AN EMPIRICAL PHASE DIAGRAM APPROACH TOWARD BIOPHYSICAL CHARACTERIZATION OF VACCINE CANDIDATES AGAINST SHIGELLA, SALMONELLA AND YERSINIA

By

XIAOTONG CHEN

Bachelor of Biotechnology
Shandong University
Jinan, China
2010

Submitted to the Faculty of the
Graduate College of the
Oklahoma State University
in partial fulfillment of
the requirements for
the Degree of
DOCTOR OF PHILOSOPHY
July, 2014

AN EMPIRICAL PHASE DIAGRAM APPROACH TOWARD BIOPHYSICAL CHARACTERIZATION OF VACCINE CANDIDATES AGAINST SHIGELLA, SALMONELLA AND YERSINIA

Dissertation Approved:

Dr. Wendy Picking

Dissertation Adviser

Dr. William Picking

Dr. Edward Shaw

Dr. Marianna Patrauchan

Dr. Joshua Ramsey

ACKNOWLEDGEMENTS

I would like to express my gratitude to all those who have helped me during my study in the Oklahoma State University. First, I would like to express my heartfelt gratitude to my mentors Drs. Wendy and William Picking who gave me their best support on both my course study and research. I gratefully acknowledge their encouragement and instruction in completion of this dissertation. Second, I would like to thank all my committee members who gave me valuable advice and shared their knowledge, which inspire me during the writing of this dissertation.

I also want to give the special thanks to Dr. Chelsea Epler for her guidance during my early research. I want to thank the past and present Picking lab members including Philip Adam, Shyamal Choudhari, Kelly Harrison, Olivia Arizmendi, Kirk Pendleton, Joshua Encinas, Dr. Francisco Martinez, Dr. Nicholas Dickenson, Dr. Julian Kissmann, Jamie Greenwood, and Mrinalini Patil for their support and help.

Name: XIAOTONG CHEN

Date of Degree: JULY, 2014

Title of Study: AN EMPIRICAL PHASE DIAGRAM APPROACH TOWARD BIOPHYSICAL CHARACTERIZATION OF VACCINE CANDIDATES AGAINST *SHIGELLA, SALMONELLA* AND *YERSINIA*

Major Field: MICROBIOLOGY AND MOLECULAR GENETICS

Abstract: Infectious diarrhea is an important public health problem and a major cause of morbidity all over the world. Infants and young children are the most vulnerable group. Vaccination is one of the most important public health tools for the prevention of infectious diseases, however, formulation of safe and effective vaccines against diarrheal disease can be challenging. *Shigella, Salmonella* and *Yersinia enterocolitica* are three highly virulent pathogens in urgent need of vaccine development. A common virulence factor is utilized by these three pathogens, the type III secretion system (T3SS), which is highly conserved across multiple serotypes within these groups. With the discovery that the *Shigella* T3SS proteins IpaD and IpaB are protective antigens, we constructed a novel IpaD-IpaB fusion protein to simplify the production and reduce the cost of vaccine production. Because of its hydrophobic IpaB portion, the DB fusion needs detergent to maintain solubility. A mild detergent called LDAO was identified and showed great promise for protein stabilization when compared to the detergent used previously (called OPOE). Inspired by the success of the DB fusion, we constructed a SipDB fusion using the homologous *Salmonella* T3SS proteins SipD and SipB. In addition to exploring the fusion strategy with regard to anti-*Shigella* and anti-*Salmonella* vaccines, a relatively new antigen delivery system called Bacterium-Like Particles (BLPs) was also explored and formulated as a potential means for delivering protective antigens from *Shigella*, *Salmonella* and *Yersinia enterocolitica* (LcrV and YopB). Derived from *Lactococcus lactis*, BLPs are peptidoglycan skeletons that are safe for newborns and can carry multiple antigens on their surface. The T3SS proteins were fused with a protein anchor domain for BLP attachment. The constructed fusion vaccine candidates and BLP-based vaccine candidates were biophysically characterized using multiple techniques including circular dichroism spectroscopy, intrinsic fluorescence spectroscopy, and static light scattering which allowed measuring the secondary, tertiary and quaternary structural changes, respectively, as a function of environmental stress. The resulting large dataset was summarized using a three-index empirical phase diagram (EPD), which is a colored representation of the overall structural integrity and conformational stability of the vaccine candidates in response to environmental conditions. The information acquired is used for identifying favorable states of protein and the proper detergent to be used for the formulation of the resulting vaccines. This approach can also be used in further studies on excipient screening for stabilizing final vaccine products, though that work was not done here.

TABLE OF CONTENTS

LIST OF TABLES

Table Page

LIST OF FIGURES

Figure Page

CHAPTER I

LITERATURE REVIEW

Historical Overview of *Shigella*

Shigella spp. are gram-negative, nonmotile, rod-shaped, facultative intracellular bacteria belonging to the family *Enterobacteriaceae*. *Shigella* was first discovered as the bacterial cause of bacillary dysentery by Dr. Kiyoshi Shiga in 1897 [1]. Over the next several years, a number of *Shigella* strains were identified and grouped into four species – *Shigella flexneri, S. sonnei, S.dysenteriae* and *S. boydii* [2]. Among these four species, *S. flexneri* and *S. sonnei* are responsible for the majority of reported *Shigella* infections[3]. Meanwhile, *S.dysenteriae* causes the most severe form of dysentery (and can lead to hemorrhagic colitis and hemolytic uremic syndrome) and contributes the majority of mortality[4]. All four species typically lead to shigellosis, an important gastrointestinal disease characterized by fever, diarrhea containing blood and mucous, and abdominal cramping. Although shigellosis is mostly self-limiting, it can be life-threatening, especially for children under 5 years of age. In 2009, WHO reported approximately 90 million cases of shigellosis leading to about 100 thousand deaths annually [5]. *Shigella* spp. are transmitted through the fecal-oral route, which is why most of these infections occur in developing countries where there are poor sanitary conditions and contaminated water supplies. Children are especially impacted by shigellosis and in the developing world repeated episodes often increase the developmental problems already caused by malnutrition and can lead to stunted growth and impaired cognitive development.

Cellular Pathogenesis of *Shigella*

Shigella have a limited host range and essentially only infect humans. After ingestion, the pathogen is able to survive the acidic environment of the stomach and passes through the small intestine [6]. Like some other pathogens, *Shigella* can down-regulate the host expression of antimicrobial peptides (AMPs) produced by phagocytes and the cells at epithelial surfaces, which enhances pathogen survival [7,8]. Instead of invading colonic epithelial cells from their apical side, *Shigella* exits the lumen of the large intestine by transcytosis across microfold cells (M cells) which are continuously sampling the contents of the gut lumen for presentation of potential invaders to underlying phagocytic and lymphoid cells [9,10]. After transcytosis, the bacteria encounter resident macrophages and are quickly engulfed. *Shigella* then rapidly induces apoptosis (pyroptosis) of these macrophages to ultimately facilitate bacterial access to the basal side of the colonic epithelium [11,12]. In this process, the dying macrophages have their caspase 1 activated which leads to the release of the proinflammatory cytokine interleukin-1β along with the release of IL-18. This triggers infiltration of polymorphonuclear leukocytes (i.e. PMNs or neutrophils) to the infection site and the stimulation of natural killer (NK) cells to produce and release IFN-γ[13,14]. After inducing macrophage cell death, the *Shigella* escape from the apoptotic macrophages which provides them access to the basal side of the overlying epithelium. The *Shigella* are able to invade the epithelial cells from this position by altering normal host cells functions using a bacterial type III secretion system (T3SS). The T3SS consists of a “needle and syringe” that allows the *Shigella* to inject effector proteins into host cells which leads to cell membrane ruffling and incorporation of the bacterium into a spacious phagosome [15]. Once inside the host cell, *Shigella* dissolves the vacuolar membrane to gain access to the host cell cytoplasm where it then replicates. While in the host cytoplasm, *Shigella* recruits host cell actin to allow it to move about the cytoplasm by a process called actin-based motility (ABM). ABM then allows the bacteria to push outward against the host membrane to enter a neighboring cell. The protrusion into the second cell then pinches off and the double membrane-bound vacuole is lysed.

In this process called intercellular spread. *Shigella* is able to spread while avoiding the extracellular environment and the host immune system [16].

Type III Secretion System

Type III secretion systems (T3SS) are needle-like molecular nanomachines that can be found in numerous plant and animal bacterial pathogens including *Salmonella* spp., *Yersinia* spp., Enteropathogenic and Enterohemorrhagic *Escherichia coli* (EPEC and EHEC, respectively), *Pseudomonas* spp. and *Shigella* spp. *Salmonella enterica* serovars Typhimurium and Typhi even possesses two T3SSs (encoded by the *Salmonella* pathogenicity islands SPI1 and SPI2) which accommodate invasion of target epithelial cells and subsequent adaptation to an intracellular lifestyle, respectively. These pathogens cause various types of diseases and have very different infection strategies. For example, *Shigella* and *Salmonella* are intracellular pathogens while *Yersinia*, EHEC and EPEC are extracellular pathogens. For all of these pathogens, however, the T3SS is an essential virulence factor that has a central role in pathogenesis.

Despite the range of infections caused by bacteria that possess T3SSs, the type III secretion apparatus (T3SA) found in all these pathogens share many structural features. The first injectisome or T3SA needle complex that was visualized by electron microscopy was from *S.* typhimurium [17], however, the *S. flexneri* T3SS is closely related to this one at the structural and protein sequence level and is also well studied. Therefore, the following discussion will focus on the *Shigella* T3SS/T3SA which is encoded on a large virulence factor by the *ipa* (invasion plasmid antigen), *spa* (surface-presentation of antigens) and *mxi* (major exporter of Ipa proteins) genetic loci. The T3SA structurally consists of a basal body, an external needle and a needle tip complex. The basal body spans the inner and outer membranes of the bacterium and supports the entire complex structure. An ATPase located on the cytoplasmic side of the basal body energizes

the system for the transport of effector proteins. The T3SA needle is composed of multiple copies of a protein called MxiH arranged helically and protruding from the basal body to the cell surface beyond the outer membrane LPS layer. The needle contains a channel that allows partially unfolded proteins to pass through when activated. The needle tip complex lies at the distal end of the T3SA needle and in its most mature form it is composed of multiple copies of a tip protein and two translocon proteins. In the case of *Shigella*, the three proteins would be IpaD (the needle tip protein), IpaB (the first hydrophobic translocator protein) and IpaC (the final hydrophobic translocator protein). Homologs of these and many other T3SA proteins can be found in other pathogens possessing T3SSs (see Table 1). The tip complex is able to respond to extracellular signals to control the secretion of effector proteins by first forming a translocon pore onto the host cell membrane and then allowing the passage of effector proteins through the pore and into the target cell cytoplasm [4,18,19,20].

Development of a Vaccine Against *Shigella*

Shigellosis continues to be an important cause of morbidity and mortality all over the world and great efforts have been made toward the development of a *Shigella* vaccine, especially one that targets children in the developing world. Unfortunately, there is still no approved vaccine available, due in part to the many obstacles impeding the development of a broadly protective *Shigella* vaccine. These obstacles include the lack of good animal models, the need to overcome the many *Shigella* serotypes, and difficulties in large scale production. Different approaches have been explored and can be categorized into serotype-based vaccines and conserved protein antigen (serotype independent) vaccines [21,22].

Table 1.1 Structural proteins of the T3SS Needle Apparatus

role	*Salmonella*	*Shigella*	*Yersinia*	EPEC	*Pseudomonas*
translocon	SipB	IpaB	YopB	EspB	PopB
translocon	SipC	IpaC	YopD	EspD	PopD
needle tip	SipD	IpaD	LcrV	EspA	PcrV
needle	PrgI	MxiH	YscF	EscF	PscF
OM ring	InvG	MxiD	YscC	EscC	PscC
inner rod	PrgJ	MxiI	YscI	EscI	PscI
IM ring	PrgK	MxiJ	YscJ	EscJ	PscJ
	PrgH	MxiG	YscD	EscD	PscD
export apparatus	SpaP	Spa24	YscR	EscR	PscR
	SpaQ	Spa9	YscS	EscS	PscS
	SpaR	Spa29	YscT	EscT	PscT
	SpaS	Spa40	YscU	EscU	PscU
	InvA	MxiA	YscV	EscV	PerD
ATPase	InvC	Spa47	YscN	EscN	PscN

Structural homologues of T3SS needle apparatus proteins are listed here for each bacterial pathogen. The general role for each in the type III secretion system is listed at the left. This table is from [19].

The genus *Shigella* is divided into four species and further includes 43 serotypes according to variations in their lipopolysaccharide (LPS) O antigen composition. Fifteen serotypes are defined for *S. dysenteriae,* 8 for *S. flexneri*, 19 for *S. boydii*, while only one for *S. sonnei*. Serotype diversity brings many difficulties into the process of vaccine development. Serotype-based *Shigella* vaccines can be further classified as LPS-protein conjugate vaccines, live-attenuated vaccine strains, and killed whole-cell formulations. Several conjugate vaccines have been formulated with perhaps the most effective ones consisting of recombinant *Pseudomonas aeruginosa* exoprotein A(rEPA) conjugated with *S. flexneri* 2a LPS [23] and *S. sonnei* LPS (developed by National Institute of Child Health and Human Development), however, these vaccines cannot prime and protect immunologically naïve young children under 2 years of age [24,25]. Another serotype-based strategy is orally administered, live-attenuated or killed whole-cell vaccines. A few live attenuated vaccine candidates have been evaluated in human clinical trials and some positive results have been observed for adults [26,27]. Unfortunately, these live attenuated vaccines are only effective against the serotypes from which they are derived and so are not broadly effective in protecting against multiple *Shigella* serotypes or species.

The use of conserved protective antigens as vaccine candidates has also been explored. One strategy has been to use outer membrane proteins prepared from *Shigella* [28,29]. A technology called ‘generalized modules of membrane antigens’ (GMMA) was developed to genetically produce outer membrane particles containing multiple *Shigella* outer membrane proteins without LPS. The GMMA were tested in a mouse model where a 65-100% protection was observed, however, it continues to remain at the preclinical stage [30].

Another strategy is to employ the Ipa proteins from the *Shigella* type III secretion system. The invasion plasmid antigens (Ipa proteins) were originally identified by the antibody responses seen in individuals convalescing from shigellosis [31,32]. These proteins have long been known to be highly immunogenic during *Shigella* infection, however, their resent identification as

surface proteins within the context of the T3SS has made them potential vaccine targets [33,34]. As discussed above, a T3SS is essential for the virulence of *Shigella* regardless of serotype and the T3SA and its components are highly conserved among all the *Shigella*. Investigators at Walter Reed Army Institute of Research initially formulated a *Shigella* invasion complex (*Shigella* Invaplex) which was composed of LPS and the highly conserved Ipa proteins (IpaB, IpaC and IpaD) and prepared from fully virulent bacteria for use as a somewhat well-defined vaccine. The Invaplex was tested in healthy volunteers and proved to be immunogenic and relatively safe [35,36]. A related LPS-containing formulation generated using purified recombinant IpaD and IpaB with adjuvant was subsequently developed and shown to grant some degree of heterologous protection in a mouse model depending upon the type(s) of LPS used [37].

More recently, IpaB and IpaD have been used in the presence of adjuvants and the absence of any LPS to provide a fully serotype-independent subunit vaccine that could be used to protect against shigellosis. Analysis of these proteins within the context of vaccine formulation will be the topic of the remaining chapters in this dissertation.

Biophysical Characterization of Proteins

A lot of effort must be put into developing vaccine formulations so that they are effective, safe and ready to be stored and/or shipped without losing activity. Macromolecule-based or higher order macromolecular complex-based vaccine formulation has developed rapidly in the last 30 years [38]. The reason for this late development is that the issue of macromolecule stability is often a tremendous problem associated with the formulation, transportation and storage of macromolecules. Such issues are typically less problematic with traditional small-molecule products. The integrity (and thus activity) of macromolecules (especially proteins) can be affected by their intrinsic instability and environmental changes such as temperature and pH

fluxes or excipient incompatibility [39]. Therefore, it's very important to ensure the maintenance of product structural integrity and conformational stability during formulation, shipping and storage. This is especially true for pharmaceutical macromolecules to be used in developing nations where shipping infrastructure and storage facilities can vary dramatically.

Traditional standard analytical methods like X-ray crystallography, nuclear magnetic resonance (NMR) and/or cryo-electron microscopy are able to obtain high-resolution structural information for proteins and their complexes. These are high-resolution and powerful techniques for assessing macromolecule structure and integrity, however, limiting conditions like crystallization or isotopic labeling make these approaches impractical for medium- to high-throughput testing of macromolecular pharmaceutical agents [40]. A set of alternative biophysical techniques with lower resolution and which provide analysis of protein secondary, tertiary and quaternary states and is amenable to high-throughput analyses is needed. Such techniques are available and while individually they provide limited information on a macromolecule, the combination could be, if used appropriately, applied to monitor the structural and conformational alterations of the macromolecules in response to different environmental conditions.

One commonly used technique for protein analysis is far-UV Circular Dichroism (CD) spectroscopy, which is used to determine the content of a protein's secondary structure and to monitor secondary structure changes. Secondary structure characteristics such as α-helical content, the presence of β sheets and the presence of turns or unfolded structure exhibit unique and quantifiable CD signals. For example, double minima at 208 and 222 nm and a prominent maximum at around 191 to 193 nm are strong indicators that a protein contains a dominant α-helical structure. Meanwhile, β sheet structures typically exhibit a strong positive maximum between 195 and 200 nm and a single minimum between 215 and 217 nm [41]. In contrast, random coil (unstructured) peptides tend to show little signal above 200 nm and a minimum near 195 nm. In folded proteins, the CD spectrum is typically a mixture of all three secondary

structure types, but there are algorithms to help quantify overall secondary structure of a protein based on a reliable signal from about 190 nm to 240 nm. Most importantly, however, CD spectroscopy can be used to monitor minor secondary structure alterations in proteins as they are exposed to different solution conditions or environmental stresses such as high temperature which can led to protein unfolding [42].

In contrast to CD spectroscopy which measures signals from the polypeptide backbone of a protein, fluorescence spectroscopy can be used to monitor the microenvironments surrounding fluorescent aromatic amino acid side chains within a protein. Extrinsic fluorescent probes can also be used to reveal tertiary structure properties of a protein as will be discussed below. Intrinsic and extrinsic fluorescence spectroscopies are frequently used as simple low-resolution measures of protein tertiary structure changes. For proteins possessing tryptophan, intrinsic fluorescence spectroscopy is typically used to assess tertiary structure changes. The indole side chain of Trp is a natural fluorophore with an absorbance near 290 nm and an emission spectrum that is highly sensitive to the polarity of the residue's microenvironment. For example, the emission peak position of Trp UV fluorescence becomes a very useful probe of the structural change. Trp residues are typically buried within the apolar core of a fully folded protein. When they move into the more polar environment of the surrounding aqueous solvent due to unfolding of the protein, a red shift in peak position is usually observed. Interactions between the Trp and solutes or other amino acids can also influence the observed fluorescence emission [43]. Alternatively, Trp emission can be used to monitor tertiary structure changes in a protein since it tends to have greater emission when in apolar environments with decreased fluorescence upon movement into a polar environment such as would be seen in aqueous solutions. The advantage of peak position over intensity, however, is that peak position can be monitored without influence from the concentration of the protein.

For proteins lacking Trp, an extrinsic fluorescence probe could be used that is very sensitive to the polarity of its microenvironment. One of the most widely used extrinsic dyes used for protein studies is 8-anilino-1-naphthalenesulfonate (ANS). ANS is nonfluorescent in aqueous solution, however, it is particularly attracted to the apolar regions of proteins where it binds to become highly fluorescent [44]. Thus, when a protein begins to unfold, apolar patches become accessible to the dye and this is observed as a dramatic increase in the fluorescence intensity of this extrinsic dye.

In addition to secondary structure content and the tertiary structure (folding state) of a protein, the oligomeric status of a protein (quaternary structure) is important to consider when exploring its use as a potential vaccine. Oligomerization can be a positive trait for proteins that naturally form discrete multimeric states, however, destabilization of a protein can often lead to aggregation which greatly compromises activity and potentially impairs use in a vaccine formulation. Static light scattering (SLS) and dynamic light scattering (DLS) spectroscopies are techniques commonly used to characterize the quaternary structure and aggregation of a protein in solution. SLS analyzes the intensity of the scattered light and it is usually obtained simultaneously with fluorescence spectroscopy data by monitoring the light scattered at a 90° angle to the incident light at the excitation wavelength. SLS increases as the aggregative state of the protein increases. DLS measures the fluctuations in intensity of scattered light due to Brownian motion and it provides a more sensitive and quantifiable measure of protein aggregation or complex formation [38]. Thus, between CD spectroscopy, fluorescence spectroscopy and light scattering, it is possible to provide a comprehensive description of the secondary, tertiary and quaternary structure properties of a protein in a manner that is amenable to moderate- to high-throughput analysis.

Three-Index Empirical Phase Diagram (Three-Index EPDs)

The techniques introduced above are practical methods for studying macromolecules to be used as biopharmaceutical agents. There are also other techniques such as Fourier transform infrared (FTIR) spectroscopy, UV-visible absorption spectroscopy, near-UV CD spectroscopy that could also be used to investigate protein structure changes at the secondary and tertiary structure levels. Each of these techniques, however, focus on one specific aspect of protein structure and do not provide a picture of the overall structural transitions that occur in a protein in response to environmental changes. Thus, a high-throughput screening approach is needed that combines the various biophysical techniques used to monitor different structural characteristics of a macromolecule (e.g. protein) including secondary, tertiary and quaternary structures. The difficult point of such an analysis, however, is the interpretation of the large quantity of data generated from multiple biophysical analyses. An empirical phase diagram (EPD) was created by the research group of Dr. C. Russell Middaugh to successfully address this problem [45]. In the EPD, the datasets obtained from different techniques are combined to form an information-rich colorful map indicating the physical stability of the macromolecules or their complexes over a range of different conditions such as temperature, pH or ionic strength. Normally, two state conditions are picked to make a two phase space, for example, a temperature-pH phase space. Multiple-dimensional vectors representing the datasets obtained from a number of experimental techniques are then fit into the temperature-pH phase space. Each dataset consists of individual values against the temperature and pH, and is normalized to values between -1 and 1. Three datasets that contribute mostly are then picked and reduced to color based on an arbitrary red/green/blue (RGB) scheme using singular value decomposition (SVD) [38,45,46]. This approach has now been well developed and applied to numerous studies on the stabilization of protein therapeutics and vaccine formulations.

Although widely applied, EPDs as originally developed do have certain deficiencies. The most critical flaw is that the color transitions that appear in an EPD represent molecular structure changes, but as designed the color itself doesn't mean anything specific with regard to these structural features. To overcome this flaw, a three-index EPD method has been recently developed. Far-UV CD spectroscopy, intrinsic fluorescence spectroscopy and static light scattering are applied to monitor the protein secondary, tertiary and quaternary structural changes, respectively. Meaningful colors are then specifically assigned to each dataset derived from an individual technique which means that there is a relationship between a specific color and a specific element of structure. In the research presented here, secondary structure has been assigned to red, tertiary structure has been assigned to green and aggregation state has been assigned to blue. A color map is thus constructed by summarizing the three color components and the resulting colors and the potential interpretation. Yellow color represents native state. Red, brown or pink usually represents variations of the molten globular state. Blue represents aggregation while black is indicative of an extensively unfolded state without aggregation [47].

CHAPTER II

MATERIALS AND METHODS

Materials

All the chemicals were purchased either from Sigma (St. Louis, MO) or Fisher Scientific (St. Louis, MO) with a small number of exceptions indicated in the text.

Buffers and Reagents

All the buffers, reagents and media recipes are listed in Appendix A and B respectively.

Bacterial strains, media and growth conditions

Escherichia coli strains containing plasmids are grown on Luria-Burtani (LB) agar plate or LB broth at 37 °C. For protein expression strains, two kinds of media are used, auto-introduction media (AI) and terrific broth (TB). Growth of liquid culture is under shaking at 200 RPM. For auto-induction media, culture is grown at 37 °C all the time. For TB, bacteria are grown at 37 °C till OD reaches 1.0 and then moved to 17 °C and IPTG is added to 1 mM for induction.

Antibiotic concentrations are 100 µg/ml ampicillin for pET15b, 34 µg/ml chloramphenicol for pACYC and 50 µg/ml kanamycin for pET28a.

Methods

Generation of plasmids for expression of the IpaD-IpaB fusion genes in *E. coli*. The pET28b plasmid containing *ipaD-ipaB* and pACYCDuet-1 plasmid containing *ipgC* were constructed as follows. The *ipaD* gene was amplified by PCR using a 5' primer with an *Nde*I restriction site and a 3' primer with *Xho*I restriction site while the *ipaB* was amplified using a 5' primer with *Xho*I site and a 3' primer with *BamH*I site. The PCR products were digested and ligated into pET15b to form the *ipaD-ipaB*. The *ipaD-ipaB* fragment was then digested and ligated into similarly digested pET28b. The constructed pET28b plasmid was used to transform *E. coli* NovaBlue. The *ipaD-ipaB* and *ipgC* plasmids were then co-transformed into *E. coli* Tuner (DE3) for co-expression and both plasmids were selected using kanamycin and chloramphenicol.

Generation of plasmids for expression of the SipD-SipB fusion genes in *E. coli*. The pET28b plasmid containing *sipD-sipB* and pACYCDuet-1 plasmid containing *scAi* were constructed as follows. The *sipD* was amplified by PCR using a 5' primer with *Nde*I restriction site and a 3' primer with *Sal*I restriction site. The *sipB* was amplified using a 5' primer with *Sal*I site and a 3' primer with *Xho*I site. The PCR products were digested and ligated into pET28b to form the *ipaD-ipaB*. The final pET28b construct was used to transform *E. coli* NovaBlue. The *sipD-sipB* and *sicA* plasmids were the co-transformed into *E. coli* Tuner (DE3) for co-expression and both plasmids were selected using kanamycin and chloramphenicol.

Generation of plasmids for expression of the tip protein and first translocator protein genes in *E. coli*. The *ipaD, sipD, lcrV, ipaB, sipB,* and *yopB* genes were amplified by PCR using a 5' primer with *Nde*I restriction site and a 3' primer with *BamH*I restriction site. The PCR products were digested and ligated into pET15b. The constructed pET15b plasmids were used to transform *E. coli* NovaBlue. The plasmids containing the tip protein genes were then purified and used to transform *E. coli* Tuner (DE3). The translocator protein chaperone genes *ipgC, sicA, sycD* were copied by PCR and ligated into pACYCDuet-1 which was used to co-

transform *E.coli* Tuner (DE3) for co-expression. Bacteria containing both both plasmids were selected using ampicillin and chloramphenicol.

Generation of plasmids for expression of PA-first translocator protein genes in *E. coli*. The *ipaB, sipB, yopB* genes were amplified by PCR using a 5' primer with *Nde*I restriction site and a 3' primer with *BamH*I restriction site while the *pa* (encoding the *L. lactis* peptidoglycan anchor peptide) was generated using both 5' primer and 3' primers with *Nde*I sites. The PCR product was digested and ligated into pET15b to form the *pa-ipaB pa-sipB* and *pa-yopB*. The constructed pET15b was used to transform *E. coli* NovaBlue cell line. The cognate translocator protein chaperone genes *ipgC, sicA, sycD* were cloned into pACYCDuet-1 and used to co-transform *E. coli* Tuner (DE3) for co-expression (except for *pa-yopB/sycD* which is transformed into the *E. coli* C43 strain) and both plasmids were selected using ampicillin and chloramphenicol.

Expression and purification of DB fusion Protein. Tuner(DE3) cells containing pET28b-IpaD/IpaB and pACYC-IpgC were grown at Auto-Induction media for 16hours started from a 6-hour LB overday culture. The bacterial pellet was resuspended, the cells ruptured using a microfluidizer and centrifuged at 12000 rpm for 20 minutes at 4°C. AEBSF protease inhibitor was added before microfludization. The IpaDB/IpgC complex was purified using Immobilized Metal Affinity Chromatography (IMAC) based on an N-terminal His-tag. This protein was further purified using Hydrophobic Interaction (HI) Chromatography and Anion Exchange Chromatography on an AKTA Explorer 10^{TM} system. A second IMAC purification was performed that included the detergent octyl-oligooxyethelene (OPOE) at 2% v/V concentration to remove the chaperone from the IpaD-IpaB complex as described before [48]. Alternatively, the detergent N,N-dimethyldodecylamine N-oxide solution (LDAO) at 0.1% v/V concentration was also used to remove the chaperone. Collected fractions were analyzed by SDS-PAGE and the

buffer was exchanged into PBS containing either 0.5% v/V OPOE or 0.05% v/V LDAO using PD-10 desalting columns.

Expression and purification of the SipDB fusion protein. Tuner(DE3) cells containing pET28b-SipD/SipB and pACYC-SicA were grown in Terrific broth media and induced with IPTG when the OD reached 1.0. The bacterial pellet was resuspended, sonicated and centrifuged as above. AEBSF protease inhibitor was added before microfluidizing. SipDB/SicA was purified using IMAC technology via the N-terminal His-tag. The partially purified protein was further purified using Anion Exchange Chromatography with a pH gradient on an AKTA Explorer 10^{TM} system. A second IMAC purification was performed that included the detergent N,N-dimethyldodecylamine N-oxide (LDAO) at 0.1% v/V in the solution. Collected fractions were analyzed by SDS-PAGE and buffer exchanged into PBS with 0.5% v/V OPOE or 0.05% v/V LDAO using PD-10 desalting columns.

Expression and purification of the tip proteins. Expression strains were grown in auto-induction media for ~16 hours and started from a 6-hour pre-culture. Bacterial pellets were resuspended , sonicated and centrifuged as above to obtain a supernatant fraction that contained the soluble protein. The His-tagged tip proteins were then purified on an IMAC system followed by anion exchange chromatography. The purified proteins were dialyzed into PBS.

Expression and purification of the translocator proteins. IpaB and IpgC (IpaB/IpgC) were co-expressed using auto-induction media while SipB/SciA and YopB/SycD were co-expressed using Terrific broth. The proteins were then purified on an IMAC system followed by HI chromatography (and anion exchange chromatography for SipB/SicA, but not YopB/SycD). A second IMAC step was applied for all three proteins to remove chaperones using buffers with 0.1% v/V LDAO. The final products were dialyzed into PBS containing 0.05% v/V LDAO.

Expression and purification of the tip-PA proteins and production of tip protein-BLPs. All the tip-PA proteins were produced by Mucosis at the company's request. *ipaD, sipD* and *lcrV* were codon-optimized for *L. lactis* and sub-cloned into the *L. lactis* expression vector Ppa224, Pmuc052 and pPA3, respectively, with a C-terminal PA domain that results in recombinant proteins secreted into the culture medium. The constructed plasmids were electroporated into *L. lactis* PA1001 and the proteins were purified from the clarified culture media using cation exchange chromatography. The proteins were then dialyzed into PBS. For the preparation of bacterium-like particles coated with antigen, the proteins were incubated with BLPs (prepared by Mucosis) at room temperature for 2 hours and washed thoroughly with PBS. The coating of the BLPs with antigen proteins was performed at Oklahoma State University. The amount of protein bound to the BLPs was determined by using Coomassie stained SDS-PAGE gels containing a bovine serum albumin (BSA) standard and with standardized amounts of the protein of interest. The final products were 85 μg of IpaD-PA, 45 μg of SipD-PA and 70 μg of LcrV-PA per mg BLPs.

Expression and purification of the PA-translocator proteins and production of translocator protein-BLPs. All three translcoator proteins possessing a PA tag were expressed using Terrific broth for growth. The proteins harvested from the cells were firstly partially purified by IMAC. PA-IpaB/IpgC and PA-SipB/SicA were further purified using anion exchange chromatography followed by a second IMAC to remove their chaperone with 0.1% v/V LDAO. The final products were dialyzed into PBS containing 0.05% v/V LDAO. PA-YopB/SycD was further purified with size exclusion chromatography with PBS containing 0.05% v/V LDAO. The final translocator protein products were incubated with naked BLPs at room temperature for 2 hours and washed thoroughly with PBS 0.05% v/V LDAO. The amount of proteins bound to BLPs was determined similar to tip-BLPs using the corresponding PA-translocator protein as standard proteins.

Biophysical characterization sample preparation. The proteins used in biophysical analyses were dialyzed into 20mM Citrate/20 mM Phosphate (CP) buffer with an ionic strength of 150mM and the pH was adjusted from 3.0 to 8.0 with either 0.5% v/V OPOE or 0.05% v/V LDAO added to the CP buffer as described in the results section for translocator protein preparations. The dialyzed protein was then filtered with 0.22 μm Millex Syringe-driven filter. The concentration of IpaDB fusion and SipDB fusion was adjusted to 0.1mg/ml. Tip proteins, tip-PA proteins and PA-translocators were adjusted to 0.15 mg/mL and translocator proteins were adjusted to 0.3 mg/mL for the biophysical studies.

For the protein-BLPs, they were centrifuged and resuspended with 20mM Citrate/20 mM Phosphate (CP) buffer with an ionic strength of 150mM and the pH adjusted from 3.0 to 8.0, 0.05% v/V LDAO was added to the CP buffer, if required. The process was repeated three times to thoroughly wash the protein-BLPs. All the protein-BLPs (IpaD-BLPs, IpaB-BLPs, SipD-BLPs, SipB-BLPs, LcrV-BLPs and YopB-BLPs) samples were diluted to 1 mg BLP/mL.

Far-UV Circular Dichroism (CD) spectroscopy. Circular Dichroism (CD) spectra of all the protein samples in CP buffer with or without the detergents OPOE (0.5%) or LDAO (0.05%) at six different pH values (3.0-8.0) were measured using a Jasco J-815 CD spectrometer equipped with a six-position Peltier temperature controller and coupled with six 0.1-cm path length cuvettes. The spectra were collected from 260 to 190 nm at 10 °C with a scanning speed of 50 nm/min, a 1.0-nm resolution and three data acquisitions. Thermal unfolding was measured by collecting the CD signal at 222 nm (225 nm for protein bound to BLPs) every 2.5 °C with the temperature increasing from 10°C to 90°C, employing a temperature ramp rate of 15 ˚C/h. Samples were equilibrated to the target temperature (± 0.1 ˚C) for 5 s prior to each data point measurement. Two repeats were obtained and all three sets of signal data were converted into molar ellipticity and plotted (Jasco Spectral manager and Origin 8.6). For protein associated with the bacterium-like particles (BLPs), the CD signal was plotted instead of molar ellipticity.

The calculation of converting CD signal into molar ellipticity is shown below:

$$\text{Molar ellipticity } [\theta] = \frac{\theta \times 100 \times M}{C \times l \times n \times 1000} \quad (1)$$

where θ represents CD signal in mDeg, M represents molecular weight of the protein, C is the concentration of protein in mg/mL, l is path length in cm, n is the number of amino acid residues present in the protein, whereas 100 is a factor to convert path length from cm into meters and 1000 is a factor to convert raw CD signal from mDeg to Degrees.

Intrinsic tryptophan (Trp) fluorescence spectroscopy. Intrinsic Trp fluorescence spectra of all the samples were obtained using a Photon Technology International (PTI) spectrofluorometer (Birmingham, New Jersey) equipped with a turreted 4-position Peltier-controlled cell holder. Trp residues were excited primarily at the wavelength of 295 nm and the emission spectra were collected from 300 to 400 nm with a step size of 1 nm and a 0.5 s integration time. Samples in CP buffers in the presence of 0.5% OPOE or 0.05% LDAO (when needed) at different pH values from 3 to 8 were placed in quartz cuvettes with 1-cm pathlengths and the emission spectra were acquired from 10 to 85 °C with an increase of 2.5 °C. Three readings were taken for each sample and a spectrum of blank buffer at each pH was subtracted from the sample spectra. Peak positions were obtained using Origin software and a mean spectral center of mass method. The emission peak position calculated by the msm method reflects the changes but not the actual value - a 10-14 nm shift occurs during the analysis.

Static Light Scattering. Static light scattering (SLS) provides a measure of thermally induced aggregation of proteins. These measurements were acquired simultaneously with intrinsic Trp fluorescence measurements using a second detector oriented 180˚ from the fluorescence photomultiplier tube but still 90˚ relative to the excitation source. Light scattering intensity at 295 nm was monitored as a function of temperature every 2.5 ˚C over a temperature

range of 10 to 85 ˚C. Buffer scans were subtracted from the sample readings prior to data analysis.

Three-index Empirical Phase Diagrams (EPDs). The substantial amount of thermal stability data acquired from the multiple techniques for each protein sample were summarized for global analysis using a three-index empirical phase diagram (EPD) to provide a comprehensive overview of the data using a standardized red, green and blue (RGB) color scheme. Briefly, structural indices defined as correlation of the degree of structural change within a given range of environmental stress conditions, are calculated for each data set. In this study, the secondary structural index was calculated from the 222 nm CD molar ellipticity (225 nm for protein associated with BLPs), the tertiary structural index was calculated from intrinsic Trp fluorescence peak position data and the aggregation index was calculated from the static light scattering data. The values for the structural index for a particular data set were normalized from 0 to 1, in which 1 represents native secondary or tertiary structure while 0 represents extensively altered secondary or tertiary structure. A value of 0 for aggregation index indicates no aggregation while a value of 1 indicates the maximum extent of aggregation seen. Each of these structural indices was assigned to a color in the standardized RGB color scheme to yield a map that provides a correlation between color and physical state of the protein at a given pH and temperature. In this case, the strongest negative CD signal represents the largest amount of secondary structure and is assigned to red while the weakest signal is assigned to black. For fluorescence peak position data, the native tertiary structure is assigned to green and the most shifted wavelength is black. Aggregation is represented by static light scattering where the minimum signal is assigned to black assuming there is no or minimal aggregation while the highest level of aggregation seen is assigned to blue. The contribution of each RGB component can be seen in the right hand panels next to the associated EPD. The three-index EPDs can then be interpreted as follows: Yellow (i.e. the sum of the “native state” colors) is associated with the native state of a protein where both

secondary and tertiary structures are intact and no aggregation has occurred. Black is associated with significantly unfolded states with minimal retention of secondary and tertiary structure and no aggregation. Blue is associated with aggregated states with minimal secondary and tertiary structure and maximal aggregation. Finally, brown is associated with intermediate states of a protein with an intermediate loss of secondary and tertiary structure.

Analytical ultracetrifugation. This approach was performed by collaborators at the University of Kansas. Fusion proteins were purified and the concentrations were adjusted to 8 μM in PBS at pH 7.4 containing 0.5% OPOE or 0.05% LDAO and covalently crosslinked by the addition of the amine-reactive crosslinking agent dithiobis[succinimidyl propionate (DSP). The reaction was maintained for 15 min at room temperature and quenched using 70 mM Tris-HCl pH7.4. The detergent was then removed by dialysis into PBS at pH 7.4. Sedimentation velocity analytical ultracentrifugation (SV-AUC) experiments were performed using a Beckman Proteomlab Optima XL-I analytical ultracentrifuge (Brea, California) equipped with a scanning UV/visible optical system housed in the Macromolecule and Vaccine Stabilization Center at the University of Kansas. Scans were collected at 20 ˚C after 1 hour of equilibration after the temperature was reached and at a rotor speed of 40,000 RPM with detection at 280 nm. Beckman charcoal-epon two sector cells with sapphire windows were used in an An-60 Ti 4 hole rotor. The data were analyzed using the Sedfit program by Peter Schuck. The default partial specific volume of 0.73 mL/g was used in the analysis, as well as values for buffer density and viscosity that were calculated using Sednterp based on buffer composition. A continuous c(s) distribution was used, with 280 scans. A range of 0 svedbergs to 15 svedbergs was used for LDA-DB and a range of 0 svedbergs to 50 svedbergs was used for OPOE-DB, after verifying that there was no material sedimenting outside of these ranges. A resolution of 400 points per distribution was used, with a confidence level of 0.95. A best-fit frictional ratio of 1.43 was used for LDAO-DB, and a best-fit frictional ratio of 1.51 was used for OPOE-DB. Baseline, radial independent noise, a and time

independent noise were also fit, while the meniscus and bottom positions were set manually. The monomer peak was assigned by comparing the experimentally observed sedimentation coefficients to the maximum theoretical sedimentation coefficient of the monomer, calculated based on molecular weight. The oligomeric state of other observed species were determined by dividing the experimentally observed sedimentation coefficient of the oligomer by that of the monomer. Percent mass assigned based on integration of the c(s) peaks in Origin. The sedimentation coefficients reported are peak maxima.

CHAPTER III

CONSTRUCTION AND BIOPHYSICAL CHARACTERIZATION OF A NOVEL DB FUSION COMPLEX FROM SHIGELLA FLEXNERI AS A CANDIATE SUBUNIT VACCINE

Introduction

Shigella spp. are the causative agents of shigellosis, a severe diarrheal and dysenteric disease having high morbidity and mortality among children and the elderly in developing countries. As a Gram-negative bacterial pathogen, *Shigella* is transmitted by the fecal-oral route. It is estimated to take only 10 to 100 organisms to cause an infection in humans [4]. There are four species of *Shigella* (*S. flexneri*, *S. sonnei*, *S. dysenteriae* and *S. boydii*) and there are approximately 50 serotypes within the genus [21,49], due to the different structures found in the O-antigen portion of the outer membrane lipopolysaccharide (LPS). Because serotype largely drives the host immune response during the course of natural infection, developing shigellosis due to one serotype of *Shigella* does not protect someone from infection by another serotype. Furthermore, this makes it difficult to develop a broadly protective vaccine that protects against all serotypes. Nevertheless, a common virulence factor called the type III secretion system (T3SS) is required for the pathogenesis of all *Shigella* serotypes. The T3SS is also an essential virulence factor for many other important Gram-negative pathogens. Components of the *Shigella* T3SS are encoded on a 220-kb invasion plasmid and they lead to the assembly of a type III secretion apparatus (T3SA) [50]. This plasmid also encodes the majority of the effector proteins secreted by the T3SS and their cognate chaperones.

The T3SA is a syringe-like structure comprised of three parts: a basal body anchoring the apparatus into the bacterial envelope; an external needle; and a needle tip complex that functions in secretion control [4,18]. Upon host cell contact, the T3SA recognizes effector proteins at the cytoplasmic face of the apparatus. The effectors are then separated from their chaperone and passed through the base, the needle and ultimately through a translocon pore that is formed in the host cell membrane by the needle tip complex. The T3SS plays an essential role in *Shigella* pathogenesis by killing macrophages immediately after crossing the epithelial layer of the large intesting and inducing subsequent internalization of the bacterium into colonic epithelial cells [51,52]. As a shared and highly conserved virulence factor among all *Shigella* species, T3SS proteins are potential candidates for the development of a serotype-independent vaccine against shigellosis.

Although much effort has been put into the development of vaccines against *Shigella*, no approved vaccine is yet available for prevention of shigellosis [22,25,26]. Our previous studies have demonstrated that a promising vaccine candidate is a novel fusion protein composed of highly conserved full length T3SS proteins IpaD and IpaB [48]. IpaD is located on the tip of the T3SA needle where it controls recruitment of other T3SA/T3SS components during translocon pore formation and host cell invasion [33,53]. Meanwhile, IpaB is part of the multimeric translocation pore that interacts with and inserts into the host cell membrane [54]. IpaB also mediates macrophage apoptosis after the pathogen is internalized into macrophages [11]. IpaD and IpaB have been shown individually to be protective antigens when delivered intranasally and intramuscularly to mice that were then challenged using the mouse lethal pulmonary infection model [37]. The development of a fusion protein sets the stage for including multiple antigens into one recombinant polypeptide which is more easily formulated than the two antigens separately. This is significant for a vaccine formulation targeting developing world since multiple antigens are delivered simultaneously and at an overall reduced cost. The fusion of IpaD with

IpaB led to what is referred to as the 'DB Fusion'. The DB Fusion was delivered through intranasal route and generated similar antibody titers to the IpaD/IpaB combination, however, higher levels of IL-17 were observed and this cytokine appears to be essential for protection against *Shigella* infection. *S. flexeri, S. sonnei* and S. *dysenteriae* were used for the lethal pulmonary challenge and an efficient protection was provided in each case [48].

Because the DB Fusion appeared to be a promising candidate for vaccine development against *Shigella* infection, a stable subunit vaccine formulation study was initiated. The work presented in this chapter focuses on the construction and preformulation characterization of this novel protein construct. The structural characteristics and stability of the DB Fusion were studied as a function of pH and temperature using biophysical techniques that included Circular Dichroism spectroscopy, intrinsic fluorescence spectroscopy and static light scattering. The data set obtained were combined and visualized using a novel three-index empirical phase diagram (EPD) that allowed analysis of the overall structural integrity and conformational stability of the protein. Because the DB Fusion only remains soluble in the presence of detergent, a mild detergent n-octyl-poly-oxyethylene (OPOE) was used in the biophysical studies presented in this chapter. An alternative detergent, Lauryldimethylamine-oxide (LDAO), was also used and found to give the DB Fusion distinct biophysical characteristics including enhanced plasticity (structural resilience) and even improved immunogenicity.

Results

DB Fusion protein construction and purification

Much like its component IpaB [50,55], the DB Fusion was only successfully made by coexpressinig it with the *Shigella* chaperone protein IpgC. It then required a mild detergent such as OPOE or LDAO to separate the protein from the chaperone. The constructed DB Fusion is a

large 101.2-kDa protein comprised of both full-length IpaD and IpaB with a two-amino acid linker (Fig. 3.1A and B). To maintain solubility, the DB Fusion requires the presence of detergent (0.5% OPOE or 0.05% LDAO which is above their individual critical micelle concentrations, respectively). Far-UV CD spectroscopy was used to investigate the protein secondary structure content and thermal stability of the secondary structures of IpaD, IpaB, and the DB Fusion. Dominant minima at 208 and 222 nm were observed in all cases indicating the proteins contain significant amount of α-helical secondary structure (Fig. 3.1C). This suggests that the fusion protein maintains a properly folded secondary structure after all the purification processes. The secondary structure thermal stabilities of all three proteins were measured by CD melt monitoring mean residue molar ellipticity at 222 nm as a function of temperature (Fig. 3.1D). As with the previously published data [33,56], IpaD had two transitions at 60°C and 80°C while IpaB had a transition at ~58°C. A major transition was found at 60°C for the DB Fusion suggesting it has characteristics intermediate to IpaD and IpaB. This is further confirmed that the DB fusion mean residue molar ellipticity values for far-UV CD scans and thermal melt curves lie between those for IpaD and IpaB alone.

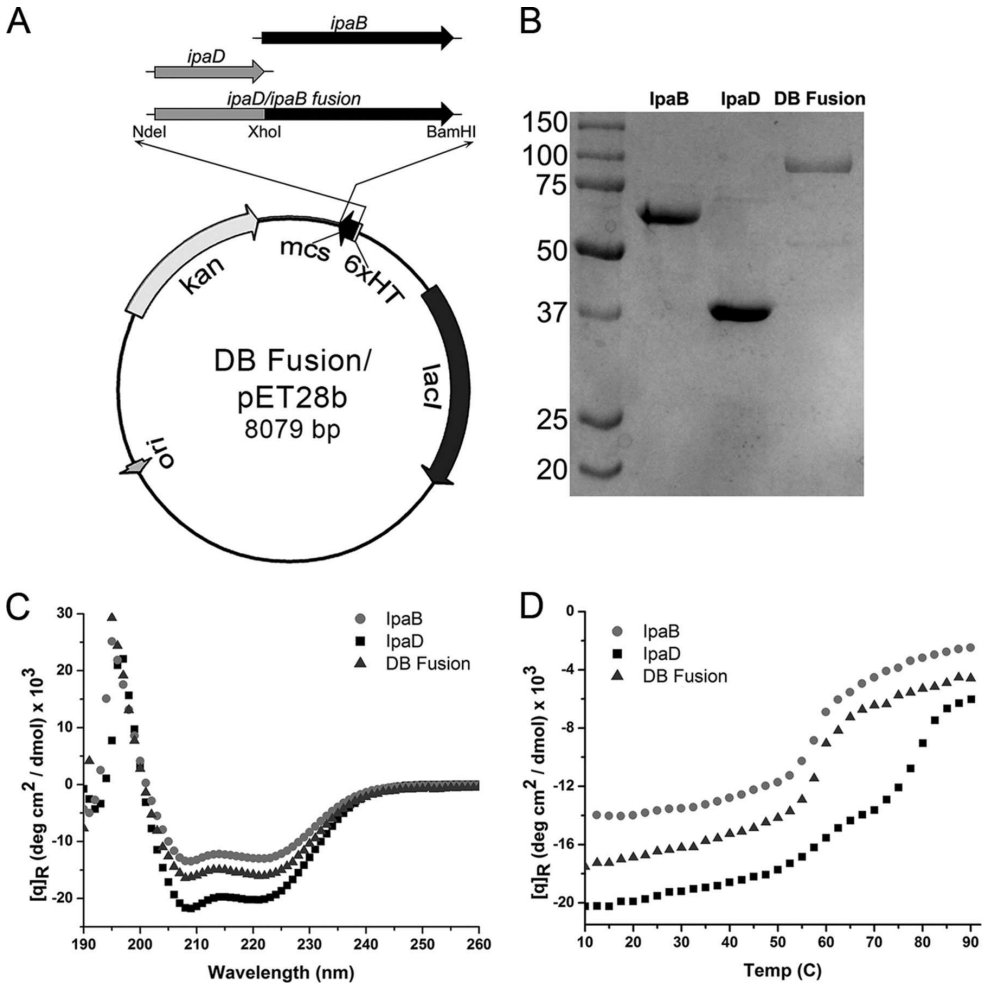

Figure 3.1 : Generation and initial biophysical analysis of the DB Fusion [48]. (A) The plasmid construct harboring the IpaD/IpaB fusion is shown. Restriction sites used for cloning are shown within a map of the commercial express plasmid pET28b. (B) Comparative SDS-PAGE profiles of IpaD, IpaB, and the DB Fusion is shown with molecular mass markers, in kDa, indicated to the left. (C) The CD spectra for IpaB in 0.5% OPOE, IpaD in PBS, and the DB fusion prepared in 0.5% OPOE all indicate predominantly α-helical contgent with the mean residue molar ellipticity ($[q]_R$) values (measured in degrees cm^2per decimol). (D) Thermal unfolding of the secondary structures of the DB fusion, IpaB, and IpaD as a function of temperature is shown.

Secondary structure stability

To analyze the secondary structure stability of the DB Fusion, different pH conditions were applied to the protein for subsequent testing of thermal stability (Fig. 3.2). CD spectra of the DB Fusion in the presence of OPOE and LDAO at 10°C (Fig. 3.2 A and E, respectively) display double minima at 208 and 222 nm, which indicates the protein contains significant amounts of α-helical structure across the entire pH range tested. A decrease in CD signal is observed in lower pH (pH 3, 4 and 5) conditions compared to the neutral pH conditions in OPOE indicating the average structure of the protein at acidic pH is slightly altered, however, the DB Fusion in OPOE shows a more intense signal overall the fusion in LDAO.

The CD melts for the DB Fusion in OPOE or LDAO indicate a loss of α-helical structure since the molar ellipticity at 222 nm increases as the temperature is increased (Fig. 3.2 B and F, respectively). For the DB Fusion in OPOE, however, the secondary structure starts a major transition at ~55°C under acidic pH conditions and at ~60°C under neutral pH. There is significant secondary structure loss after the major transition in all cases. Meanwhile, the DB Fusion in LDAO shows a lower degree of structure alteration as a function of temperature. A gradual linear increase is present for samples at pH3-5 without apparent transition, while protein at pH6-8 there is a subtle transition at around 50°C. Although a structural alteration occurs, the DB Fusion in LDAO maintains significant secondary structure under all the experimental conditions used here.

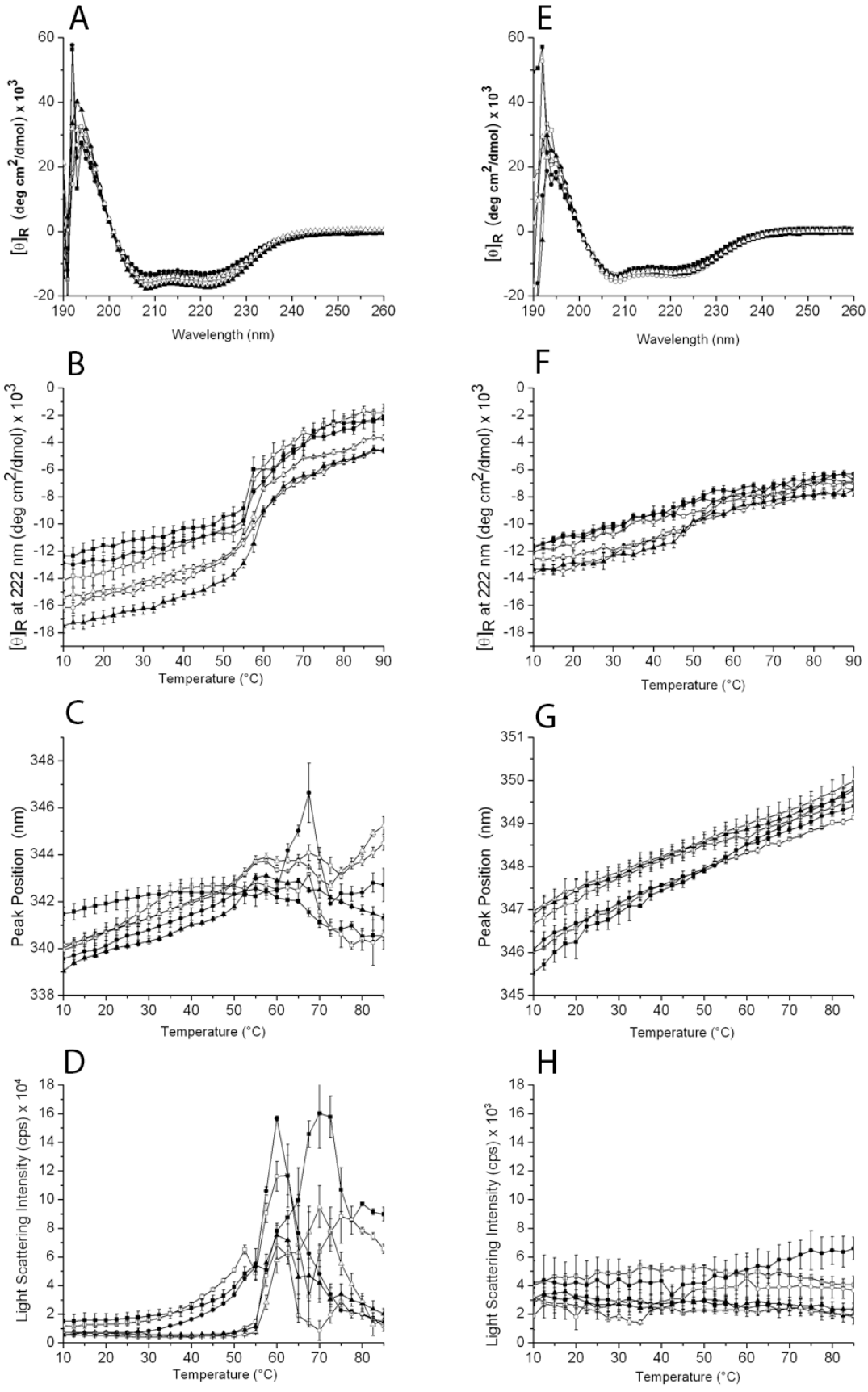
A
E
B
F
C
G
D
H
Wavelength (nm)
Temperature (°C)
Peak Position (nm)
Light Scattering Intensity (cps) x 10^4
Light Scattering Intensity (cps) x 10^3

Continued…

Figure 3.2 : Biophysical characterization data for the DB Fusion in the presence of OPOE (A, B, C and D) and LDAO (E, F G and H). The far-UV CD scan for the DB Fusion from pH 3 to pH 8 indicates predominantly α-helical content with the mean residue molar ellipticity ($[q]_R$) values at 10 °C (A, E). Thermal unfolding of the secondary structures of the DB fusion CD molar ellipticity at 222 nm monitored as a function of temperature from 10 to 90 ˚C (B, F). Intrinsic Trp fluorescence peak position wavelength (C, G), and light scattering intensity monitored at 295 nm as a function of temperature from 10 to 85 ˚C (D, H). Error bars represent standard deviation from three different experiments. Symbols: pH 3 (■), pH 4 (□), pH 5 (●), pH 6 (○), pH 7 (▲) pH 8 (Δ).

The CD spectra of the DB Fusion in both detergents after the thermal unfolding process were also measured and compared to the spectral data before unfolding to further investigate protein stability. These spectra were taken with the temperature returned to 10°C. The α-helical secondary structure of the DB Fusion in the presence of OPOE is clearly lost following the unfolding event (Fig. 3.3A, open symbols), however, the spectra of the DB Fusion in LDAO after prior unfolding and renaturation overlay perfectly with that generated before the thermal unfolding process (Fig. 3.3B). This provides strong evidence that the protein recovers its secondary structure fully.

Tertiary structure stability

Tertiary structure changes in the DB Fusion in the presence of OPOE or LDAO were characterized by monitoring changes in the intrinsic Trp fluorescence peak position wavelength as a function of temperature and pH (Fig. 3.2 C and G). The DB Fusion contains five Trp residues, four from IpaD and one from IpaB. For the DB Fusion in 0.5% OPOE (Fig. 3.2C), initial peak position at pH 3 was near 342 nm, which indicates only partial burial of Trp residues (on average) probably due to conformational alterations under these acidic conditions. As the temperature increases, a subtle red shift appeared followed by a blue shift after 65°C which is probably due to burial of indole side chains caused by aggregation. Peak positions of samples at pH4 to 8 are near or under 340 nm, which suggests that the Trp residues are largely buried. A red shift was obvious as a function of temperature in the beginning at these pHs, suggesting increased exposure of Trp residues to the polar aqueous environment. At pH 4, two transitions are seen, one at around 32°C, indicating formation of a conformationally altered state, and another at 65°C, suggesting aggregation (which was later confirmed by static light scattering). Samples at pH to pH 8 behave similarly with a transition at approximately 55~60°C, however, a sharp transition is observed at pH5, while samples showed a red shift from pH 7 to pH 6 and pH 8, suggesting the protein is most stable at pH 7.

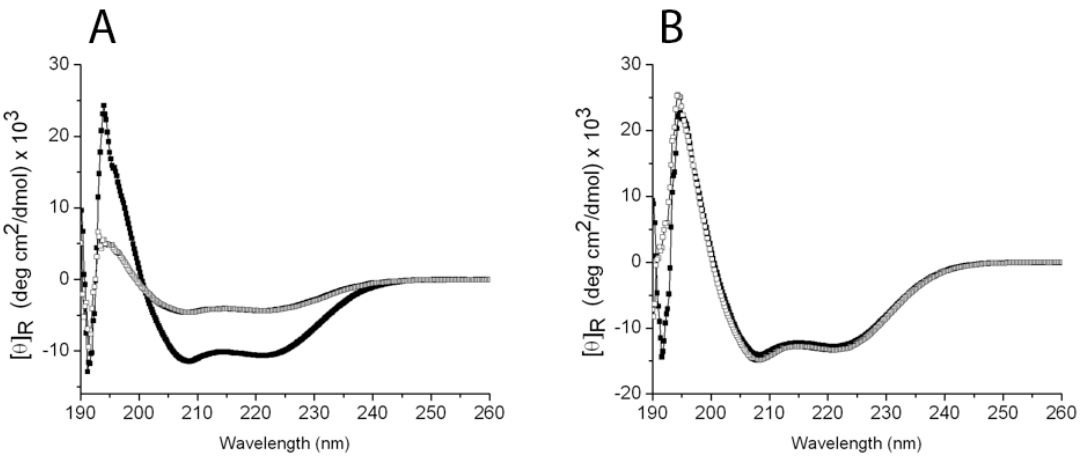

Figure 3.3 : Far UV Circular Dichroism spectra for DB fusion before and after thermal melt of the secondary structure. The DB fusion with the presence of PBS 0.5% OPOE (A) and 0.05% LDAO (B) were used for circular dichroism spectrum at 10 °C before (■) and after (▲) thermal denaturation.

In the presence of LDAO, the DB Fusion behaved differently (Fig. 3.2G and H). For all samples the Trp emission maxima at 10°C are higher than 345nm and showed a gradual red shift as the pH increased, suggesting the indole side chains are only partially buried at the start and gradually become more exposed to the aqueous environment at higher pHs. As a function of temperature the peak position wavelength increased linearly without any obvious transitions which can be attributed to an intrinsic thermal effect on the internal conformational alteration of the Trp residues. Thus, no major structural transitions are indicated.

Quarternary structure stability

Static light scattering measurements were performed simultaneously with the intrinsic fluorescence to examine the aggregation behavior of the DB Fusion protein (Fig. 3.2 D and H). The DB Fusion in the presence of OPOE undergoes aggregation at all pHs tested with the onset of aggregation at pH 3 to 5 are seen at around 35°C while samples at pH 6 to 8 didn't start to aggregate until 55°C. The decrease of the signal after the initial red fluorescence shift suggests that aggregation leads to precipitation of the protein which then settles out of solution at approximately 60°C for samples at pH 4 to 7, and around 70°C for samples at pH 3 and pH 8. The static light scattering data indicate the DB Fusion maintains highest stability in relative neutral environment with regard to aggregation. No significant increase in light scattering is observed as a function of temperature and pH for the DB Fusion in LDAO, indicating no significant aggregative behavior. These data are consistent with the results from intrinsic fluorescence which show that the DB Fusion is significantly stabilized by the presence of LDAO.

Three-index empirical phase diagram (EPD) provides an overall assessment of the biophysical stability of the DB Fusion

A data visualization approach, the three-index empirical phase diagram (EPD), was generated using the datasets obtained from far-UV CD spectroscopy, intrinsic Trp fluorescence spectroscopy and static light scattering as a function of temperature and pH. This was done for the DB Fusion protein with the presence of OPOE and LDAO. In the three-index EPDs, different colors are assigned to the changes in different protein structural states. Red is assigned to secondary structure (molar ellipticity at 222nm), green to tertiary structure (Trp fluorescence peak position wavelength), and blue to quaternary structure or aggregation (light scattering intensity at 295nm).

For the DB fusion in OPOE, the EPD can be divided into four phases (Fig. 3.4A). Phase 1 is the yellow region covering pH 6 to pH8 below 55°C, pH 5 below 45°C, and pH 4 below 30°C. This portion of the EPD suggests that the fusion protein stays in its most stable native state here, which is consistent with the presented CD and fluorescence data. In phase 2, the dark color defines the samples in a highly structurally altered state (secondary and tertiary structure are lost) with a lower degree of aggregation compared with phase 4. Phase 3 indicates that the protein samples are in a partially unfolded state either because of relatively high temperature (pH 6-8) or due to acidic environment (pH 3-5). The blue color of phase 4 suggests the acidic pH and high temperature cause complete aggregation. Overall the DB Fusion protein is maintained in its most stable state at around neutral pH and below 55°C in OPOE.

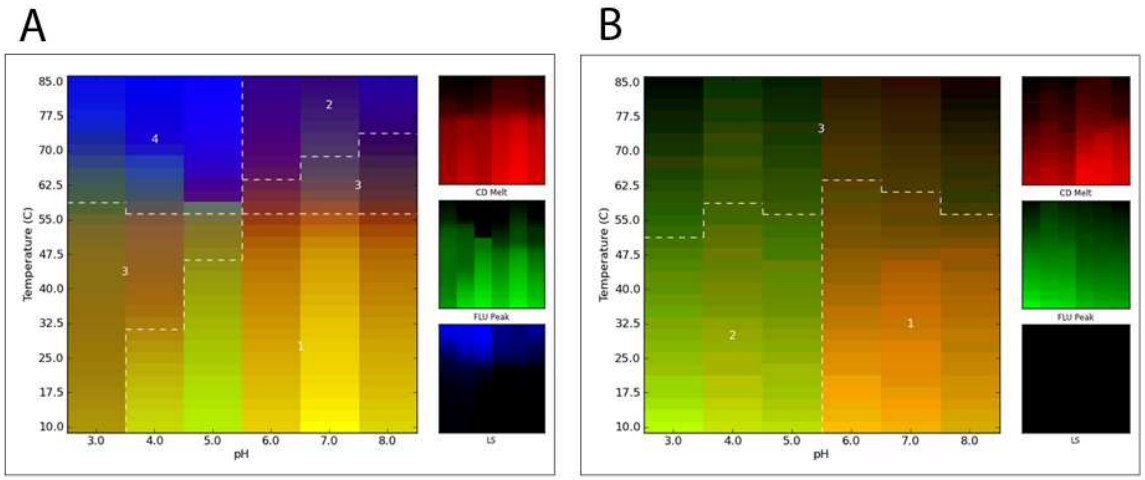

Figure 3.4 : Three index empirical phase diagram (EPD) for DB fusion with presence of 0.5% OPOE (A), and 0.05% LDAO (B), representing conformational stability of the DB Fusion as a function of pH and temperature. Data obtained from multiple techniques shown in Figure 3.2 were synthesized into this colored map with different physical states represented by different colors. Four different phases were defined for the DB Fusion with 0.5% OPOE. Region A1: most favorable state of the protein. Region A2: Relatively unstable states at either low pH or high temperature. Region A3: transition state between different phases. Region A4: completely unfolded and aggregate state. On the other hand, the EPD of the DB Fusion in 0.05% LDAO shows no clear transition states and three phases with borders characterized by subtle transitions were defined. Regions B1 and B2 are relatively favorable states and B3 is a relatively unfavorable structural state.

The three-index EPD of the DB Fusion in the presence of LDAO shows a pattern that is quite distinct from that in OPOE (Fig. 3.4B). As temperature increases, all measurements (except for static light scattering) show gradual and constant changes without sharp color divisions. This is consistent with the presented biophysical data. Since there is no drastic change, it is hard to find clusters over temperature extremes except the difference between pH 3-5 and pH 6-8. Data at pH 3-5 show more apolar microenvironments around the Trp residues (indicated by fluorescence peak position) and less secondary structure (CD) than pH 6-8 in the lower temperature region. No aggregation is observed across all the pH and temperature ranges tested in LDAO.

Chemical stability of DB fusion at 50 °C incubation

The high throughput biophysical techniques used here provide evidence that the DB Fusion with OPOE is stable at neutral pH under 55°C, but the DB Fusion in LDAO behaves quite differently. To further expand these studies by exploring the chemical stability of the two proteins, the DB Fusion in PBS with either OPOE or LDAO was incubated at 50 °C and monitored for 7 days. Samples were removed daily and the same amount of protein was subjected to SDS-PAGE with Coomassie staining (Fig. 3.5). The DB Fusion in OPOE (Fig. 3.5A) started degrading at day one and more than 90% of protein was lost by day five. Meanwhile, the DB Fusion in LDAO (Fig. 3.5B) also showed mild degradation, but approximately 50% of the protein remained in its full-length form even after 7 days. This phenomenon indicates that even though the DB Fusion in LDAO is in a different structural state than in OPOE, it maintains this state stably and even shows signs of greater chemical stability.

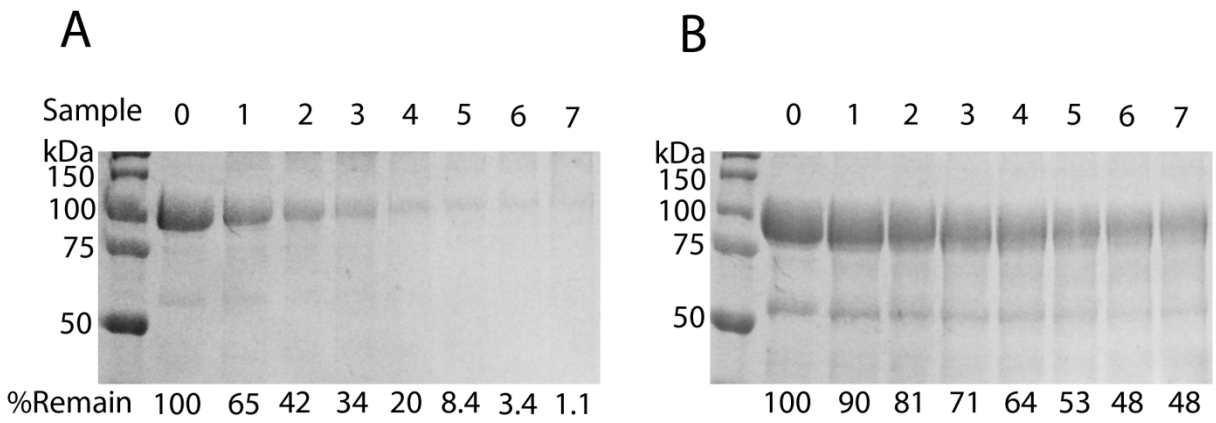

Figure 3.5 : The DB Fusion chemical stability was examined after storage at 50 °C. The DB Fusion in PBS containing either 0.5% OPOE (A) and 0.05% LDAO (B) was maintained at 50 °C for 7 days. Samples were taken each day and same amount of sample for each was subjected to SDS-PAGE and stained with Coomassie blue. The densitometry of the DB fusion protein band were taken and the percentage of protein remained were calculated and labeled below the SDS-PAGE gel.

Analytical ultracentrifugation to determine the association state of DB fusion

To better understand the effect of different detergents on the DB Fusion, sedimentation velocity analytical ultracentrifugation was conducted to compare the oligomerization state of the soluble DB Fusion in the presence of OPOE (Fig. 3.6A) or LDAO (Fig. 3.6B). The DB Fusion in OPOE and DB Fusion in LDAO were cross-linked and dialyzed into PBS without detergent and subjected to AUC analysis to provide an accurate measurement of sedimentation. Because the sample contained some degradation products, a contaminant peak showed up for each sample, however, the DB Fusion in LDAO contained a dominant monomer peak with a sedimentation coefficient of 4.82 s, and then a dimer (7.03 s) and linear trimer (9.6 s). The sedimentation velocity results for the DB Fusion in OPOE were more complicated and were analyzed by c(s) are shown in Figure 5B and Table 3.1. Although a trimer is not indicated in Table 3.1, a different scale reveals a shoulder on the 11.15 s peak at about 9.8 s (data not shown), the sedimentation coefficient expected of a trimer. There were many higher order aggregates for the sample cross-linked in OPOE, such as hexamers (15.29 s) and octamers (17.67 s) along with some other higher order species. Additionally, the trimer/tetramer peak was much larger in the OPOE-prepared sample, suggesting that this detergent favors the formation of oliogmers as was demonstrated for IpaB prepared in OPOE [57].

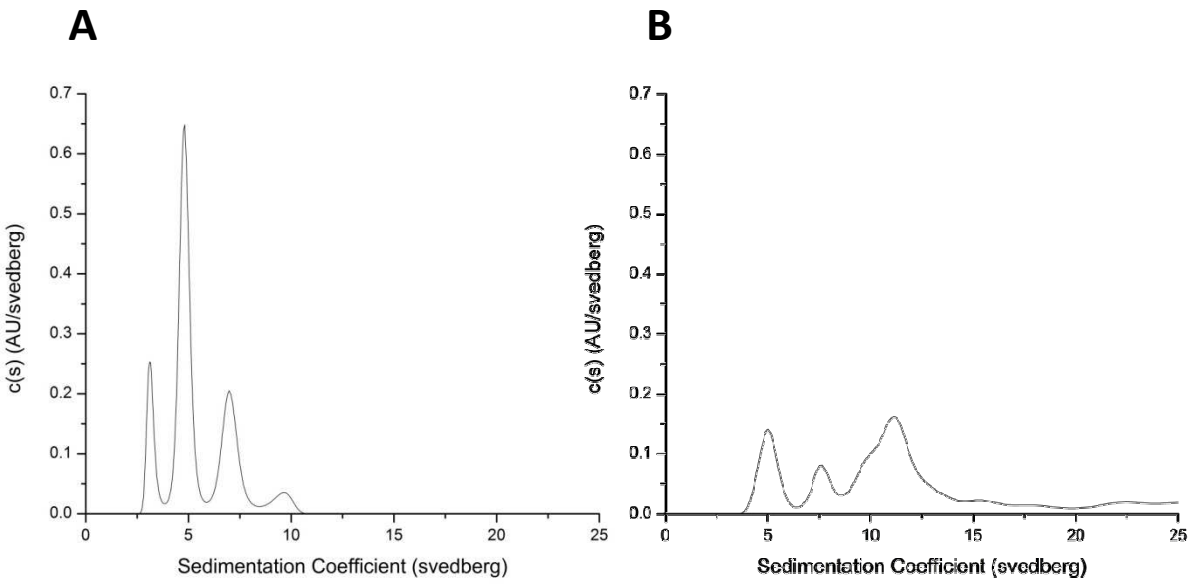

Figure 3. 6 : Determination of the precise DB Fusion oligomerization state by analytical ultracentrifugation (AUC). The DB Fusion in 0.5% OPOE (A) and 0.05% LDAO (B) were chemically cross-linked and thoroughly dialyzed into PBS without any detergent. Sedimentation velocity AUC radial absorbance scans were obtained for each DB Fusion sample and analyzed using SEDFIT program.

Table 3.1. Sedimentation coefficient of each DB fusion species in the presence of LDAO or OPOE and the relative percent of mass that can be attributed to each DB Fusion species as determined by SV-AUC.

Species	Sedimentation coefficient (Svedberg)	Relative Percent of Mass for Each Species
With LDAO		
Fragment	3.19	15%
Monomer	4.82	54%
Dimer	7.03	26%
Trimer	9.60	6%
With OPOE		
Monomer	5.01	16%
Dimer	7.64	9%
Trimer and tetramer	11.15	45%
Hexamer	15.29	5%
Octamer	17.67	3%
Higher order aggregates	22.43	6%
	25.19	11%
	34.84	2%
	41.23	1%

In the presence of different detergents, the DB Fusion forms different species. In the presence of LDAO more than 50% of the species are monomeric, with some dimer and a little trimer formation. In contrast, the DB Fusion in OPOE forms various oligomers, with mostly trimers and tetramers.

Discussion

Subunit vaccines are considered safer than live attenuated vaccines, especially in people with compromised immune systems and in children. As previously described, IpaD and IpaB have been shown to be protective antigens and are candidates for a possible subunit vaccine formulation containing multiple antigens. Unfortunately, there are several obstacles to overcome, such as defining appropriate formulation conditions for both antigens. This is often difficult and the cost of the production would be higher for two antigens relative a single recombinant protein [58]. The development of the novel recombinant DB Fusion protein as a *Shigella* vaccine candidate provides an alternative way to making a broadly protective vaccine that is more affordable, especially for the developing world.

In this work, we successfully constructed a novel DB Fusion and obtained highly purified protein. A band was found at around 50 kDa which proved to be degradation product containing parts of IpaD and IpaB based on western blot analysis (data not shown). The conformational stability of the DB Fusion was extensively characterized by employing a variety of biophysical techniques. CD spectroscopy, intrinsic fluorescence spectroscopy and static light scattering were used to monitor the stability of protein at the secondary, tertiary and quaternary (aggregative) levels, respectively, as a function of temperature and pH. The large data set obtained was summarized in a three-index empirical phase diagram (EPD) which allows visualization of protein structure changes in response to environmental conditions via a graded color scheme. Due to the hydrophobicity of IpaB, the presence of detergent was necessary for maintaining the DB Fusion in solution during all of the biophysical analyses. The two different detergents considered were used just above their critical micelle concentrations (CMCs). Thus, we used 0.5% OPOE and 0.05% LDAO and found that they both led to very different properties in the DB Fusion. With OPOE, the DB Fusion lost the majority of its α-helical secondary structure after thermal unfolding regardless of the pH used. In contrast, the DB Fusion in LDAO maintained a

significant degree of secondary structure even after thermal unfolding followed by reducing the temperature back to 10°C. With regard to tertiary structure, the indole side chains of the five Trp residues of the DB Fusion in LDAO were more exposed than for the protein in OPOE, however, there was no sharp transition (indicating full unfolding) for the protein in LDAO compared to DB Fusion in OPOE. Furthermore, there was no observed aggregation for the DB Fusion prepared in LDAO under any of the conditions tested. Overall, the EPD profiles clearly indicated that in the presence of OPOE, the DB Fusion is most stable at pH 6 to 8. It starts to unfold sooner at lower pHs as the temperature is increased, and it completely aggregates after 60°C at pH 3 to 5. Meanwhile, in LDAO the protein is in a state that provides the protein more structural elasticity (resiliency) to adapt to a wide range of pH and temperature conditions. The pattern of EPD for the DB Fusion in LDAO indicates that the protein structure is less tightly packed than when it is in OPOE. This may be because LDAO is a non-denaturing zwitterionic surfactant with a positively charged N^+ group and negatively charged O^- group. These groups might interact with charged protein residues located on the DB fusion protein surface but not disrupt the apolar core of the protein [56]. Despite the fact that LDAO interacts with DB fusion to impart a unique structural state, this does not appear to be the case for all proteins.

Full development of a protein subunit vaccine requires formulation which often includes the identification of excipients that serve to stabilize antigen. Identification of excipients was not included in this study, but this will be done in future studies. Nevertheless, we have already progressed in the formulation of DB Fusion with the use of the detergent LDAO, which allows the protein to remain stable both physically and chemically. The effect that the two detergents used here (OPOE and LDAO) have on the DB Fusion's structural state suggests that they interact with the protein differently. A previous study on detergent effects on IpaB indicated that IpaB in LDAO exclusively forms a monomeric species while IpaB in OPOE forms a distinct tetramer that may dimerize into an octomer [57]. Thus, we used analytical ultracentrifugation in this study

because it is very informative in the respect of evaluating hydrodynamic properties of biomolecules and macromolecular complexes [38]. It should be noted that AUC can be compromised by the difficulties posed by trying to remove all of the degradation from a protein preparation. Furthermore, degradation products can influence the accuracy and interpretation of AUC data since they could potentially associate with the full-length IpaB or the DB Fusion (or with each other to form higher order species). This is reflected in the AUC data presented here. The AUC data however still provided insight into the oligomerization state of the fusion in OPOE which differs markedly from that in LDAO. As with IpaB [56], the DB Fusion forms higher order quaternary species which is dominanted by a tetrameric form when in OPOE. Meanwhile, the DB Fusion in LDAO favors the formation of a monomeric species. The effect of the detergents on the DB Fusion oligomerization status is very much in line with that of IpaB, but the reason behind this is not yet clear.

Perhaps unlike many normally employed excipients, LDAO is believed to interact with the DB Fusion to alter its structure – apparently in a positive manner. This raises the concern that the structural alteration of the DB Fusion in LDAO may influence the immunogenicity of the protien. Moreover, as discussed above, the DB Fusion tends to favor an oligomeric form in the presence of OPOE, but a monomer is favored in the presence of LDAO. Some studies have shown that multimeric antigens tend to induce better memory immune responses than do monomeric antigens [59]. For the DB Fusion, this is clearly not the case. The DB Fusion in the presence of LDAO actually induces greater protection in a mouse model of shigellosis than its counterpart in OPOE.

In summary, the novel DB Fusion protein is a promising *Shigella* vaccine candidate that is highly immunogenic and broadly protective (serotype and species independent). It provides an advantage over using IpaD and IpaB separately in that as a single protein it is less costly in its production. Moreover, this preformulation study has identified a detergent (LDAO) that appears

to provide enhanced biophysical and chemical stability. Perhaps most importantly, LDAO reduces (eliminates) the aggregative properties of the antigen which is highly undesirable for vaccine formulation because it reduces the likelihood of loss of efficacy/activity [60,61,62]. LDAO not only stabilizes the DB Fusion, it also increases the immunogenicity and is in line for testing in phase 1 human trials within the next two years. Nevertheless, basic research on this vaccine formulation must continue since the structural and immunogenic principles behind the phenomena observed here require further characterization.

CHAPTER IV

CONSTRUCTION AND BIOPHYSICAL CHARACTERIZATION OF A NOVEL SipDB FUSION COMPLEX FROM SALMONELLA TYPHIMURIUM AS A CANDIDATE SUBUNIT VACCINE

Introduction

In addition to the *Shigella* spp. discussed in Chapter III, we have also worked with another important bacterial pathogen from the *Enterobacteriaceae* which falls into the genus *Salmonella*. *Salmonella* spp. are gram-negative, motile, facultative intracellular, rod-shaped facultative anaerobes. The genus *Salmonella* consists of two species, *Salmonella enterica* and *Salmonella bongori*. *S. enterica* is the most commonly encountered cause of foodborne diarrhea with about 1.2 million illnesses and 450 deaths annually in the United States and more than 1.3 billion cases annually worldwide [63,64]. There are more than 2500 serovars of *S. enterica* with three main groups involved in causing human disease. There are 22 million cases of enteric fever with 200,000 deaths every year around the world. These cases occur mostly in pre-school and school-age children. *S. enterica* serovars Typhi and Paratyphi A and B are the main groups responsible for this disease [65,66,67]. A second group of serovars includes *S. enterica* serovar *Choleraesuis* and Paratyphi C, which are important causes of septicemia and multiple organ dysfunction in humans. The last group is known collectively as the non-typhoidal *Salmonella* (NTS), which is usually self-limiting in healthy humans but can be severe or even fatal in the very young, the elderly, and immunocompromised people. NTS includes a large number of serovars, most

notably *S. enterica* serovar Typhimurium (which I'll refer to as *S. typhimurium*) and *S. enterica* serovar Enteritidis (which I'll refer to as *S. enteritidis*) which are the most commonly encountered pathogens [68].

A lot of effort has been put into the development and formulation of vaccines against *Salmonella*, however, there is still no broadly protective *S. enterica* vaccine available which can protect across serovar boundaries. A live-attenuated *S.* typhi vaccine, called Ty21a, is available and confers cross-protection against *S.* Paratyphi B but not *S.* Paratyphi A. The Ty21a vaccine requires three oral doses taken every other day, however, being a live vaccine, there are safety concerns for some individuals. Another licensed vaccine in the U.S. is formulated based on the capsular polysaccharide of fully virulent *S.* typhi, but it is rather poorly immunogenic and only effective against *S.* typhi [69,70]. Neither of these licensed vaccines can be considered "broadly protective" since they do not protect against a wide range of *Salmonella* serovars.

Just like *Shigella* and a number of other Gram-negative pathogens, *Salmonella* possesses a type III secretion system (T3SS) as an important virulence factor. In fact, it possesses two T3SSs encoded by two distinct gene clusters termed *Salmonella* pathogenicity islands 1 and 2 (SPI-1 and SPI-2, respectively). The T3SSs are essential for the human infections caused by *Salmonella* [71,72,73]. The *Salmonella* SPI-1 T3SS is very similar to the *Shigella* T3SS and it is responsible for induction of membrane ruffles and invasion of epithelial cells [73,74,75]. Moreover, the SPI-1 T3SS is responsible for having a cytotoxic effect on macrophages during the early stages of infection [76]. The SPI-2 T3SS is also an essential virulence factor and it is associated with intracellular growth of *Salmonella* following SPI-1 mediated invasion [77,78,79]. After invasion of the host cell, the pathogen remains confined to the "Salmonella-containing vacuole" (SCV) and uses its SPI-2 T3SS to deliver effectors into the host cell cytosol for maintenance of the SCV where it grows until rupture and release from the cell [80].

As mentioned above, the *Salmonella* SPI-1 T3SS is very similar to the *Shigella* T3SS. The *Shigella* T3SS tip protein IpaD and the first translocator protein IpaB have been shown to be effective as protective antigens using the mouse lethal pulmonary model for *Shigella* challenge [37]. Our previous studies have also demonstrated that we have successfully developed a promising vaccine candidate with a novel DB fusion protein composed of these two proteins [48]. The IpaD homolog from *Salmonella* SPI-1 is SipD which has been demonstrated to be localized on the *Salmonella* surface. The IpaB homolog from SPI-1 is SipB which has been shown to be a cholesterol binding protein just like IpaB. Moreover, as with IpaD and IpaB, SipD and SipB are conserved across all the important *Salmonella* serovars. Thus, these proteins may be able to provide potential serotype independent protection when used for immunization. Inspired by the success of the IpaD-IpaB fusion from *Shigella*, I generated a novel SipD-SipB fusion protein whose construction will be described here. Successful expression of the SipDB fusion requires co-expressioin with SipB's chaperone SicA. The mild detergent N,N-lauryl dimethyl amine oxide (LDAO) is then used to separate the chaperone from the SipB portion of the fusion protein. In preparation for use of the protein in future vaccine formulations, the biophysical and chemical stability of the SipBD fusion was examined as a function of temperature and pH. In the end, we found that in the presence of LDAO, the SipDB fusion behaves more stably than in other detergents with a high degree of plasticity, much like its counterpart from *Shigella*.

Results

SipDB fusion protein is expressed and stably purified with the presence of detergent LDAO

As with construction of the *Shigella* DB Fusion, I introduced a two-amino acid linker between SipD and SipB protein when fusing the two proteins and I used the SipB chaperone SicA for co-expression with the final SipDB fusion. After an initial IMAC purification step followed

by a pH gradient anion exchange chromatography step, SicA was removed from the SipDB fusion with detergent (0.1% LDAO) followed by a second IMAC column. The bound SipDB fusion was then eluted and maintained as a soluble fusion protein in 0.05% LDAO. This concentration of LDAO was just above its critical micelle concentration (CMC) and was optimal in maintaining SipDB fusion solubility. SDS-PAGE of SipD, SipB and SipDB fusion is shown in Fig. 4.1A. The lower molecular weight bands in the SipDB fusion lane are minor degradation products of SipD and SipB as confirmed by western blot analysis. Far-UV Circular Dichroism (CD) spectroscopy was then used to determine the secondary structure content of the SipDB fusion for comparison with the spectra of SipD and SipB individually. The spectra of all three preparations showed double minima at 208 and 222 nm, indicating that the secondary structure of each protein is highly α-helical (Fig. 4.1B). It is known that SipD is rich in α-helical secondary structure based on its crystal structure [81] and the N-terminal portion of SipB is highly α-helical [82] and both proteins have CD spectra that are in agreement with this. As for the SipDB fusion, these data strongly suggest that the protein is properly folded and stably purified.

SipDB fusion with the presence of LDAO maintains secondary structure stability

The protein secondary structure content and stability was further investigated using Far-UV CD spectroscopy and thermal unfolding. At 10 °C the spectra of the SipDB fusion at pH3 through pH8 all show a similar pattern with dominant minima at 208 and 222 nm, thus indicating significant α-helical content. The protein shows a slightly stronger signal at pH values near neutral, suggesting a structural preference for this pH range (Fig. 4.2A).

When the CD signal at 222 nm (a minimum seen for α-helical structures) was monitored as function of temperature, a gradual increase in signal without a clear transition to indicate full unfolding suggested that the SipDB fusion's secondary structure in the presence of LDAO was

thermostable at all pH values tested (Fig. 4.3A). This is similar to what was observed for the *Shigella* DB Fusion as discussed in Chapter III. Moreover, when the protein was cooled back down back to 10 °C, the CD spectrum at each pH was to the scan taken before the temperature increase. These data suggest that just the SipDB fusion in LDAO not only maintains its secondary structure under extreme conditsoin, but it is also able to regain its original secondary structure content following thermal stress.

Tertiary structure of SipDB with the presence of LDAO is more open but relatively stable

Intrinsic Trp fluorescence spectroscopy was used to study potential tertiary structure changes in SipDB fusion as a function of environmental pH and temperature. Tryptophan is an intrinsic fluorophore found in many proteins that has emission properties that are sensitive to the immediate environment of the residue. Thus, properties such as fluorescence intensity and peak position wavelength can be used to monitor changes to the overall or tertiary structure of a protein. The fluorescence intensity of Trp in the SipDB fusion decreased gradually without any sharp transition, indicating the gradually exposure of the native Trp residues to the aqueous solvent as the temperature increased (Fig. 4.3B). Meanwhile, the peak position wavelength of Trp emission increased with the temperature at all pH conditions, which likewise indicates that the tertiary structure is entering a more open state that allows solvent exposure to the typically buried Trp residues (Fig. 4.3C). At 10 °C, there is a gradual red shift that occurs as the pH increases, suggesting the Trp is more buried under acidic environmental conditions, but becomes more exposed at neutral pH. Overall, the intrinsic Trp fluorescence spectroscopy shows that LDAO stabilizes the protein against sudden major unfolding events, which is consistent with what was observed for the secondary structure as monitored by CD spectroscopy.

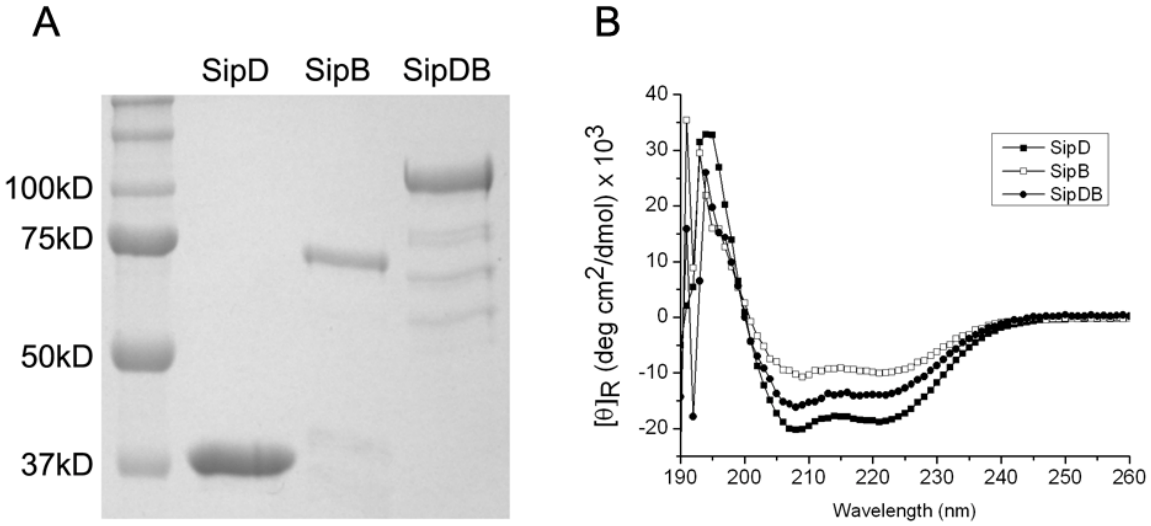

Figure 4.1 : Purification and secondary structure analysis of the SipDB fusion protein from *Salmonella.* (A) SDS-PAGE of purified SipD, SipB, and the SipDB fusion protein. The molecular mass markers are in the left lane with sizes labeled up to 100 kD. (B) The Far-UV Circular Dichroism (CD) spectra for SipD, SipB, and the SipDB fusion in citrate-phosphate buffer (pH 7) after conversion to mean residue molar ellipticity ($[q]_R$) values (measured in degrees cm^2per decimol). For SipB and SipDB, 0.05% LDAO was included to maintain solubility. The double minima at 208 and 222nm are present in all cases and are indicative of predominantly α-helical protein content within each of the proteins.

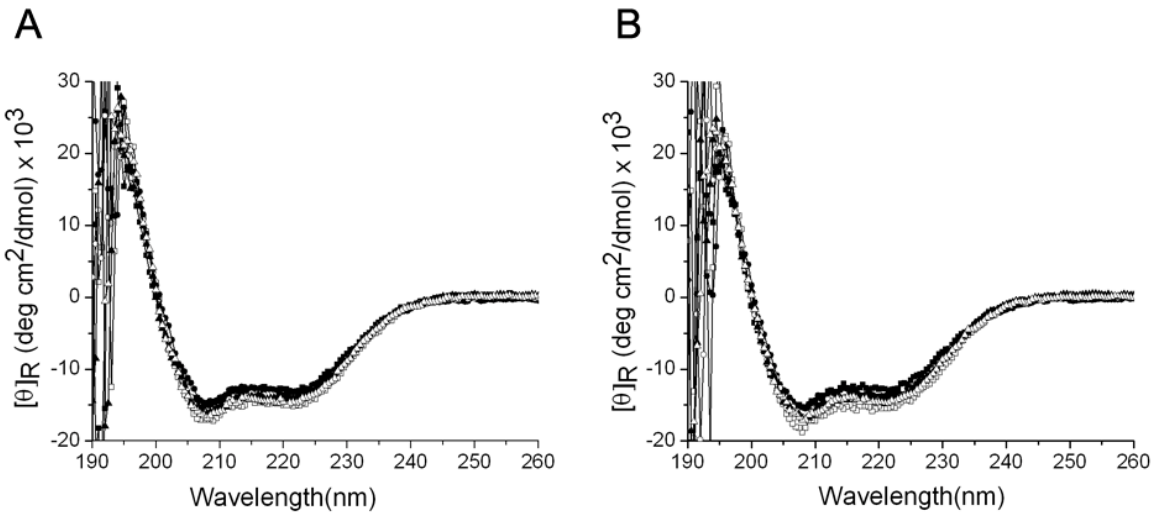

Figure 4.2 : Far UV Circular Dichroism (CD) spectra for the SipDB fusion at pH 3 to 8.

These spectra were obtained in the presence of 0.05% LDAO before (A) and after (B) thermal unfolding at 90 ^{o}C. The SipDB fusion was prepared in citrate-phosphate buffer in the presence of 0.05% LDAO at each of the indicated pH values. All of these spectra were obtain were obtained at 10 °C before or after thermal treatment and are expressed here as mean residue molar ellipticity ($[q]_R$) values (measured in degrees cm^2per decimol). Symbols: pH 3 (■), pH 4 (□), pH 5 (●), pH 6 (○), pH 7 (▲) pH 8 (Δ).

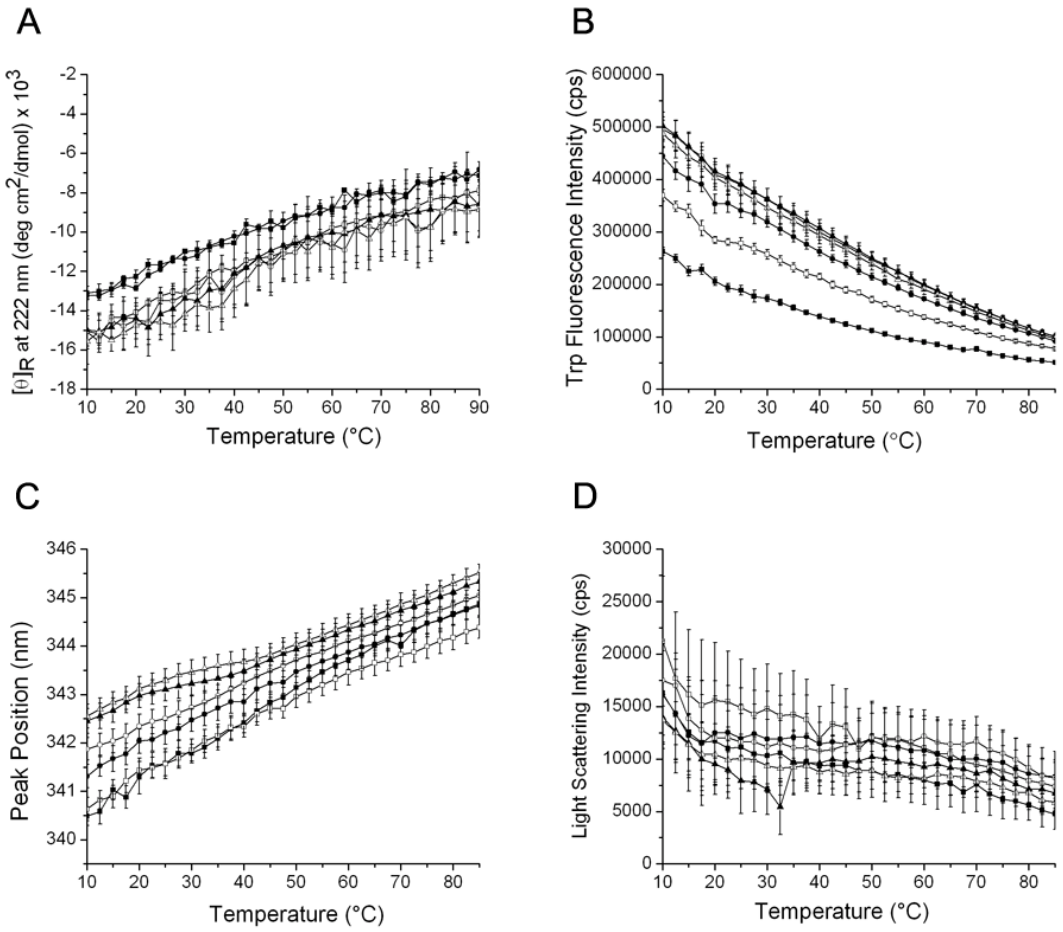

Figure 4.3 : Biophysical characterization data summary for SipDB fusion with the presence of LDAO. (A) Thermal unfolding was monitored by following the loss of secondary structure (via the minimum at 222 nm) for the SipDB fusion which is expressed as mean residue molar ellipticity as a function of temperature from 10 to 90 ˚C. (B) Intrinsic Trp fluorescence intensity changes were monitored as a measure of tertiary structure integrity as a function of pH and temperature. (C) Intrinsic Trp fluorescence peak position wavelength was monitored as a second measure of tertiary structure integrity as a function of pH and temperature. (D) Static light scattering intensity was monitored at 295 nm as a function of pH and temperature from 10 to 85 ˚C to measure protein quaternary structure or aggreation. Error bars represent standard deviation from three different experiments. Symbols: pH 3 (■), pH 4 (□), pH 5 (●), pH 6 (○), pH 7 (▲) pH 8 (Δ).

SipDB fusion protein aggregation is prevented with the presence of LDAO

Static light scattering (SLS) rises as the size of the particles being examined in a solution increase in size. Thus, SLS provides a means for monitoring increases in quaternary status of a protein, which is typically an indicator of protein aggrergation. Thus, aggregation of the SipDB fusion protein was investigated by SLS which was performed simultaneously with the intrinsic Trp fluorescence measurement (Fig. 4.3D). Consistent with observations for the *Shigella* DB fusion protein, there was no significant increase in static light scattering observed regardless of the various pH conditions used. Similarly, no increase in light scattering was observed as the temperature was increased from 10 to 85 °C. This indicates that no aggregation occurs for this protein during the thermal stresses applied here. This is consistent with the intrinsic fluorescence data which suggested no major changes in tertiary structure which could expose the hydrophobic core and lead to aggregation of the protein. This is also consistent with the observation that the SipDB fusion in LDAO can be heated to 90 ^{o}C and the cooled back to 10 ^{o}C where it retains its original secondary structure as indicated by CD spectroscopy.

Three-index empirical phase diagram (EPD) visualizes the biophysical stability of SipDB fusion

As discussed in chapter III, the three-index empirical phase diagram (EPD) provides a platform for combining a large amount of data into a single diagram that allows analysis of a protein's shift between structural states. The EPD approach as applied here summarizes the stability of a protein based on its secondary, tertiary and quaternary structures based on data obtained by CD spectrscopy, intrinsic Trp fluorescence spectroscopy and static light scattering. To improve this form of data visualization for analyzing changes in macromolecular structural, the three-index EPD assigns colors to different protein structural states so that a meaningful relationship between color and molecular features can be formed. In this case, red is assigned to secondary structure, green is applied to tertiary structure, and blue is assigned to aggregation.

The three-index EPD for the SipDB fusion prepared in LDAO exhibits a pattern that is very similar to that of the *Shigella* DB fusion prepared in LDAO (Fig 4.4). As temperature increases, CD and intrinsic Trp fluorescence spectroscopies indicate constant, gradual changes in secondary and tertiary structure, respectively, without any sharp structural transitions or changes occurring. This is indicated by the gradual shifts in color in Figure 4.4 (top and middle panels on the right, respectively) and this is consistent with the biophysical measurements presented in Figure 4.3 (panels A-C). Due to the resistance to aggregation, no color change is observed for light scattering in the EPD (Fig. 4.4, bottom right panel). When these data are considered as a whole, there is no drastic color change in the combined diagram except for the difference between low pH conditions (pH 3 to 5) and high pH conditions (pH 6 to 8). At lower temperature region, the protein secondary structure is more partially unfolded at low pH than at high pH. Meanwhile, the Trp is slightly more buried at lower pH, perhaps indicating that the protein tertiary structure is somewhat more open at pH values of 6 and higher. It is difficult to define conformational clusters that are dependent upon the temperature increase. This pattern is also observed for the *Shigella* DB fusion prepared in the presence of LDAO. Considering the two components of SipDB fusion are quite similar to their homologous IpaD and IpaB counterparts from *Shigella*, and they are fused here using strategy similar to that of the *Shigella* DB Fusion, it's not surprising that we obtained this result. For the *Shigella* protein, this was quite distinct from what was observed in the presence of the detergent octyl polyoxyethylene (OPOE) in which the DB Fusion displayed clear structural transitions in response to elevated temperature and these were not reversible. A similar study in OPOE was not performed on the *Salmonealla* SipDB fusion protein because the prior work with *Shigella* proteins indicated that LDAO was the detergent that would be used in future vaccine formulations.

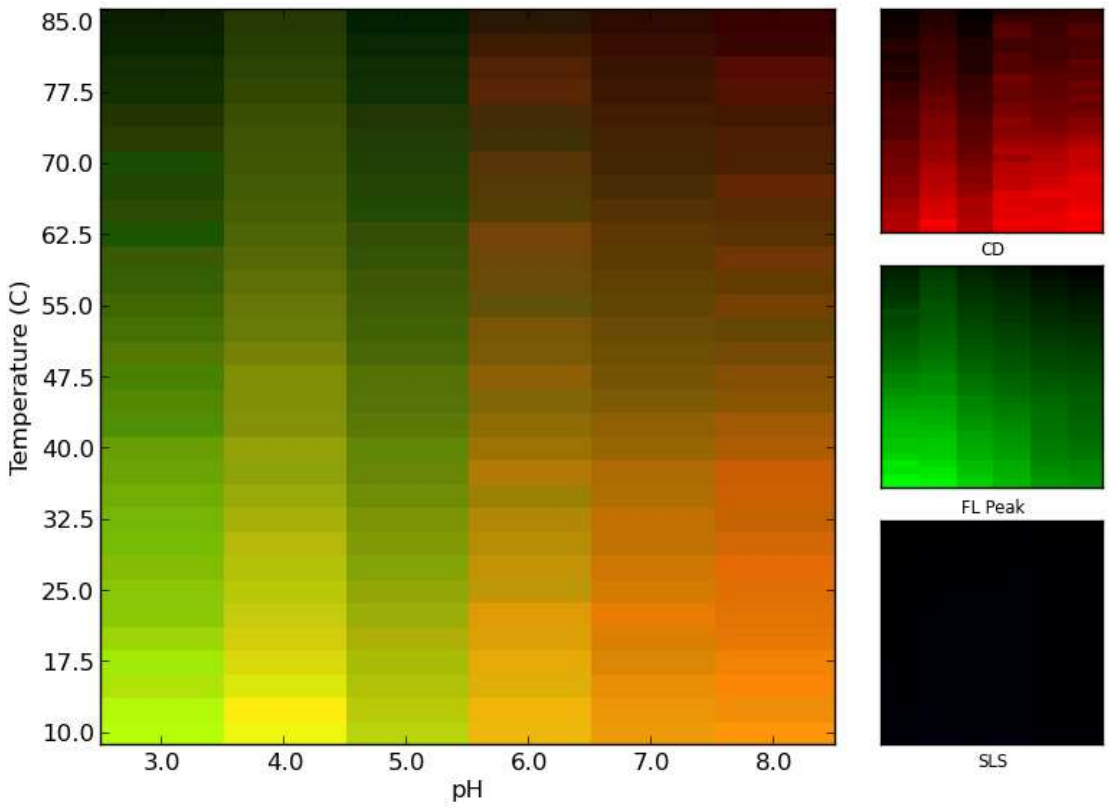

Figure 4.4 : Three index empirical phase diagram (EPD) for SipDB fusion with presence of 0.05% LDAO, representing conformational stability of the SipDB fusion as a function of pH and temperature. Data obtained from multiple techniques shown in Figure 4.3 were synthesized into this colored map with different physical states represented by different colors. EPD of SipDB fusion shows no clear transition state and the state of the protein gradually altered as the temperature increase.

Discussion

A tremendous amount of effort has been expended for the development of vaccines against *Salmonella*, however, much of the research focus here has been on generating live, attenuated vaccine strains that, in the end, always give rise to serotype-specific immunity. Thus, a broadly protective vaccine is strategy is needed. As described in Chapter III, we have successfully constructed a subunit vaccine called DB fusion – a fusion protein consisting of IpaD and IpaB from *Shigella*, which are homologous to the T3SS proteins SipD and SipB, respectively, from *Salmonella*. The DB Fusion was shown to protect against all *Shigella* species and serotypes tested. Inspired by this success, a *Salmonella* version of the DB Fusion, called the SipDB fusion, was created. The hydrophilic SipD portion is not sufficient to maintain the whole fusion protein soluble due to the hydrophobic characteristics of the SipB portion (data not shown). Thus, the SipDB fusion had to be co-expressed with the SipB chaperone, SicA. The SicA could then be removed using the detergent LDAO. LDAO is a mild detergent, was previously found to stabilize the *Sihgella* DB Fusion and, more importantly, it imparted an improved immune response on the DB Fusion. Thus, we immediately elected to use LDAO as the detergent for removing SicA from the SipDB fusion and to maintain its solubility.

In this study, a battery of biophysical techniques was used to characterize the conformational stability of the SipDB fusion in the presence of LDAO. The techniques used here included Far-UV CD spectroscopy, intrinsic Trp fluorescence spectroscopy and static light scattering. These were analyzed separately to allow for the monitoring of protein secondary, tertiary and quaternary structures, respectively, as a function of pH and temperature. The collective data obtained from these diverse techniques were summarized using a three-index empirical phase diagram to provide an overall view of protein structure changes in response to the environmental conditions. These changes were visualized via different colors and shifts in color change in response to pH and temperature changes. Based on the EPD of the SipDB fusion,

thermal stress causes both the secondary and tertiary structures to undergo a gradual, but only partial loss of integrity, regardless of pH used. However, the SipDB fusion protein recovers its original structural state after cooling down from thermal stress, most probably because the LDAO prevents aggregative events that would lead to irreversible protein-protein interactions.

Just like the *Shigella* DB Fusion in LDAO, with the presence of LDAO in the SipDB fusion preparation appears to allow the protein to stay in a structurally resilient and rather elastic state that readily adapts to changes in pH and temperature. This may be possible because LDAO is non-denaturing Zwitterionic surfactant with distinct positively charged N^+ and negatively charged O^- groups. These groups may interact with charged protein residues within the fusion proteins to shield it from deleterious interactions [56]. Thus, LDAO may play a role beyond simply being a detergent. It may also interact with certain proteins to strongly affect their surface features which might protect them from the negative effects of environmental stress. The SipDB fusion is now being characterized for its immunogenicity using a mouse model of *Salmonella* infection.

To summarize this work, we have successfully generated a recombinant SipD-SipB fusion protein that is a strong *Salmonella* vaccine candidate that may lead to broad protection against infectin by multiple *Salmonella* serovars. This pre-formulation study introduces the detergent LDAO as a vaccine component that causes the protein to become more elastic with regard to its structural features and more resilient to its environment. Most important, LDAO prevents aggregation of the SipDB fusion which is an important property when considering the need for a stable vaccine that is not adversely affected during long term storage and shipping [60,61].

CHAPTER V

BIOPHYSICAL CHARACTERIZATION OF THE TYPE III SECRETION TIP PROTEINS AND TRANSLOCATOR PROTEINS ALONE AND ATTACHED TO BACTERIUM-LIKE PARTICLES AS POTENTIAL VACCINE CANDIDATES AGAINST *Shigella, Salmonella* AND *Yersinia*

Introduction

Shigella and *Salmonella* (discussed in chapters III and IV) have been listed as Category B agents of bioterrorism by CDC. Category B includes agents that are easily spread through contaminated water or food. As previously addressed, *Shigella* can cause severe gastrointestinal illness that includes bloody diarrhea, cramping and fever. *Salmonella* is an important cause of gastroenteritis with a broad host range and more than 2500 serovars, many of which are responsible for human disease. Both of these organisms have the potential to become weaponized pathogens due to specific characteristics including low infective dose (*Shigella*), high morbidity rates [83], ease of transmission [84], increasing incidence of antibiotic resistance, and the absence of effective vaccines. In addition to these two pathogens, *Yersinia enterocolitica* is a category B agent capable of causing severe gastroenteritis. Although the overall incidence of *Yersinia* infections is lower than for *Shigella* and *Salmonella*, at one time it was the most common agent of diarrheal disease among African-American children [85].

Yersinia enterocolitica is the causative agent of a broad range of gastrointestinal syndromes, from self-limited enteritis to life-threatening systemic infection [86]. It's also an important cause of seasonal bacterial gastroenteritis among young children in urban communities

in the southeast United States where the infection rate is only lower than that of *Salmonella* spp. in infants under 12 months of age [87]. *Y. enterocolitica* enters the host via oral route and crosses the intestinal epithelial barrier through M cells [88]. Just like *Shigella* and *Salmonella*, *Yersinia* uses a type III secretion system (T3SS) to form a translocon pore in host cell membranes for delivering effector proteins into the cytoplasm of host cells which causes the blockage of phagocytosis by macrophages and results in macrophage death [52,89,90]. It is worth noting that the T3SS of *Y. enterocolitica* is identical to that of its close relative *Yersinia pestis*, the causative agent of plague which is probably the most dangerous and well known bioterror pathogens. It is likely that any vaccine effective against *Y. enterocolitica* will be effective against all *Yersinia* spp.

In addition to being potential candidates for bioterror weapons, *Shigella, Salmonella* and *Yersinia enterocolitica* are major public health problems that mostly affect infants and young children who are most vulnerable to the dehydration and growth defects associated with diarrheal diseases. Even without direct contact with contaminated water, children can still be infected by association with ill individuals via the fecal-oral route. Thus, development of vaccines against these pathogens is in urgent need. Vaccination is one of the most important public health tools for the prevention of infectious diseases, however, formulation of safe and effective vaccines for newborns and infants against infectious disease can be challenging. Subunit vaccines are usually safe but require a suitable adjuvant and delivery system to increase the efficacy. Dr. K. Leenhouts at Mucosis (http://www.mucosis.com/) has developed a novel technology using modified *Lactococcus lactis* cell wall particles as a platform for antigen delivery and referred to as Bacterium-Like Particles (BLPs), previously designated as Gram-positive Enhancer Matrix (GEM) [91,92]. *L. lactis* is a Gram positive, non-pathogenic lactic acid bacterium that is widely used in the production of dairy-based food products and generally regarded as safe (GRAS) entity [93]. *L. lactis* is one of the probiotics which have been shown to be safe for children and even newborns [94]. The BLPs are produced from fresh *L. lactis* bacteria that are harvested, boiled in

acid, and extensively washed with PBS. The DNA, RNA, lipids and almost all of the bacterial proteins are removed in this harsh treatment, but the intact peptidoglycan envelope still maintains structural integrity. The whole production process is simple and low cost, besides the final product is stable at room temperature. BLPs can be administered at mucosal sites, which is more "friendly" to infants when compared to needle injection. In addition to these excellent features, BLPs possess immune-stimulation properties conveyed by the peptidoglycan nature of the envelope that can activate the innate immune system through TLR2-mediated signaling [95,96].

As a delivery system, BLPs provide a scaffold for carrying multiple subunit antigens on their surface. To attach antigens to the BLP surface, the antigens need to be produced as fusions proteins containing a peptidoglycan anchoring (PA) domain that is also derived from *L. lactis*. The recombinant antigen-PA fusion proteins can non-covalently bind to BLPs but the association is extremely tight [97]. Because of the nature of the platform, single or multiple antigens can be displayed on a single BLP surface or BLPs carrying different antigens can be mixed, thus the BLPs can carry a wide variety of protein antigens from different pathogens. Pneumococcal, malaria and influenza proteins have been displayed on BLPs and investigated for the protective efficacy against their corresponding infections [98,99,100].

Like many other Gram-negative bacteria, *Shigella*, *Salmonella* and *Yersinia* all possess a common virulence mechanism, the TT3S, which is a syringe like structure that forms an energized conduit for the injection of effector proteins into host cells. Located at the needle tip is a "tip complex" that is involved in protein secretion control [4,52]. These include IpaD, SipD and LcrV for *Shigella*, *Salmonella* (from *Salmonella* pathogenicity island 1 or SPI-1) and *Yersinia*, respectively [101,102,103]. Upon contact with a host cell membrane, these T3SS deliver the first translocator protein which is also located at the needle tip for the formation of the translocon pore which allows later passage of effector proteins into the host cell cytoplasm. These proteins are IpaB, SipB and YopB for *Shigella, Salmonella* and *Yersinia*, respectively. These T3SS proteins

are attractive targets for inclusion in a protective vaccine due to their surface exposure and their essential roles in virulence. IpaD and IpaB have been found to protect against *Shigella* infection using the mouse pulmonary lethal infection model when administered intranasally with an appropriate adjuvant [37]. The T3SS of *Shigella* and *Salmonella SPI-1* are closely related, suggesting that SipD and SipB are also potential vaccine candidates. Although a little more distantly related, LcrV and YopB of *Yersinia enterocolitica* are functional homologs and thus are potential vaccine candidates. More importantly, since the tip proteins and first translocator proteins are very highly conserved at the sequence level within a given genus, they have the potential to be broad spectrum vaccine candidates capable of providing serotype-independent protection with, for example, the expansive genus *Salmonella*. Thus, this study will explore whether these T3SS proteins can be attached to the bacterium-like particles and then formulated to become T3SS protein-BLPs vaccines for later testing in animal models of infection against multiple category B agents.

As protein based vaccines, the major concern regarding formulation is stability in aqueous solution during storage and transport. Temperature and pH are the dominant factors that affect protein stability. The naked BLPs are stable even at room temperature, but for the BLPs with associated proteins, formulation becomes something to be concerned about. Therefore, a variety of biophysical techniques are used here to characterize the stability as a function of pH and temperature. The main techniques used here are Circular Dichroism (CD), intrinsic fluorescence and static light scattering spectroscopies. These multiple methods give rise to rather large amounts of data, so the findings generated here are summarized in a three-index empirical phase diagram (EPD). Furthermore, to better understand the effect of binding of PA fusion proteins to BLPs, we compared the biophysical studies of T3SS proteins alone, fused with the PA domain, and the fusion after attachment to BLPs. The PA domain was added at the C terminus of each tip protein, but this strategy led to poor expression and stability for the translocator proteins.

Thus, the translocator proteins have the PA domain attached at their N termini. Furthermore, IpaB, SipB and YopB are hydrophobic proteins and need to be co-expressed with their specific chaperones IpgC, SicA and SycD, respectively. This also applies for expression of PA-IpaB, PA-SipB and PA-YopB. Then the chaperones were removed with the mild detergent LDAO which is also needed to maintain the solubility of the resulting individual translocator proteins. Thus for the characterization of the translocator proteins, the PA-fusions and PA-fusions associated with BLPs, 0.05% LDAO was present at all times.

Results

Biophysical characterization summary of IpaD, SipD and LcrV

Biophysical characterization of the tip proteins described here has been previously published [104,105], however, due to improvements in the purification scheme used to prepare them, it was necessary to repeat some of this work to be able to accurately compare the effects of fusing the PA moiety to them. Furthermore, use of the new three-index EPD allows for direct comparisons of properties between different proteins, which also necessitated redoing several of these biophysical measurements. For IpaD, SipD and LcrV the far-UV CD spectroscopy revealed double minima at 208 and 222 nm in their spectra regardless of pH, indicating dominant α-helical content in all cases (Figs. 5.1A, 5.2A and 5.3A respectively). The spectra for each protein are similar at pH values with relatively minor differences except for the LcrV at pH 5 which is dramatically altered and suggests partially unfolding at pH 5. The thermal stability of each protein's secondary structure was determined by monitoring the CD signal as molar ellipticity at 222 nm as a function of increasing temperature (Fig 5.1-5.3B respectively). An increase in signal indicated a loss of α-helical structure due to unfolding of the protein. At neutral pH conditions (especially pH 7 and 8), all three proteins maintained strong α-helical secondary structure until

~50 °C and significant unfolding was observed above 75 °C. IpaD and SipD behaved quite similarly in that there was a slight reduction in stability at pH which became much more prominent at pH 4 and 3. For LcrV there is a slight reduction in the transition of unfolding at pH since and a greater reduction at pH 5 and 4. Interestingly, LcrV at pH3 appeared to retained its structure until 80 °C. The reason for this latter observation is unclear, but it does appear that secondary structure stability is maximum in neutral pH conditions where the proteins tend to be quite stable.

Tip protein tertiary structure was monitored by following intrinsic fluorescence peak position as a function of pH and temperature (Figs. 5.1C, 5.2C and 5.3C). As with secondary structure, all the proteins appear to lose stability at low pH values. For IpaD and SipD, which behaved similarly to each other, the initial red shift in peak position occurs somewhat earlier than the initial signal change at seen in CD measurements, however, both proteins show an increase in peak position wavelength (a red shift) as the temperature is increased, suggesting exposure of the buried Trp residues to the aqueous environment as the temperature increases. At pH 5, 4 and 3, there is an increasing loss of thermal stability for IpaD and SipD with the greatest loss of stability seen at pH 3. At these lower pH values, the noise seen in the signal at higher temperatures is probably due to aggregation events.

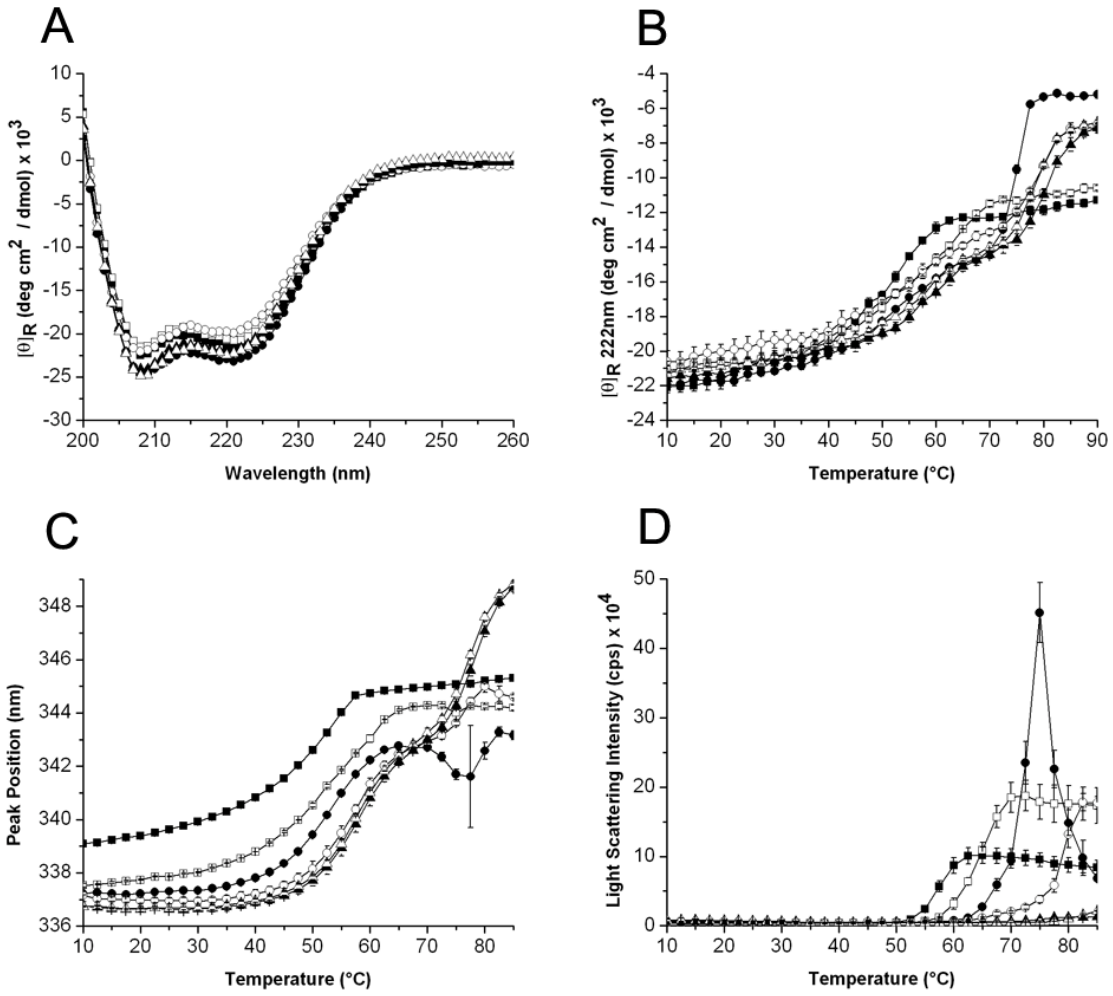

Figure 5.1 : Biophysical characterization of IpaD. Far-UV Circular Dichroism (CD) spectra of IpaD, recorded at different pH conditions (A). Far-UV CD molar ellipticity at 222 nm monitored as a function of temperature from 10 to 90 ˚C (B). Intrinsic Trp fluorescence peak position wavelength (C) and light scattering intensity monitored at 295 nm (D) as a function of temperature from 10 to 85 ˚C. Error bars represent standard deviation from three different experiments. Symbols: pH 3 (■), pH 4 (□), pH 5 (●), pH 6 (○), pH 7 (▲),pH 8 (Δ).

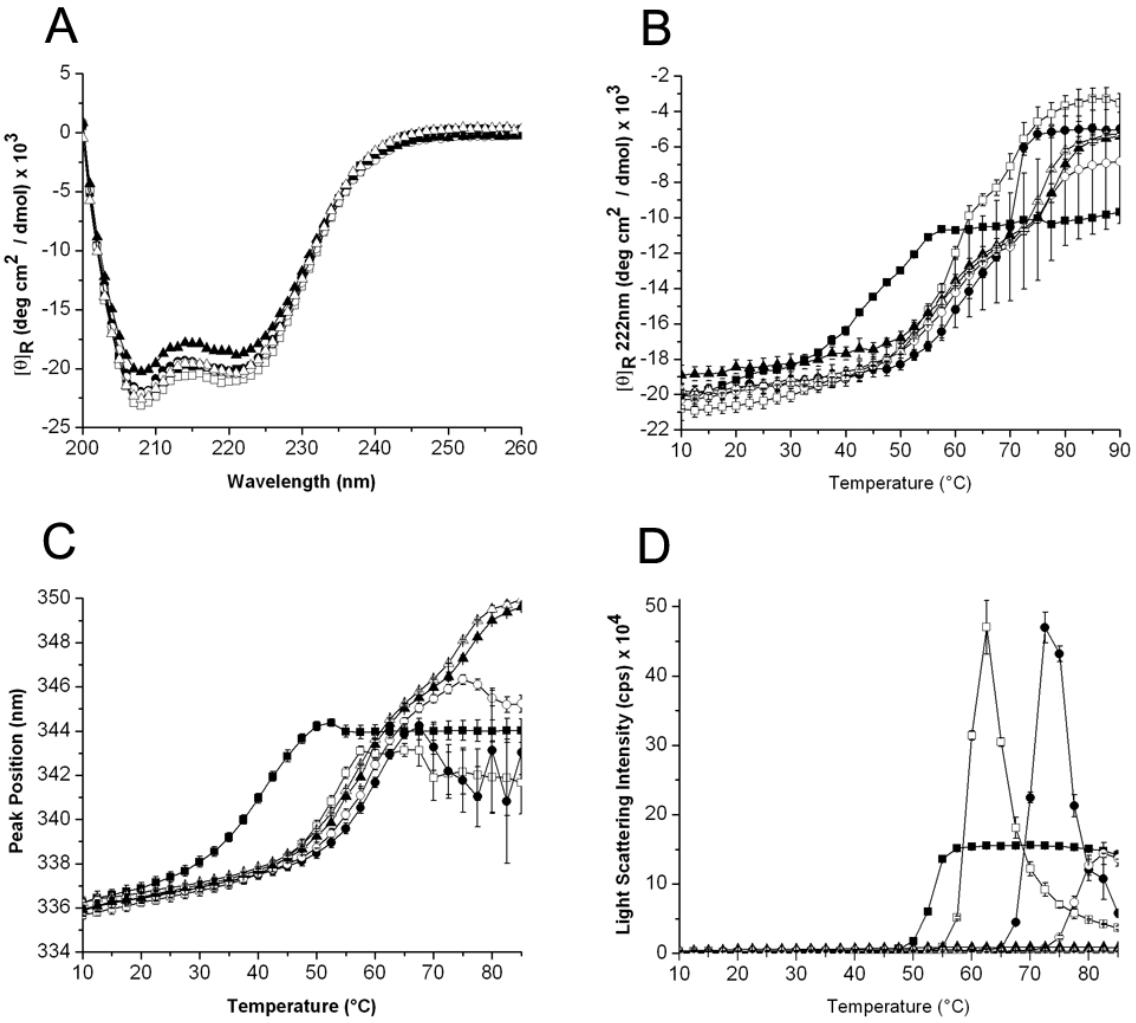

Figure 5.2 : Biophysical characterization of SipD. Far-UV Circular Dichroism (CD) spectra of SipD, recorded at different pH conditions (A). Far-UV CD molar ellipticity at 222 nm monitored as a function of temperature from 10 to 90 ˚C (B). Intrinsic Trp fluorescence peak position wavelength (C), and light scattering intensity monitored at 295 nm (D) as a function of temperature from 10 to 85 ˚C. Error bars represent standard deviation from three different experiments. Symbols: pH 3 (■), pH 4 (□), pH 5 (●), pH 6 (○), pH 7 (▲),pH 8 (Δ).

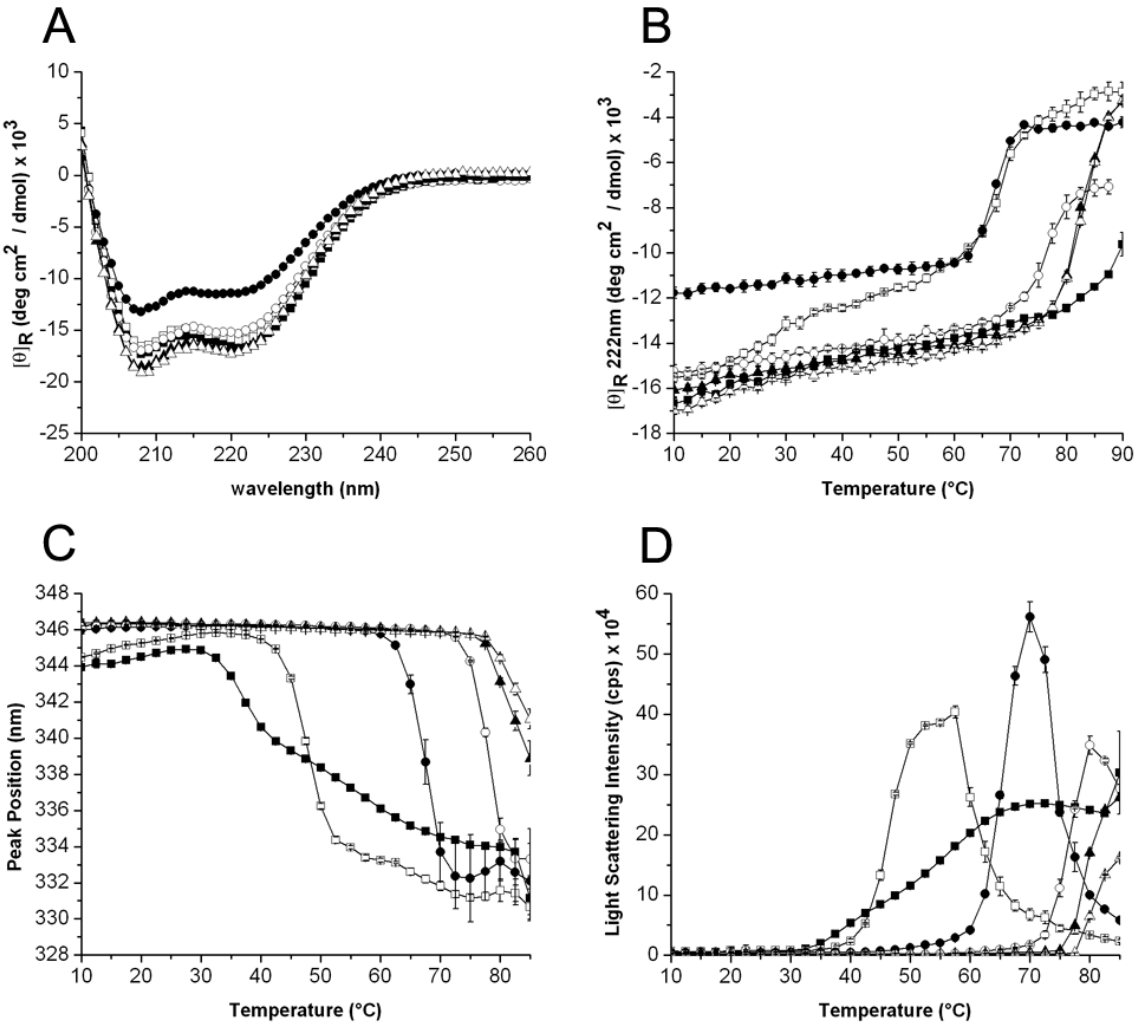

Figure 5.3 : Biophysical characterization of LcrV. Far-UV Circular Dichroism (CD) spectra of LcrV, recorded at different pH conditions (A). Far-UV CD molar ellipticity at 222 nm monitored as a function of temperature from 10 to 90 ˚C (B). Intrinsic Trp fluorescence peak position wavelength (C) and light scattering intensity monitored at 295 nm (D) as a function of temperature from 10 to 85 ˚C. Error bars represent standard deviation from three different experiments. Symbols: pH 3 (■), pH 4 (□), pH 5 (●), pH 6 (○), pH 7 (▲), pH 8 (Δ).

The tertiary structure of LcrV is very stable at neutral pHs with the transition temperature then decreasing as the pH is lowered. Compared to IpaD and SipD, LcrV maintains its tertiary structure well and almost no red shift is observed before it undergoes a blue shift which is probably caused by aggregation and the trapping of Trp residues within the hycrophobic core of the resulting aggregates. It's noteworthy that LcrV at pH 3 starts its thermal destabilization at around 40 °C although it maintains its secondary structure until higher temperatures. This could be due to initial formation of soluble aggregates that maintain secondary structure content while collapsing around the core Trp residues.

Static light scattering was used to explore aggregation of IpaD, SipD and LcrV as a function of pH and temperature (Figs. 5.1D, 5.2D and 5.3D, respectively). Aggregation is probably the most difficult property to overcome in the storage of proteins in solution and it can occur by factors including protein unfolding, chemical degradation and by simple time-dependent protein-protein interactions. Based on light scattering, IpaD and SipD once again tend to behave similarly. Both proteins show good stabilitiy at netural pH are fairly stable at pH 6. A substantial reduction in stability as monitored by protein aggregation was observed at pH 5, 4 and 3. At these more acidic pH values, the loss of signal at higher temperatures is due to the formation of visible precipitates that fall out of solution. For LcrV, a similar trend is observed, but it seems to be a bit more exaggerated relative to what is seen for the other two tip proteins.

The biophysical data accumulated in the above experiments set were summarized using a three-index EPD. In these updated versions of the EPD model of data presentation, each parameter (secondary structure, tertiary structure and quaternary structure/aggregation) is assigned a specific color which allows for determination of the factor that most greatly influences each protein's overall stability and it allows for comparison of the summarized data between proteins. Three predominant regions were defined for IpaD (Fig. 5.4 A). Region 1 is yellow and it represents IpaD's native state over the entire pH range and under 45-55 °C.

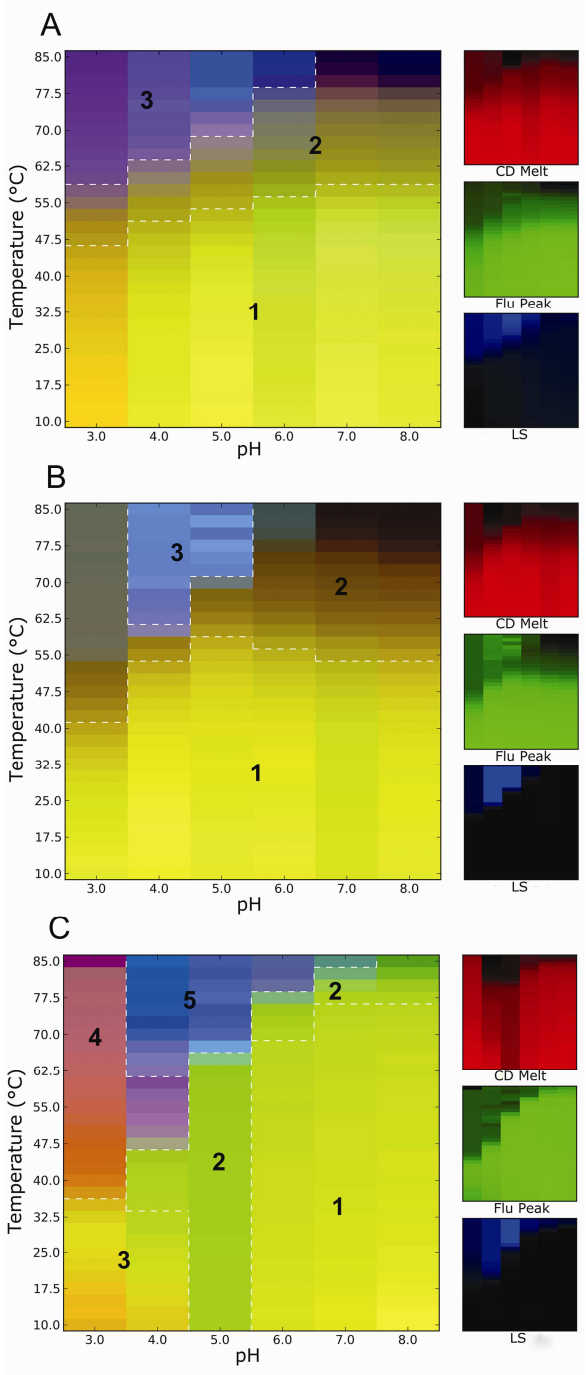

Figure 5.4 : Three-index empirical phase diagrams (EPDs) for IpaD (A), SipD (B) and LcrV (C), representing the conformational stability of the tip proteins as a function of pH and temperature. The red, green and blue panels at the right define individual component indices for secondary structure (CD), tertiary structure (fluorescence peak position) and aggregation behavior (LS), respectively.

IpaD is most stable over this relative large range of parameters. Region 2 represents a structurally altered state mostly caused by the loss of protein secondary and tertiary structure and it seems to almost overlay with the red and green at the right in Fig. 5.4A. Region 3 is mainly an aggregated (denatured) state for IpaD from pH 3 to 6 and above 60°C. Overall, IpaD is most stable at lower temperature at all pH values examined. It takes both an acidic environment and high temperature to grossly perturb IpaD structure and this disruption seems to be irreversible due to aggregation.

The EPD for SipD seems rather similar in pattern to that of IpaD (Fig. 5.4B). Region 1 again represents the native state at all pH values with slightly better thermostability at pH 4 and 5 relative to IpaD. Region 2 is once again an altered structural state with minimal aggregation caused by the thermal unfolding. Significant aggregation activity attributed to the blue color in region 3 at pH 4 and 5. It is worth noting that a gray color was observed at pH 3 over 40 °C due to partial loss of secondary and tertiary structure, but with less aggregation compared to pH 4, 5 and 6. This is another feature that differentiates SipD from IpaD.

For LcrV, the EPD was more complicated and divided into 5 regions (Fig. 5.4C). Like in the other cases, region 1 describes the native conformational state at neutral environment and up to ~ 75 °C. Region 2 represented a transition state or partially unfolded state that appears at high temperature at near neutral pH and at lower temperatures at around pH 5. It was stated above, LcrV behaved oddly at pH 5 with regard to secondary structure and that likely contributes to the split pattern seen for region 2. Region 3 is close to region 1 with regard to overall color, but it may differ slightly due to there being a slight alteration in tertiary structure as appeared as a red shift in the fluorescence peak position (Fig. 5.4C, green color in panel at right). At pH 3 LcrV maintained its secondary structure well while losing some of its tertiary and quarternary structure pretty quickly as the temperature increased. This phenomenon is reflected on region 4 on the composite EPD map. Region 5 represents the completely aggregated/denatured state of LcrV. To summarize, IpaD and SipD EPDs demonstrate similar patterns to indicate similar behavior for

these two T3SS tip proteins while LcrV possesses greater stability under neutral pH conditions with much lower structural integrity in acidic environments.

Biophysical characterization summary of IpaD-PA, SipD-PA and LcrV-PA

Before being able to ascertain the influence that binding to BLPs has on the T3SS tip proteins IpaD, SipD and LcrV, the proteins had to be prepared as fusion proteins the a peptidoglycan anchor (PA) domain prepared from a cell wall repair enzyme from *L. lactis*. It was thus, also important to determine the influence that fusion with the PA had on the biophysical properties of these tip proteins. Far-UV CD spectroscopy was used to measure the secondary structure content of IpaD-PA, SipD-PA and LcrV-PA (Figs. 5.5A, 5.6A and 5.7 A, respectively). Double minima at 208 and 222 nm were observed with the minimum at 208 nm being more intense than the one at 222 nm, suggesting that there was conservation of α-helical secondary structure within the tip proteins, however, fusion with the PA domain did appear to introduce more random coil into the final secondary structure content of the proteins. To monitor retention of α-helical structure as a function of temperature, CD spectroscopy was used and the molar ellipticity at 222 nm was monitored.

For IpaD-PA, the molar ellipticity gradually decreased at each pH with increasing thermal stress (Fig 5.5B), suggesting partial unfolding in response to temperature, however, there was no major and clear cut transition as seen for IpaD alone (see Fig. 5.1B). A similar pattern was observed for SipD-PA except at pH 5 and 6 where a complete unfolding transition was seen at 75 °C (Fig. 5.6 B). This may suggest that these two proteins tend to retain secondary structure content well in response to elevated temperature except for SipD at pH 3 and 4. The effect of fusing PA to LcrV was interesting in that insoluble aggregates formed during dialysis into CP

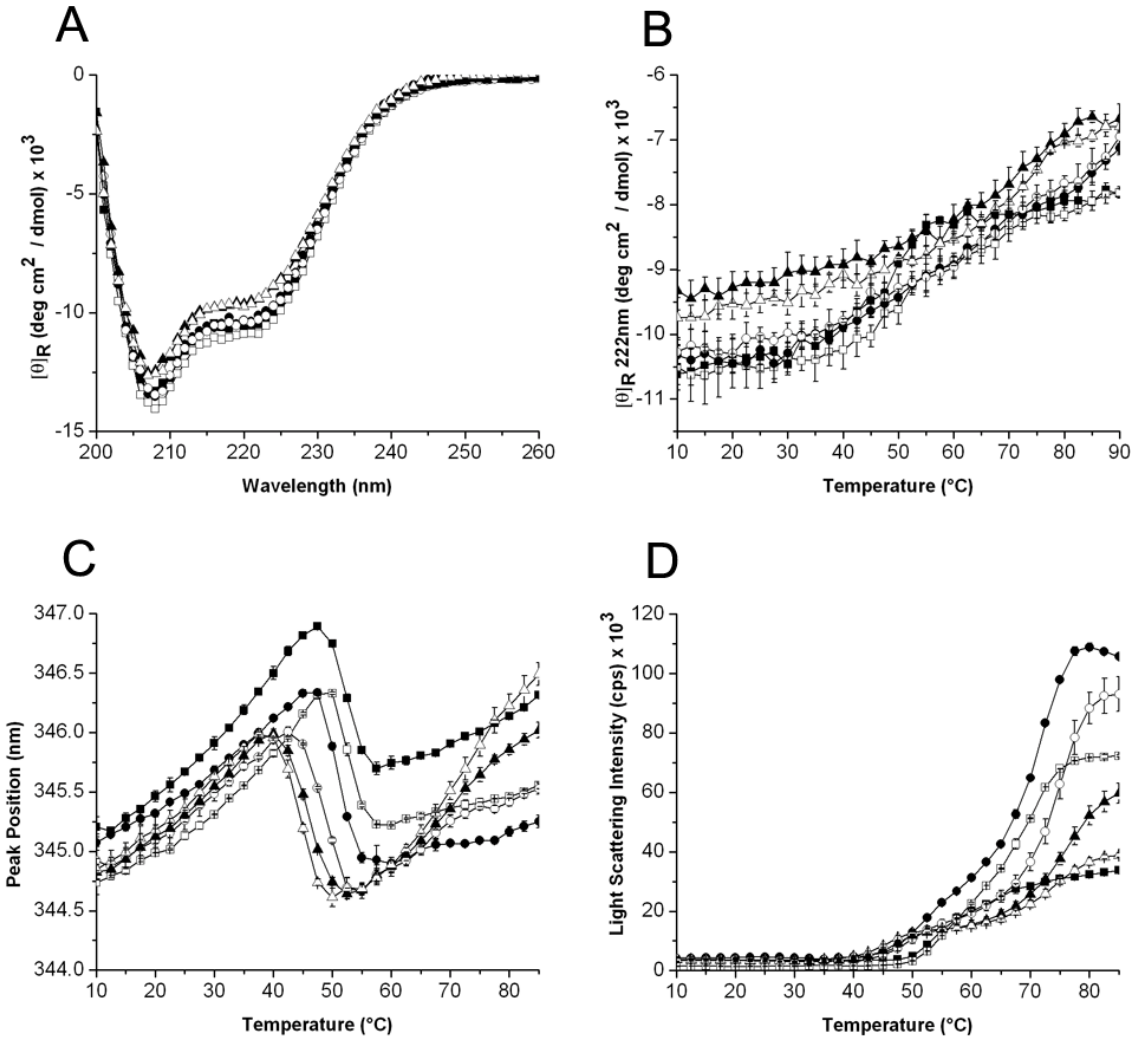

Figure 5. 5: Biophysical characterization data for IpaD-PA. Far-UV Circular Dichroism (CD) spectra of IpaD-PA, recorded at different pH conditions (A). Far-UV CD molar ellipticity at 222 nm monitored as a function of temperature from 10 to 90 ˚C (B). Intrinsic Trp fluorescence peak position wavelength (C) and light scattering intensity monitored at 295 nm (D) as a function of temperature from 10 to 85 ˚C. Error bars represent standard deviation from three different experiments. Symbols: pH 3 (■), pH 4 (□), pH 5 (●), pH 6 (○), pH 7 (▲),pH 8 (Δ).

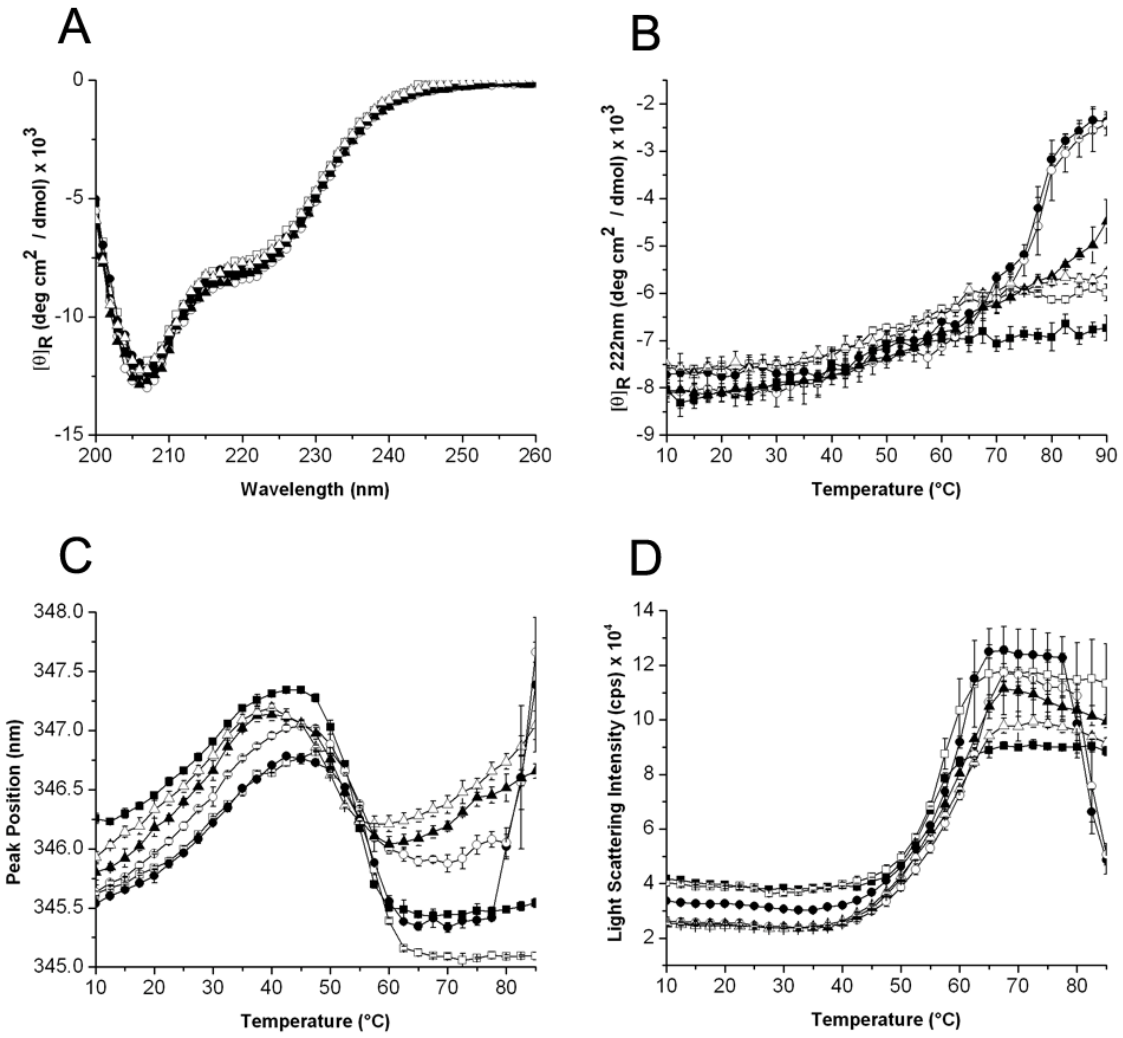

Figure 5.6 : Biophysical characterization data for SipD-PA. Far-UV Circular Dichroism (CD) spectra of SipD-PA, recorded at different pH conditions (A). Far-UV CD molar ellipticity at 222 nm monitored as a function of temperature from 10 to 90 ˚C (B). Intrinsic Trp fluorescence peak position wavelength (C) and light scattering intensity monitored at 295 nm (D) as a function of temperature from 10 to 85 ˚C. Error bars represent standard deviation from three different experiments. Symbols: pH 3 (■), pH 4 (□), pH 5 (●), pH 6 (○), pH 7 (▲),pH 8 (Δ).

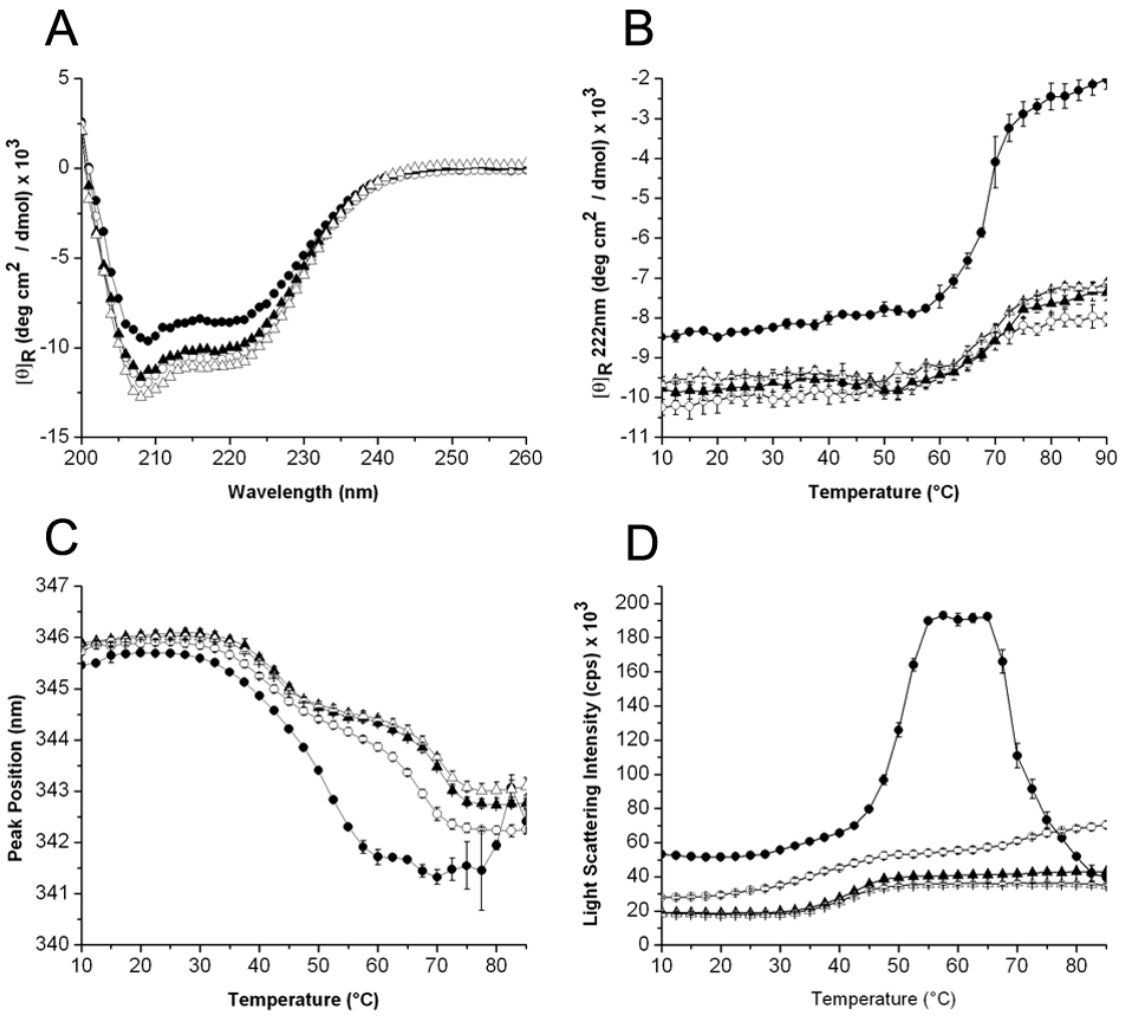

Figure 5.7 : Biophysical characterization data for LcrV-PA. Far-UV Circular Dichroism (CD) spectra of LcrV-PA, recorded at different pH conditions (A). Far-UV CD molar ellipticity at 222 nm monitored as a function of temperature from 10 to 90 ˚C (B). Intrinsic Trp fluorescence peak position wavelength (C) and light scattering intensity monitored at 295 nm (D) as a function of temperature from 10 to 85 ˚C. Error bars represent standard deviation from three different experiments. Symbols: pH 5 (●), pH 6 (○), pH 7 (▲), pH 8 (Δ).

buffer at pH 3 and 4. Thus, biophysical data for LcrV-PA were only collected at pH 5 through 8 (Fig,. 5.7B). From pH 6 to 8, only minor changes in secondary content were seen for LcrV-PA until ~65 °C, however, at pH 5 the LcrV-PA had reduced α-helical signal even at 10 ^{o}C and then completely unfolded after 70 °C.

The tertiary structure stability of IpaD-PA and SipD-PA, as determined by fluorescence peak position, appears to be similar to though maybe slightly less stable than each tip protein without the PA addition (Fig. 5.6C). A large blue shift (to a lower wavelength) was observed at ~45-50 °C regardless of the pH with the degree of shift being greater at pH 3 (Fig. 5.5C and 5.6C, respectively). The pattern once the transition started was different than for these two proteins alone, however, this is likely due to the state of the protein once the major portion of the tertiary structure is lost. Fusion with the PA also decreases the stability of LcrV, however, instead of remaining steady and then undergoing a major blue shift, a unique double transition scheme was observed at neutral pH while a completely loss of tertiary structure was seen above 50 ˚C at pH 5 (Fig. 5.7C).

As before, static light scattering was used to monitor the aggregation of the tip-PA protein fusions (Figs. 5.5D, 5.6D and 5.7D). Minor aggregation was observed for IpaD-PA at pH values of 3, 7 and 8 as thermal stress was applied, however, much greater aggregation was seen at pH 4, 5 and 6 as the temperature was increased. The data seem to suggest greater resistance to aggregation at the pH extremes, but not between. SipD-PA started to aggregate at around 45 ˚C and showed a midpoint of transition at around 55 ^{o}C regardless of pH (Fig. 5.6D). LcrV-PA seems to resist aggregation induced by thermal stress at pH values from pH 6 to 8 but completely early on at pH 5. Further reduction in the pH resulted in LcrV precipitation even before analyses could be performed, as mentioned above.

As was done for the tip proteins alone, the biophysical data were viewed as a whole using empirical phase diagrams. The EPD for IpaD-PA was divided into three regions that were loosely similar to the regions seen for IpaD alone, but with the overall appearance that the PA domain reduces overall stability (Fig 5.8A). Region 1 (yellow color) depicts the native state of the fusion protein with minor color differences occurring at high pH due to the minor loss of secondary structure at lower temperatures. Region 2 represents a transition into a mildly altered conformational state that results from thermal stress with minor aggregation activity. Region 3 then represented a major loss of structural integrity that is largely characterized by aggregation. For SipD-PA, only two regions were defined (Fig. 5.8B) mostly depend on the thermal increase. Under ~55 ˚C was the native state as defined by region 1 with the most stable state being observed at pH 6 and 7 according to the color scheme. Region 2 was mainly a denatured state where loss of tertiary structure and aggregation dominated. The EPD for LcrV-PA was once again quite complicated and differentiated into six regions based upon the cluster analysis (Fig. 5.8C). The native state defined by region 1 was at neutral pH under 40 ˚C. Region 2 and 3 most likely represent different forms of the molten globular and partially unfolded states, respectively. Region 4 was defined based on the decrease of secondary structure at pH 5. Region 5 and 6 were differentiated from each other because partial secondary structure was still maintained at in region 5 relative to region 6 where there is complete denaturation. The structure trends in this EPD with regard to pH would appear to provide a clue as to why no data could be obtained at low pH with aggregation becoming the dominant factor as pH is lowered.

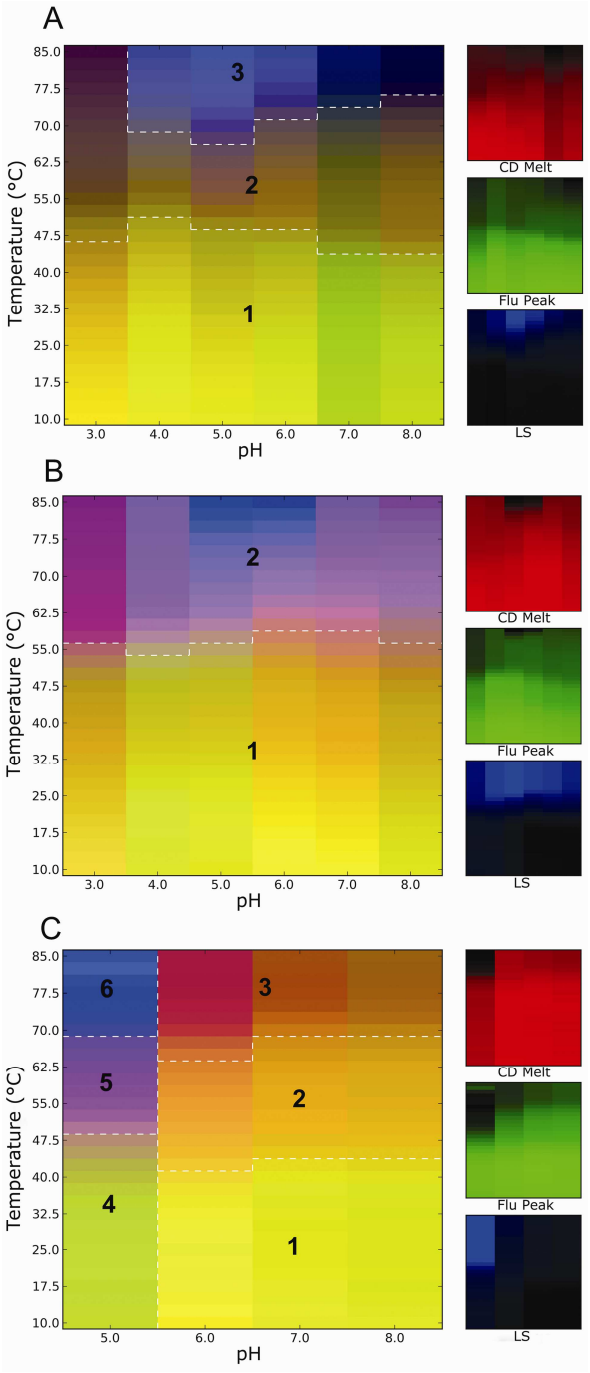

Figure 5. 8 : Three-index empirical phase diagrams (EPDs) for IpaD-PA (A), SipD-PA (B) and LcrV-PA (C), representing the conformational stability of the proteins as a function of pH and temperature. The red, green and blue panels at the right define individual component indices for secondary structure (CD), tertiary structure (fluorescence peak position) and aggregation behavior (LS), respectively

Biophysical characterization summary of IpaD-BLP, SipD-BLP and LcrV-BLP

The biophysical techniques used here tend to become complicated when trying to characterize proteins attached to bacterium-like particles (BLPs) because the BLPs tend to dominate the majority of the spectroscopic signals and create a great deal of noise in the signal. Nevertheless, we can still obtain stability information of the tip-BLPs as a whole using these methods. In some cases, other difficulties arise such as the degradation that is observed when IpaD-BLPs and SipD-BLPs were transferred into pH 3 buffer. In these cases, no biophysical data were collected and such data are omitted from this study. The far-UV CD spectra at 10 ˚C for all the tip-BLPs showed a single minimum at ~ 225 nm (Figs. 5.9A, 5.10A and 5.11 A). Such a phenomenon was previously seen in the characterization of a live, attenuated *Salmonella* in a vaccine formulation [106]. As a general trend, signals at neutral pH for the protein-BLPs are more intense than that at acidic pH. A decrease in CD signal intensity was observed at pH 4 to 6, but not at pH 7 and 8 except for SipD-BLP at pH 7 (Figs. 5.9B, 5.10B and 5.11 B). Clearly tip protein-BLPs prefer higher pH values to maintain their overall secondary structure integrity.

When tertiary structure was examined, the fluorescence peak position for IpaD-BLPs showed a maintenance of wavelength at pH 7 and 8 in response to thermal stress while there was a graduate but substantial blue shift in response to increasing temperature that could be attributed to aggregative events at pH 4 to 6 (Fig. 5.9C). Although the pattern differed, increased stability for SipD-BLPs also appears to occur at pH 7 and 8 (Fig. 5.10C). This same trend seems to occur for LcrV-BLPs with the neutral pH data sets also having much less noise, suggesting they are more stable than below pH 7 (Fig. 5.11C).

With regard to aggregation as determined by static light scattering, similar stability trends were observed with LcrV showing marginal stability relative to IpaD and SipD once attached to the BLPs (Figs. 5.9D, 5.10D and 5.11D). Under all of the pH conditions used, IpaD maintains a relatively steady level of light scattering though it begins to drop at relatively low temperatures at

pH 4, 7 and 8 (Fig. 5.9D). It should be noted that in these plots of light scattering versus temperature, the graduate decrease that is seen is probably due to the large BLP particles falling out of solution. On the other hand, while increased light scattering is probably due to aggregation, a rapid drop in scattering is most likely due to large aggregates rapidly settling out of solution. It should be noted that the contribution from small soluble proteins (even in soluble aggregate form) would not be expected to contribute here due to the dominant nature of the large BLP particles. Thus, IpaD appears initially to be more stable to gross aggregation at all pH values with minor aggregation occurring at pH 5 and 6 with some aggregation pH 4. It should be noted that the large error bars seen from pH 4 to 6 are probably caused by the distribution of aggregates as larger particles begin to rapidly settle out of solution. At about 65 ^{o}C, the IpaD-BLPs then rapidly fall out of solution indicating major aggregative events. The gradual decrease in light scattering at pH 7 and 8 may suggest little true aggregation is occurring here.

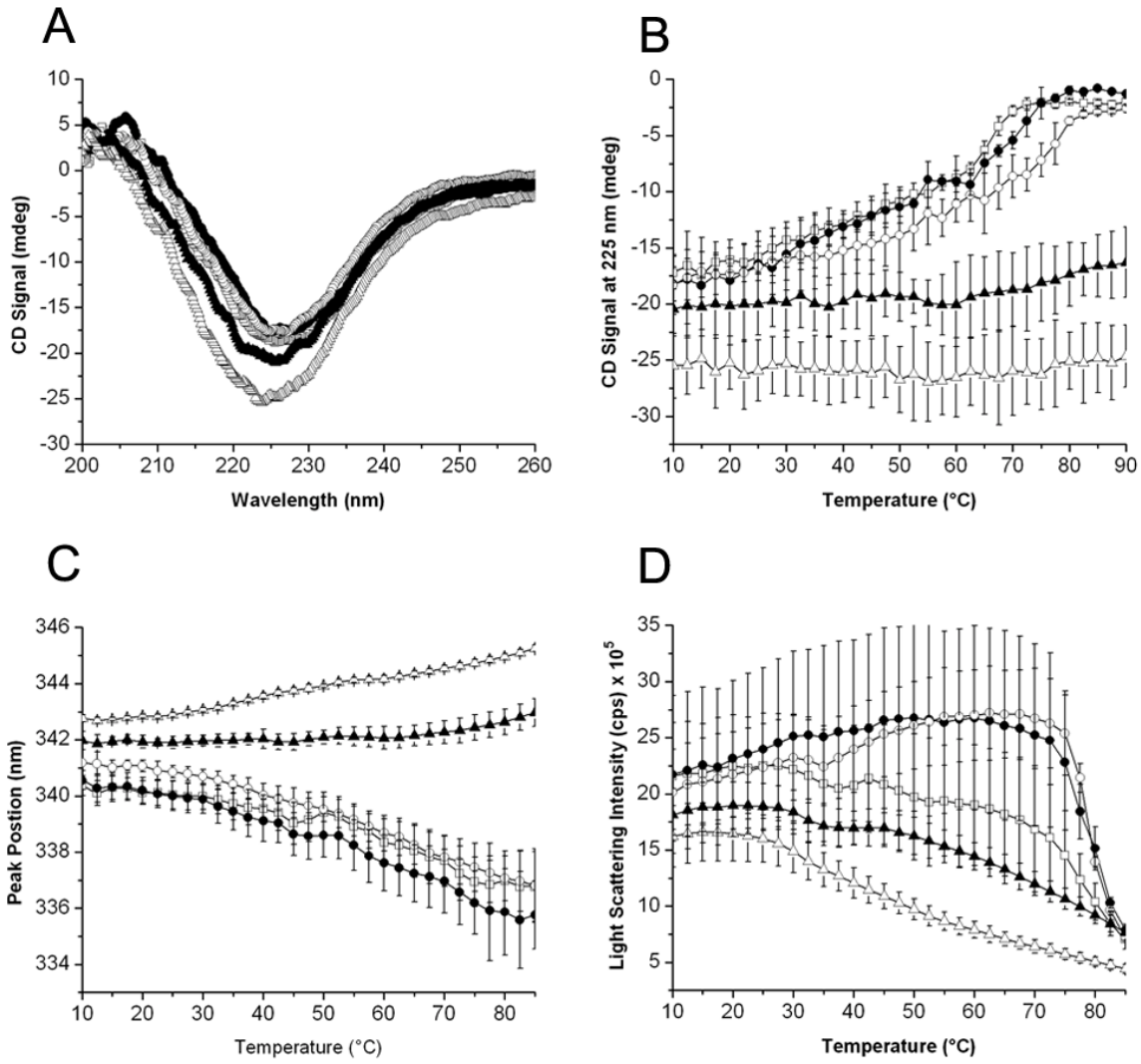

Figure 5. 9 : Biophysical characterization data for IpaD-BLPs. Far-UV Circular Dichroism (CD) spectra of IpaD-BLPs, recorded at different pH conditions (A). Far-UV CD signal at 225 nm monitored as a function of temperature from 10 to 90 ˚C (B). Intrinsic Trp fluorescence peak position wavelength (C) and light scattering intensity monitored at 295 nm (D) as a function of temperature from 10 to 85 ˚C. Error bars represent standard deviation from three different experiments. Symbols: pH 4 (□), pH 5 (●), pH 6 (○), pH 7 (▲),pH 8 (Δ).

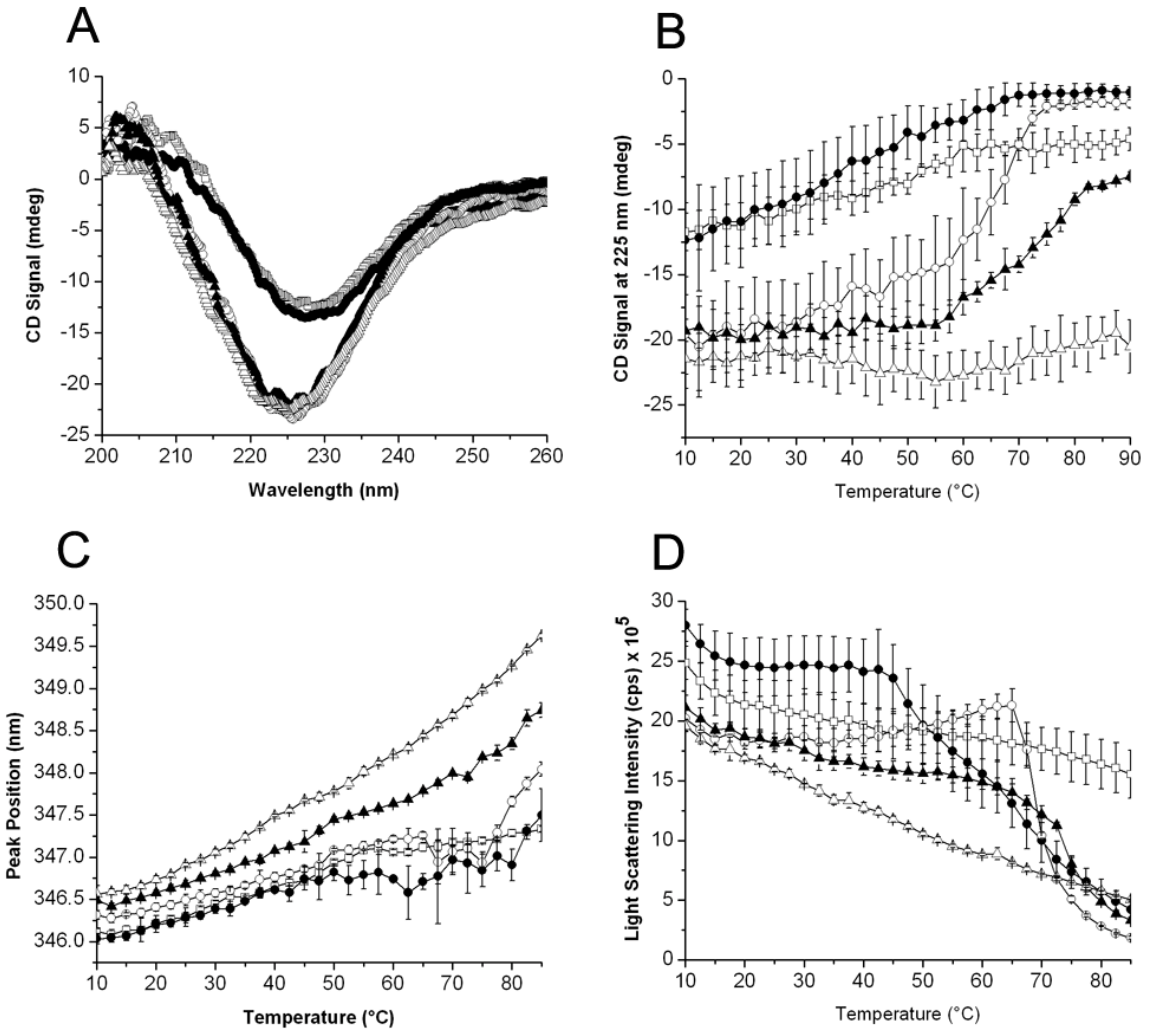

Figure 5. 10: Biophysical characterization data for SipD-BLPs. Far-UV Circular Dichroism (CD) spectra of SipD-BLPs, recorded at different pH conditions (A). Far-UV CD signal at 225 nm monitored as a function of temperature from 10 to 90 ˚C (B). Intrinsic Trp fluorescence peak position wavelength (C) and light scattering intensity monitored at 295 nm (D) as a function of temperature from 10 to 85 ˚C. Error bars represent standard deviation from three different experiments. Symbols: pH 4 (□), pH 5 (●), pH 6 (○), pH 7 (▲), pH 8 (Δ).

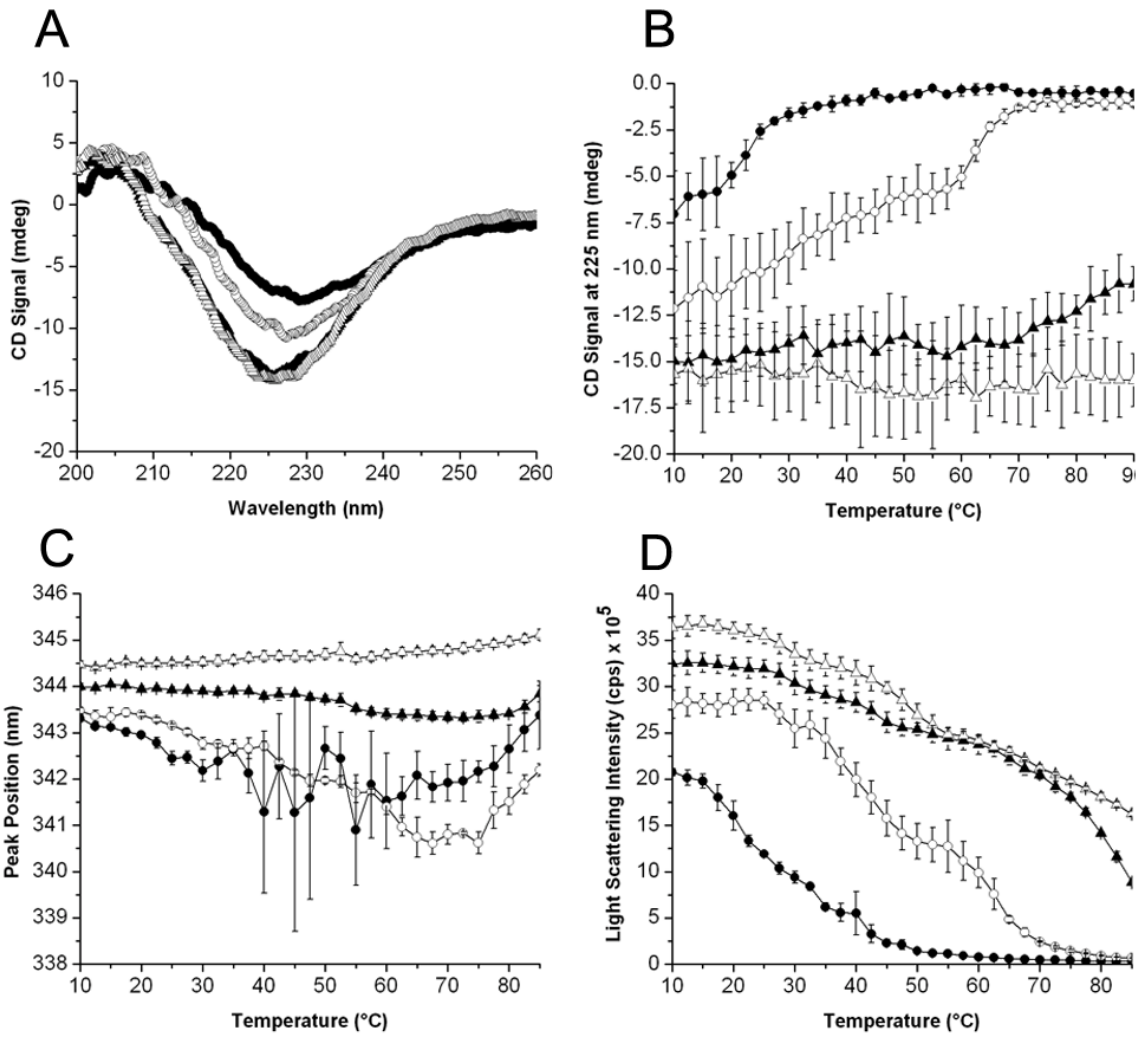

Figure 5. 11: Biophysical characterization data for LcrV-BLPs. Far-UV Circular Dichroism (CD) spectra of LcrV-BLPs, recorded at different pH conditions (A). Far-UV CD signal at 225 nm monitored as a function of temperature from 10 to 90 ˚C (B). Intrinsic Trp fluorescence peak position wavelength (C) and light scattering intensity monitored at 295 nm (D) as a function of temperature from 10 to 85 ˚C. Error bars represent standard deviation from three different experiments. Symbols: pH 5 (●), pH 6 (○), pH 7 (▲),pH 8 (Δ).

In a somewhat similar manner, SipD-BLPs tend to show an early but slight decrease in light scattering suggesting there little aggregation in all cases. This is followed by an increase in light scattering at pH 5, and 6 as would occur with mild aggregation. At pH 7 and 8, the SipD-BLPs show a graduate and steady drop in light scattering from the start and continuing until the end suggesting there is little gross aggregation at these pH values (Fig. 5.10D). At pH 4 there is also a rather gradual decrease in light scattering suggesting perhaps less aggregation occurring here relative to all the other pH conditions. Interestingly, at pH 6 (and to a lesser extent at pH 5), the SipD-BLPs start to show a gradual increase in scattering (after the initial drop) and then they rapidly fall out of solution at about 70 ^{o}C (45 ^{o}C for pH 5), perhaps due to slowly accumulating aggregation until a complete collapse occurs as large aggregates form. As for the LcrV-BLPs, the light scattering continually decreases throughout the experiment for all the pH values tested but the aggregation appears to be greatest at pH 5 which appears to be consistent with what was observed for tertiary structure (Fig. 5.11D and C, respectively). The trend for the LcrV-BLPs is that as acidity increases, stability decreases.

The association of the proteins to the BLPs ended up making the EPDs more complex than for the proteins alone. The EPD for IpaD-BLPs was divided computationally into three regions (Fig. 5.12A). Region 1 is the most stable state which is limited to pH 7 and 8, regardless of temperature. This was largely dictated by secondary structure and aggregation status though at higher temperatures at pH 7, tertiary structure begins to have an influence (see panels at right). Region 2 is a relatively less stable with a lower CD signal and transition at 65 $^{\circ}$C. Settling of the tip-BLPs caused by protein aggregation is largely responsible for region 3. The EPD of SipD-BLP is divided into 4 regions with region 1 defined as the most favorable state at relatively low temperatures under mostly neutral pH conditions (Fig. 5.12B). Region 2 was identified as less stable region due to the low CD signal. Higher temperatures at pH 8 gave rise to region 3 which represents a structurally altered state based on the loss of tertiary structure. Finally, region 4

represents the settling of protein-BLP complexes out of solution due to substantial protein aggregation. Meanwhile, the most stable region (region 1) for LcrV-BLPs was at pH 7 and 8 under ~50 ˚C (Fig. 5.12C). Regions 2 and 3 represent a partially unfolded state due to loss of secondary structure caused by thermal stress or pH stress, respectively. Region 4 is observed at higher temperatures under neutral pH conditions and it corresponds to a relatively low level of aggregation while region 5 results from significant aggregation that leads to clumping. In general, the tip protein-BLP complexes prefer neutral environment and relatively low temperatures.

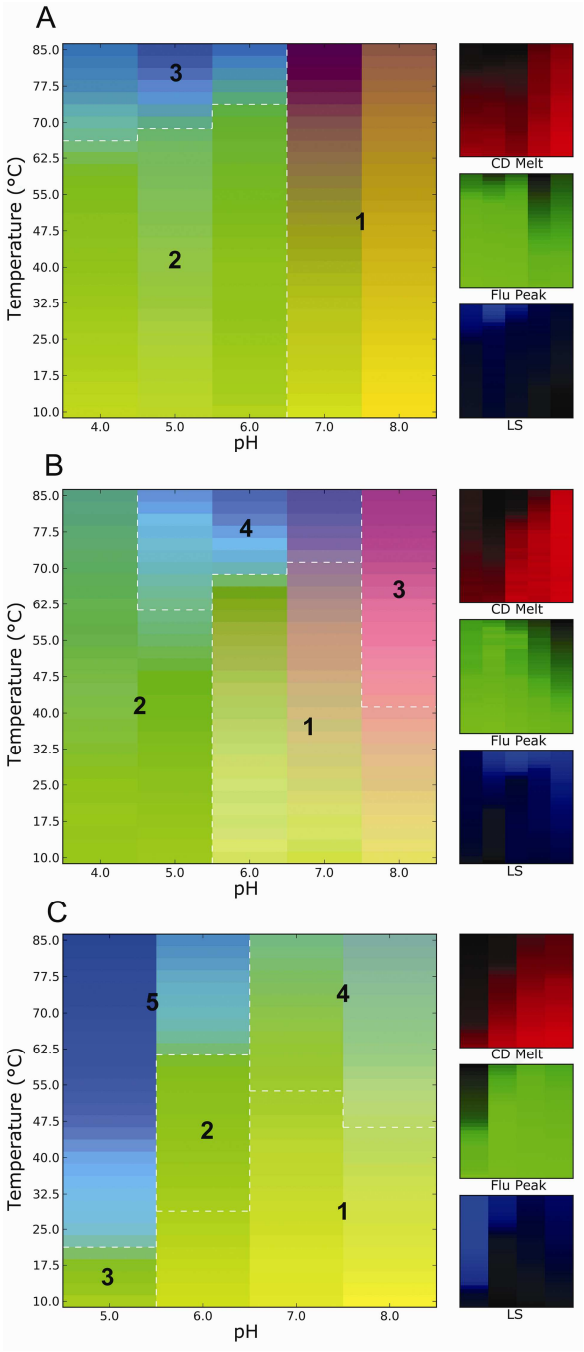

Figure 5. 12: Three-index empirical phase diagrams (EPDs) for IpaD-BLPs (A), SipD-BLPs (B) and LcrV-BLPs (C), representing the conformational stability of the tip proteins attached to the BLPs as a function of pH and temperature. The red, green and blue panels at the right define individual component indices for secondary structure (CD), tertiary structure (fluorescence peak position) and aggregation behavior (LS), respectively.

Biophysical characterization summary of IpaB, SipB and YopB

The translocator proteins IpaB, SipB and YopB need to be co-expressed with their chaperones which are removed with detergent LDAO (or a suitable alternative mild detergent). In this case, the biophysical characterization of these proteins was all conducted with the presence of LDAO. For IpaB and SipB, minor chemical degradation was seen at pH 3, which became even more obvious for PA-IpaB and PA-SipB. Thus, to reduce the complexity and focus on the effect the PA domain brings to these proteins, pH 3 was eliminated from the study. In contrast, no degradation was seen YopB, so it was studied at pH 3 to 8. Far-UV CD spectroscopy revealed double minima at 208 and 222 nm in all the translocator protein spectra, indicating dominant α-helical content in all cases (Figs. 5.13A, 5.14A and 5.15A). As seen in for the DB Fusion and SipDB fusion, the presence of LDAO lessened the destabilizing effect of low pH for the translocator proteins (although IpaB at pH 7 showed a relatively stronger signal than at the other pH values). The thermal stability of each protein's secondary structure was determined by monitoring the CD signal as molar ellipticity at 222 nm as a function of increasing temperature (Fig 5.13, 5.14B and 5.15B). The secondary structure of IpaB at pH 4 to 6 diminished gradually and a transition at ~ 45-50 °C was seen at pH 7 and 8. A similar partially unfolded state was reached at all pH values after reaching 90 °C. An important thing to mention here is that when the protein was cooled down after the thermal melt, it exhibited an identical CD spectrum as before the melt, which indicates that the IpaB in LDAO recovered its secondary structure. The same pattern was shared by SipB without any relatively obvious transition. For YopB, the secondary structure was dramatically lost at pH 5 and 6 with transitions at ~ 70°C and 60 °C, respectively, while it was partially unfolded at the other pH values.

The protein tertiary structure was monitored by following intrinsic fluorescence peak position as a function of pH and temperature (Figs. 5.13C, 5.14C and 5.15C). As with secondary structure, IpaB maintained its tertiary structure to over ~50 °C after the initial red shift, while a

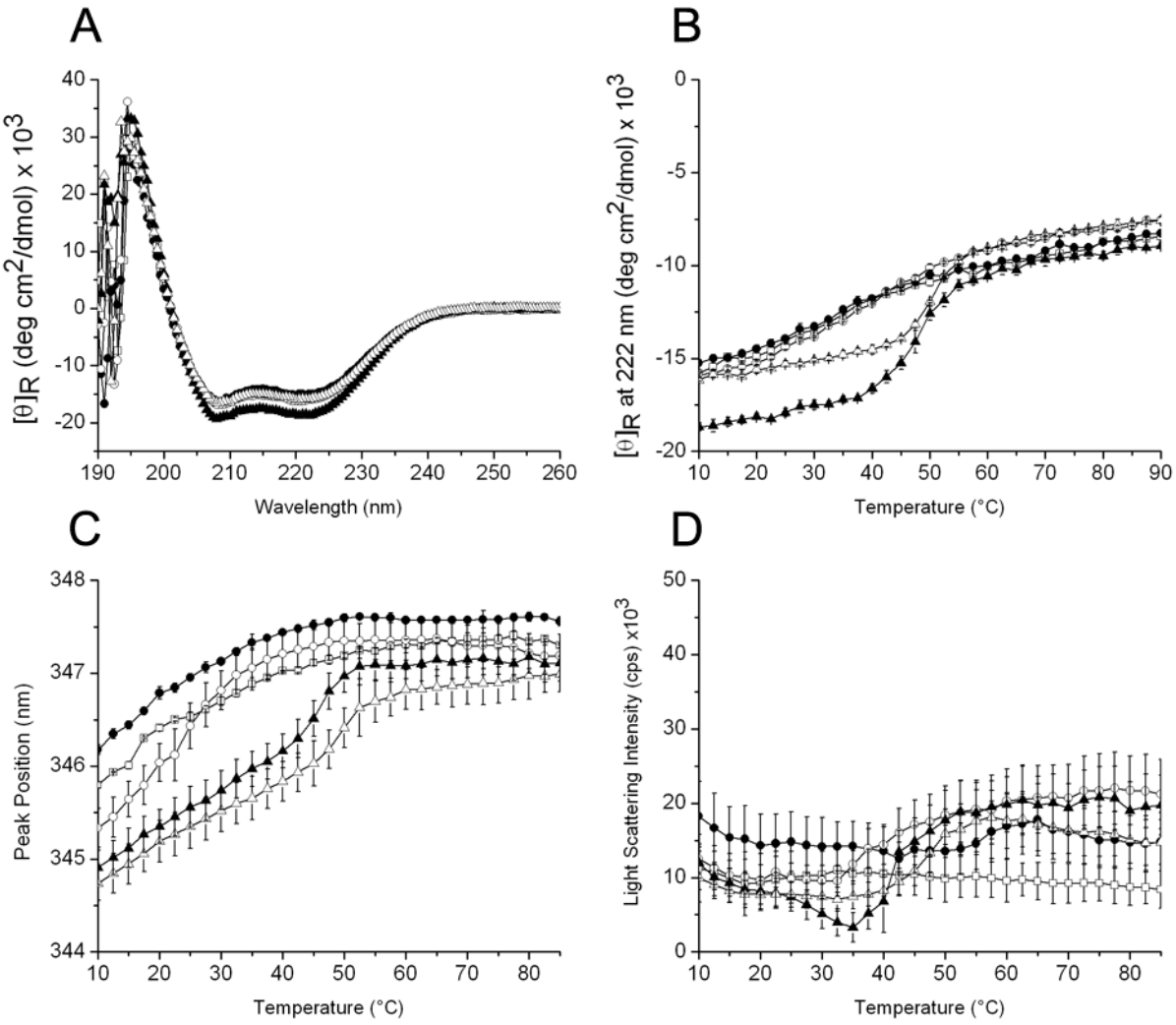

Figure 5.13: Biophysical characterization of IpaB with the presence of LDAO. Far-UV Circular Dichroism (CD) spectra of IpaB, recorded at different pH conditions (A). Far-UV CD molar ellipticity at 222 nm monitored as a function of temperature from 10 to 90 ˚C (B). Intrinsic Trp fluorescence peak position wavelength (C) and light scattering intensity monitored at 295 nm (D) as a function of temperature from 10 to 85 ˚C. Error bars represent standard deviation from three different experiments. Symbols: pH 4 (□), pH 5 (●), pH 6 (○), pH 7 (▲), pH 8 (Δ).

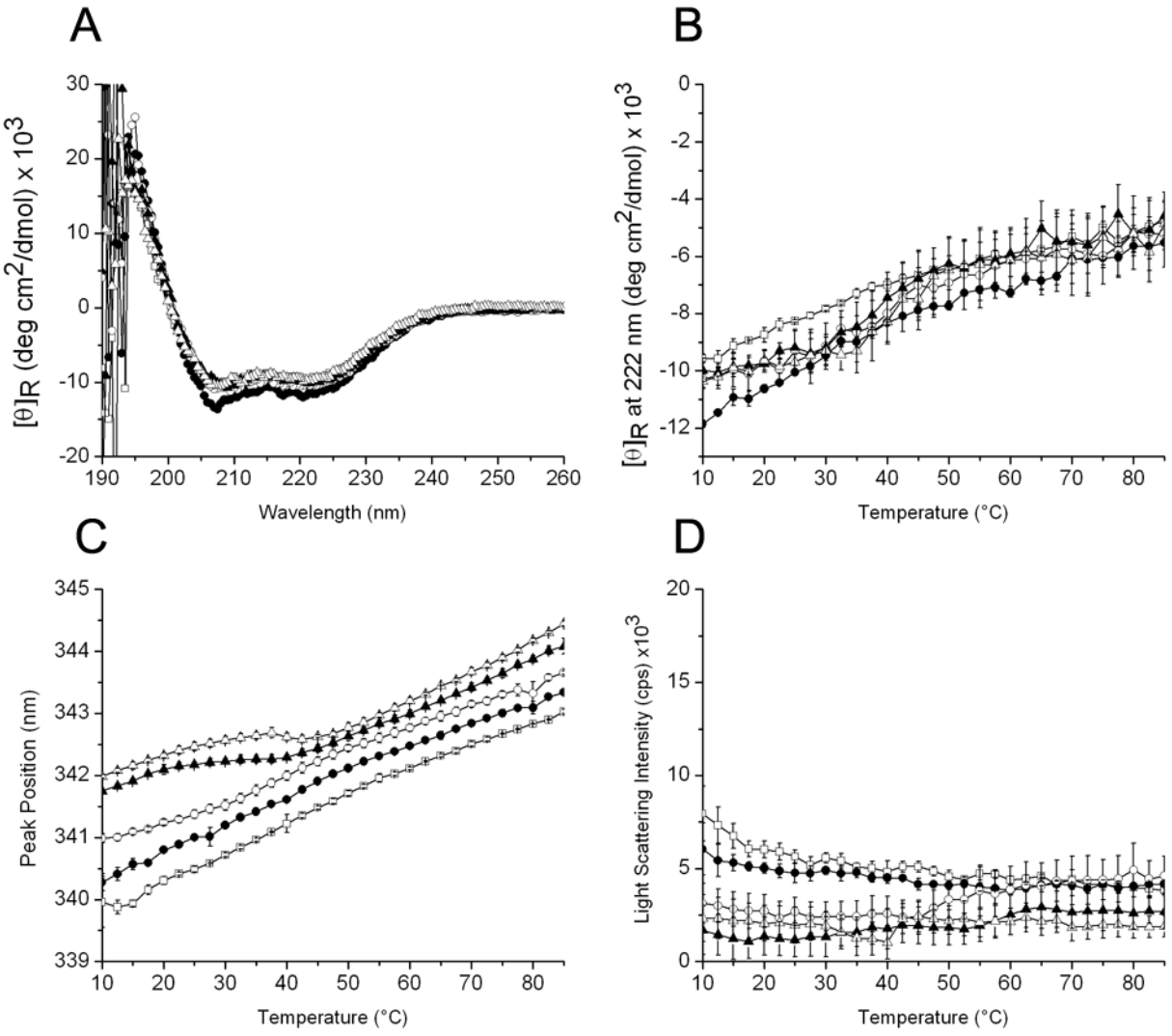

Figure 5.14: Biophysical characterization of SipB with the presence of LDAO. Far-UV Circular Dichroism (CD) spectra of SipB, recorded at different pH conditions (A). Far-UV CD molar ellipticity at 222 nm monitored as a function of temperature from 10 to 90 ˚C (B). Intrinsic Trp fluorescence peak position wavelength (C) and light scattering intensity monitored at 295 nm (D) as a function of temperature from 10 to 85 ˚C. Error bars represent standard deviation from three different experiments. Symbols: pH 4 (□), pH 5 (●), pH 6 (○), pH 7 (▲), pH 8 (Δ).

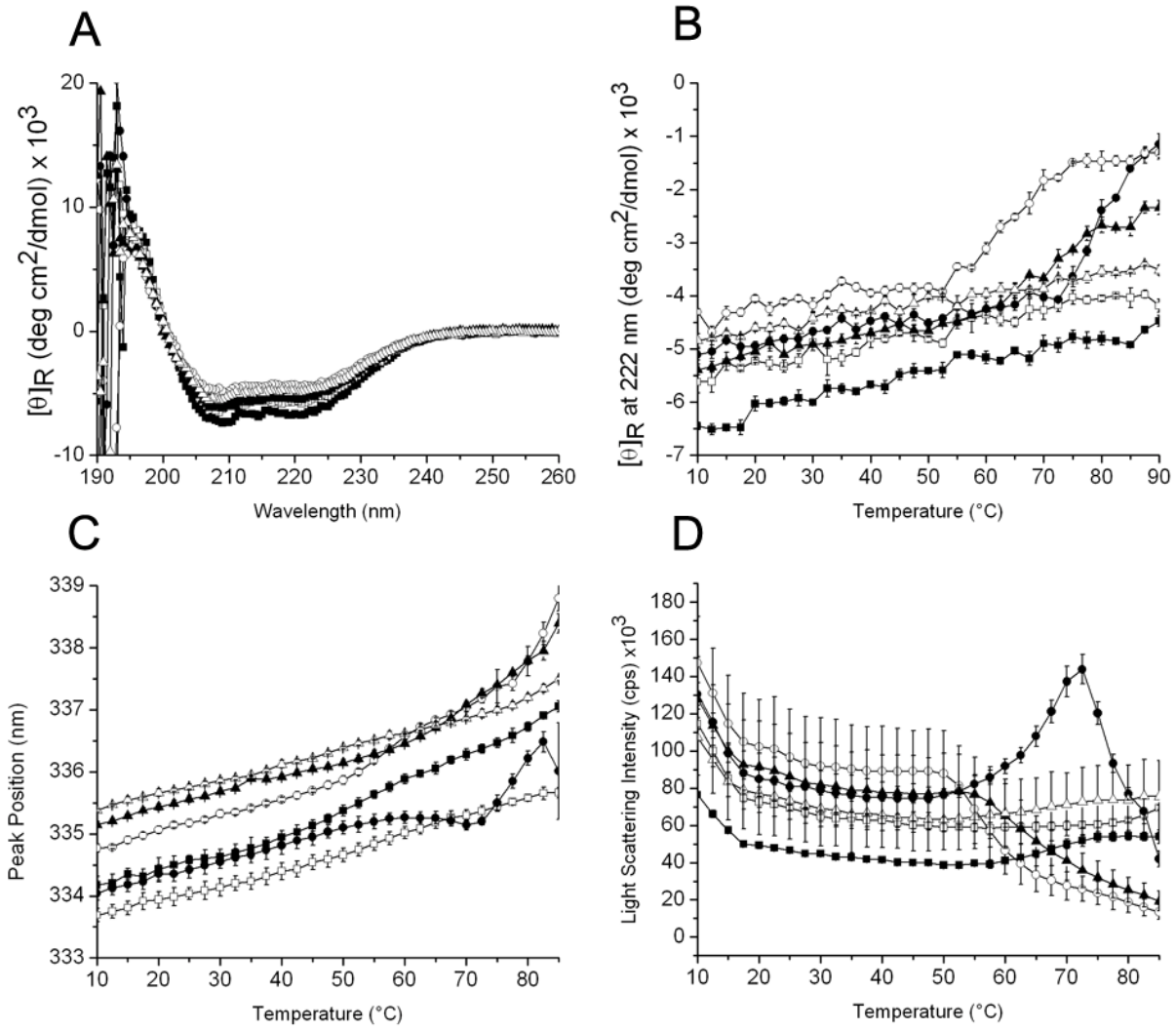

Figure 5.15: Biophysical characterization of YopB with the presence of LDAO. Far-UV Circular Dichroism (CD) spectra of YopB, recorded at different pH conditions (A). Far-UV CD molar ellipticity at 222 nm monitored as a function of temperature from 10 to 90 ˚C (B). Intrinsic Trp fluorescence peak position wavelength (C) and light scattering intensity monitored at 295 nm (D) as a function of temperature from 10 to 85 ˚C. Error bars represent standard deviation from three different experiments. Symbols: pH 3 (■), pH 4 (□), pH 5 (●), pH 6 (○), pH 7 (▲), pH 8 (Δ).

gradual increase in signal was observed for SipB, suggesting a gradual, probably mild change in tertiary structure occrs. For YopB, a similar transition was observed as seen in the CD melt although it was not very sharp at pH 5 and 6. Static light scattering was performed simultaneously with the intrinsic fluorescence to explore aggregation of IpaB, SipB and YopB as a function of pH and temperature (Figs. 5.13D, 5.14D and 5.15D, respectively). LDAO has been shown to prevent aggregation for the DB Fusion and SipDB fusion. Consistent with being a major component of these fusion proteins, IpaB and SipB were also found to resist to aggregation activity in the presence of LDAO. No significant increase in light scattering was observed for IpaB regardless of temperature and pH, indicating no significant aggregation behavior, however, the light scattering intensity did increase a small amount at higher temperatures. Although the signal shows small changes, the transition temperature appear to match that seen using the other techniques. Therefore, minor aggregation could occur though no visible aggregates were observed. As for the YopB, a relatively higher light scattering signal was observed compared to IpaB and SipB. A significant increase in scattering is seen over 60 °C at pH 5 and this is followed by a decrease due to settling of the resulting protein aggregates.

The biophysical data for the translocator proteins were then viewed as a whole using the three-index EPD (Fig. 5.16). For IpaB, lower temperature regions at pH 7 and 8 show the most native-like state which is shown as region 1, which is based on the strong CD signal and fluorescence peak position see under these conditions. Region 2 represents the molten globular state of the protein which is seen in low pH environments. Minor aggregation was suggested for at region 3, which is probably caused by thermal stress. It’s notable that the light scattering increase was very limited which might indicate the formation of smaller soluble particles. The EPD for SipB showed similar pattern as SipDB fusion with gradual changes in color and definitely no aggregation regardless of pH conditions. There are thus only two regions indicated for SiipB. As for the YopB, interestingly the most stable region (region 1) is seen at lower pHs.

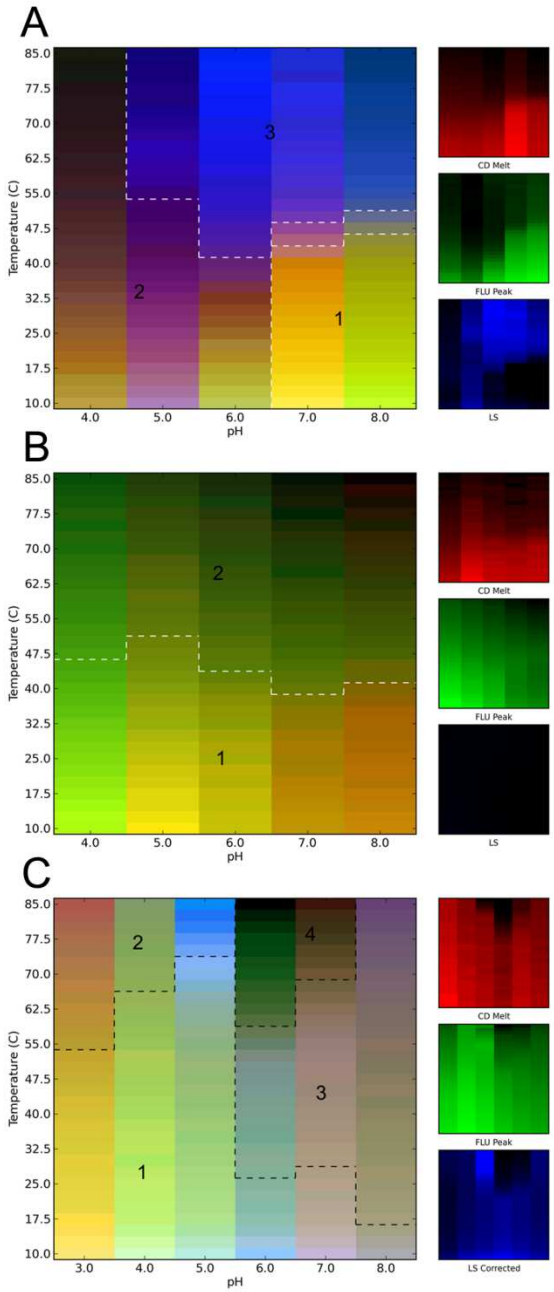

Figure 5.16: Three-index empirical phase diagrams (EPDs) with the presence of LDAO for IpaB (A), SipB (B) and YopB (C), representing the conformational stability of the translocator proteins as a function of pH and temperature. The red, green and blue panels at the right define individual component indices for secondary structure (CD), tertiary structure (fluorescence peak position) and aggregation behavior (LS), respectively.

Overall, the color pattern seen for YopB looks very different from those of IpaB and SipB, which most likely is caused by the light scattering data which initially decreased as the temperature increased. It is possible that this could be due to micelle formation from LDAO, though it was not seen for the other translocator proteins. The micelle particles would disperse with increasing temperature and the intensity would thus go down. The only exception is the region with higher temperature at pH 5 where actual protein aggregation causes an increase in LS signal.

Biophysical characterization summary of PA-IpaB, PA-SipB and PA-YopB

As mentioned above, it is important to determine the influence that fusion with the PA has on the biophysical properties of these translocator proteins before we study their binding to BLPs. PA placed at the C terminus of the translocator proteins led to poor expression and instability. Therefore, we constructed the fusions with PA at the N terminus and LDAO was included to maintain the solubility of the proteins after the chaperones were removed. Chemical degradation was observed for PA-IpaB and PA-SipB at pH 3, so this condition was deleted from the study. PA-YopB formed visible aggregates when dialyzed into the CP buffers at pH 3 to 5, so only pH 6 to 8 were included in the study for this fusion protein. Far-UV CD spectroscopy was used to measure the secondary structure content of PA-IpaB, PA-SipB and PA-YopB (Figs. 5.17A, 5.18A and 5.19A, respectively). Double minima at 208 and 222 nm were observed suggesting that there was conservation of α-helical secondary structure within these translocator fusion proteins.

To monitor retention of α-helical structure as a function of temperature, CD spectroscopy was used and the molar ellipticity at 222 nm was monitored (Figs. 5.17B, 5.18B and 5.19B). For PA-IpaB, the molar ellipticity signal gradually decreased at each pH with increasing thermal stress until it reached ~50 °C, suggesting gradual and partial loss of secondary structure. At pH

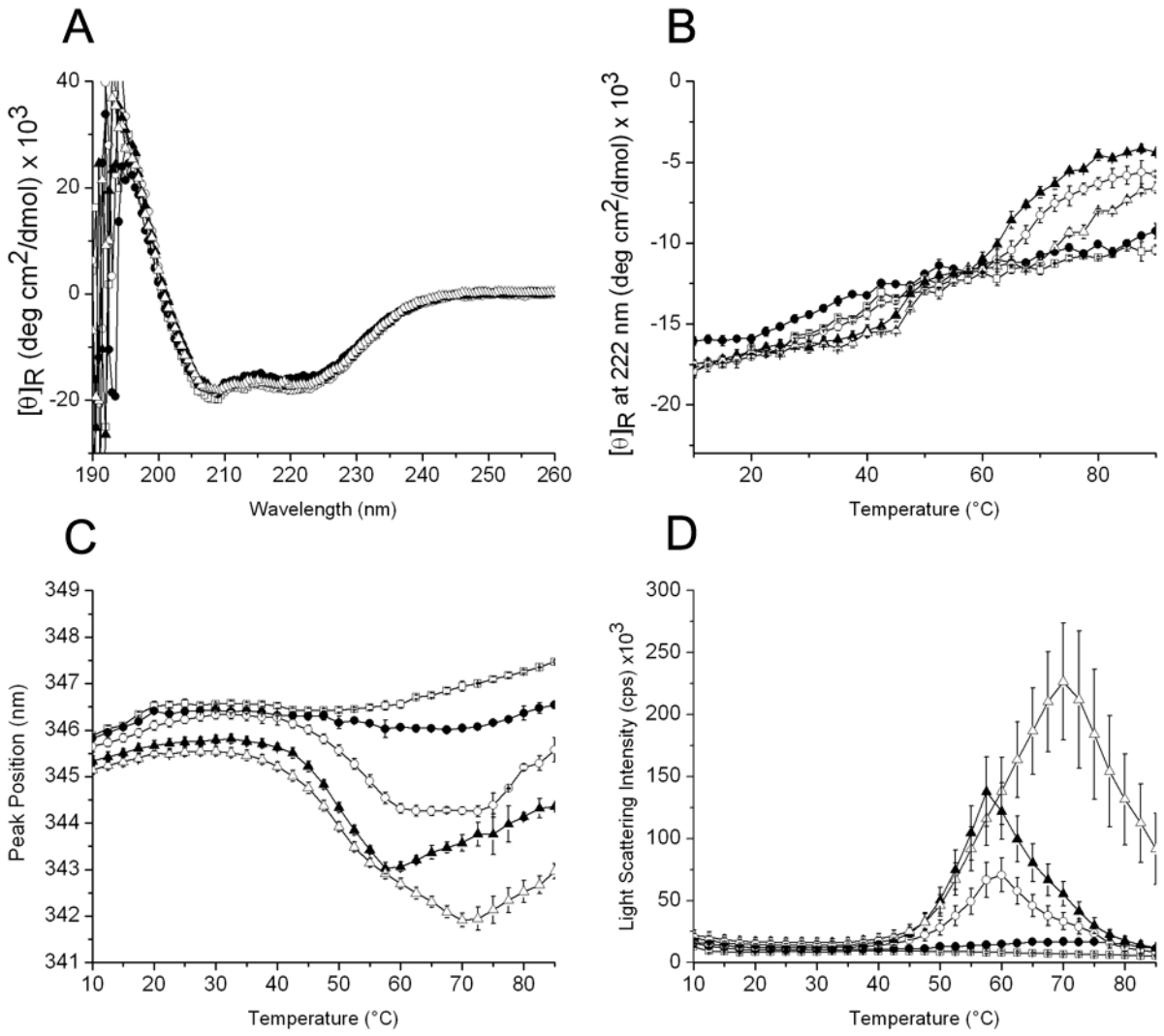

Figure 5.17: Biophysical characterization of PA-IpaB with the presence of LDAO. Far-UV Circular Dichroism (CD) spectra of PA-IpaB, recorded at different pH conditions (A). Far-UV CD molar ellipticity at 222 nm monitored as a function of temperature from 10 to 90 ˚C (B). Intrinsic Trp fluorescence peak position wavelength (C) and light scattering intensity monitored at 295 nm (D) as a function of temperature from 10 to 85 ˚C. Error bars represent standard deviation from three different experiments. Symbols: pH 4 (□), pH 5 (●), pH 6 (○), pH 7 (▲), pH 8 (Δ).

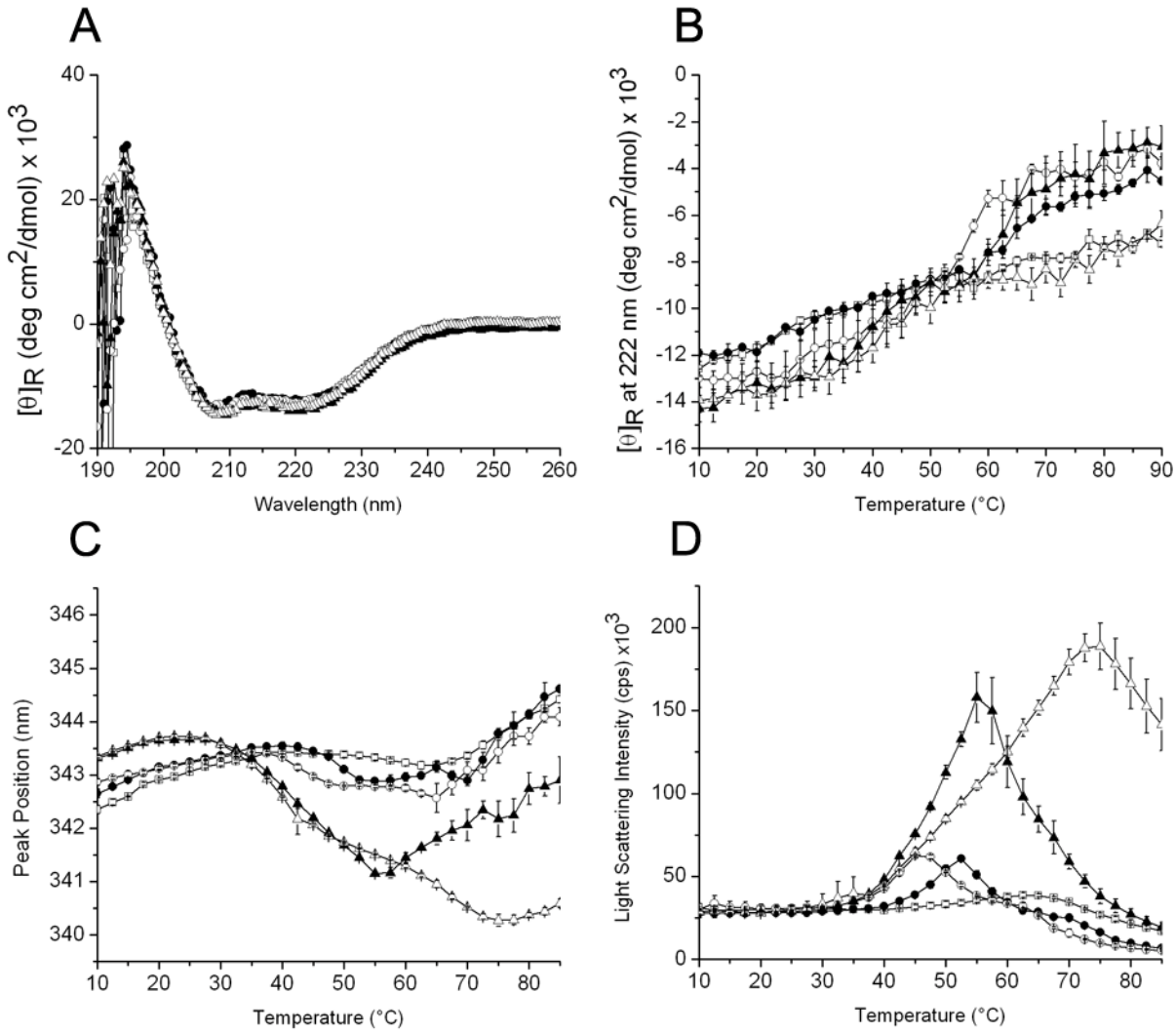

Figure 5.18: Biophysical characterization of PA-SipB with the presence of LDAO. Far-UV Circular Dichroism (CD) spectra of PA-SipB, recorded at different pH conditions (A). Far-UV CD molar ellipticity at 222 nm monitored as a function of temperature from 10 to 90 ˚C (B). Intrinsic Trp fluorescence peak position wavelength (C) and light scattering intensity monitored at 295 nm (D) as a function of temperature from 10 to 85 ˚C. Error bars represent standard deviation from three different experiments. Symbols: pH 4 (□), pH 5 (●), pH 6 (○), pH 7 (▲), pH 8 (Δ).

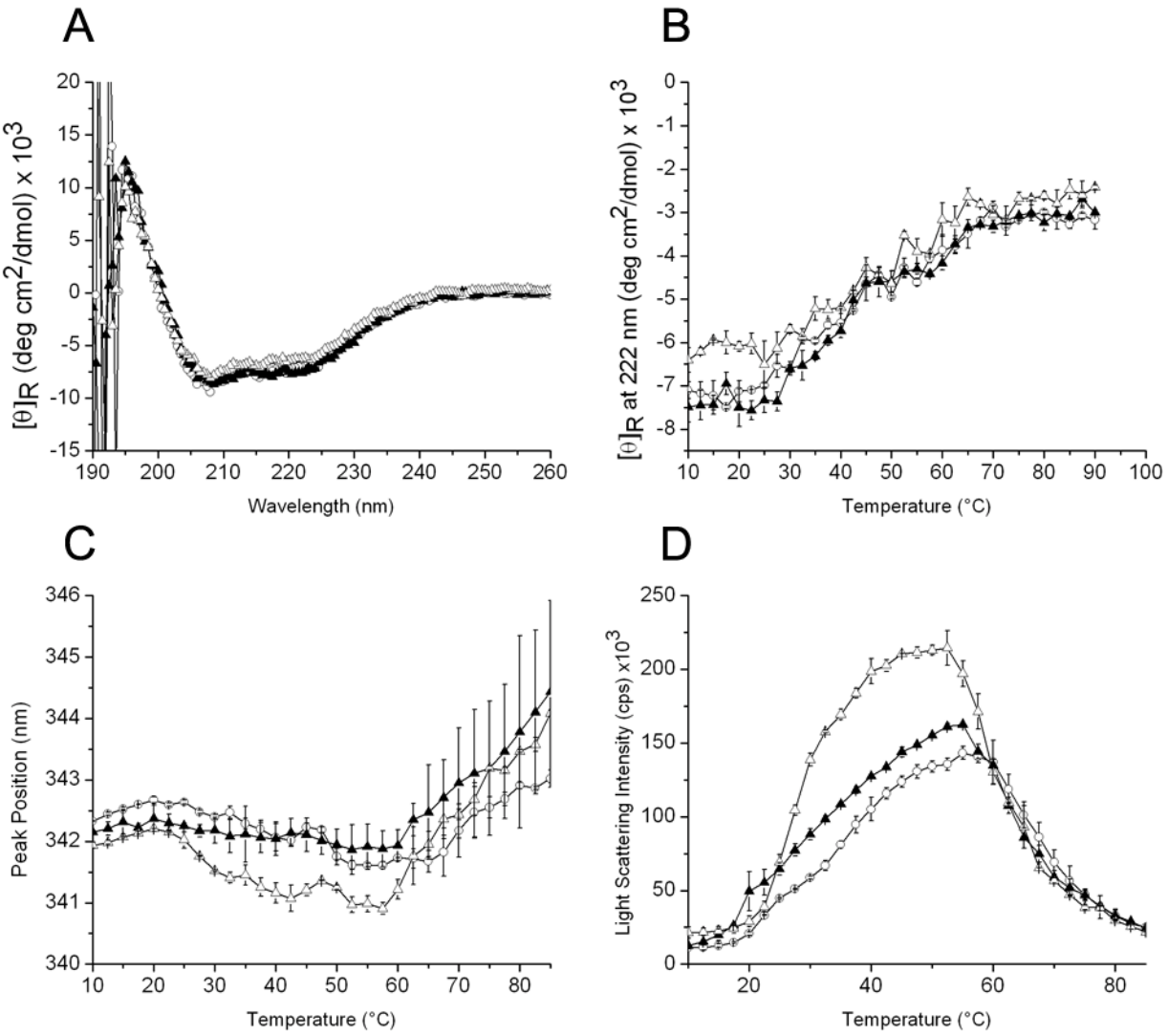

Figure 5.19:Biophysical characterization of PA-YopB with the presence of LDAO. Far-UV Circular Dichroism (CD) spectra of PA-YopB, recorded at different pH conditions (A). Far-UV CD molar ellipticity at 222 nm monitored as a function of temperature from 10 to 90 ˚C (B). Intrinsic Trp fluorescence peak position wavelength (C) and light scattering intensity monitored at 295 nm (D) as a function of temperature from 10 to 85 ˚C. Error bars represent standard deviation from three different experiments. Symbols: pH 6 (○), pH 7 (▲), pH 8 (Δ).

6 to 8 there is a bit of a transition at about 50 ^{o}C and a major transition after 60 °C, which represents a possible substantial structural alteration. Meanwhile the secondary structure continued to only gradually change at pH 4 and 5. No such apparent conformational change was observed for IpaB alone (Fig. 5.13B). PA-SipB shared similar pattern as PA-IpaB but with different pH conditions in that the protein at pH 4 and 8 resisted rapid structural changes due to thermal stress while unfolding was observed from pH 5 to 7 (Fig. 5.18B). As for PA-YopB, the molar ellipticity started decreasing at ~28 °C and underwent a second subtle transition at ~60 °C (seen as a leveling off of the signal change) regardless of pH. For all three proteins, the PA domain dramatically affected the secondary structure and the influence of temperature on thermal stability.

The tertiary structure stability of PA-translocator proteins, as determined by fluorescence peak position, appears to also be significantly influenced by the addition of the PA tag in comparison to each translocator protein alone (Fig. 5.17C, 5.18C and 5.19C). A somewhat similar pattern was observed for all three proteins that started with a gradual red shift followed by a blue shift which was mostly likely caused by protein aggregation. As temperature firstly started to increase, the tertiary structure start to loosen for each and as the Trp residue became exposed a red shift was observed for the peak position. Then, when aggregation started to occur (as confirmed from light scattering data in Fig. 5.17D, 5.18D and 5.19D), the Trp became buried and the peak position then decreased (blue shifted). The light scattering signal went down due to the settling of aggregates. When considered separately, PA-IpaB at all pH values starts to lose tertiary structure and aggregate between 40 and 50 ^{o}C. PA-SipB does the same thing at about 30 ^{o}C at pH 7 and 8 but then becomes more stable to aggregation as the pH decreases. Then, PA-YopB appears to be the least stable as it loses tertiary structure and aggregates starting at about 20 ^{o}C at each pH.

The EPDs of PA-IpaB and PA-SipB showed similar pattern (Fig. 5.20A and B). Region 1 represented the most native-like state at all pH values below about 40 to 50 ^{o}C. Partial unfolding is represented in region 2 for PA-IpaB and the related regions 2 and 3 for PA-SipB. Regions at neutral pH over 50 °C, however, clearly showed signs of aggregation. PA-YopB is clearly much less stable than the other two with a lower aggregation ignition temperature which is obvious in its EPD with the large amount of blue color in regions 2 and 3. The overall structural stability of translocator proteins are highly affected by the addition of the PA domain. Even with the presence of LDAO, which was shown to prevent the translocator proteins from complete conformational destruction and aggregation, dramatic structural changes are observed under various pH conditions when the PA domain is present. Among the three proteins, YopB was mostly influenced by the presence of the PA domain in that it started aggregating just after 20 °C.

Biophysical characterization summary of IpaB-BLP, SipB-BLP and YopB-BLP

As seen for the tip protein-BLP complexes, the BLPs tend to dominate the majority of the spectroscopic signals for the translocator-BLP complexes. Due to problems with either protein degradation or early aggregation of the PA-translocator proteins (as mentioned previously), IpaB-BLP and SipB-BLP complexes were only characterized from pH 4 to 8 conditions while YopB-BLP was studied from pH 6 to 8. The far-UV CD spectra at 10 ˚C for all the tip-BLPs also showed a single minimum at ~ 225 nm (Figs. 5.21A, 5.22A and 5.23A), with much less signal at pH 4 and 5 for IpaB-BLPs, and pH 4 to 6 for SipB-BLPs. As a general trend for IpaB-BLPs and SipB-BLPs, signals at pH 4 and 5 decrease immediately after thermal stress started to be applied where it is already in a completely altered state. As the pH increases, their overall secondary structure was maintained relatively longer (Figs. 5.21B and 5.22B) for both proteins, although it was much less stable compared to the proteins alone. Clear transitions were observed with sharp decreases seen in the signals. Further, the secondary structure appeared to be completely lost after

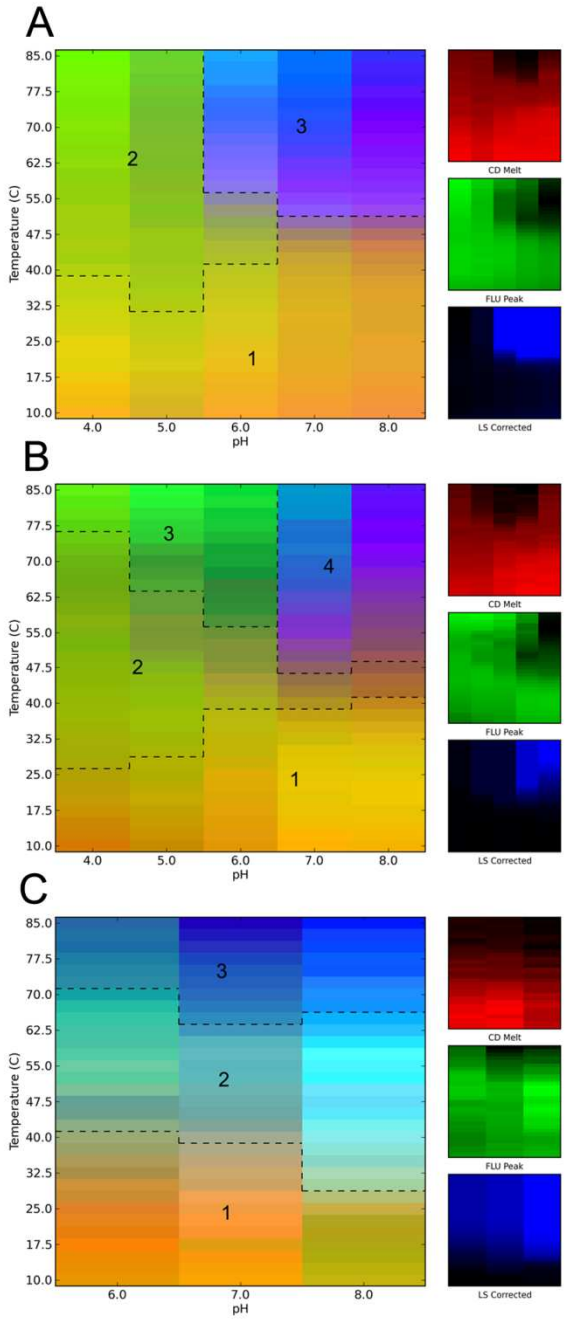

Figure 5.20: Three-index empirical phase diagrams (EPDs) with the presence of LDAO for PA-IpaB (A), PA-SipB (B) and PA-YopB (C), representing the conformational stability of the PA-translocator proteins as a function of pH and temperature. The red, green and blue panels at the right define individual component indices for secondary structure (CD), tertiary structure (fluorescence peak position) and aggregation behavior (LS), respectively.

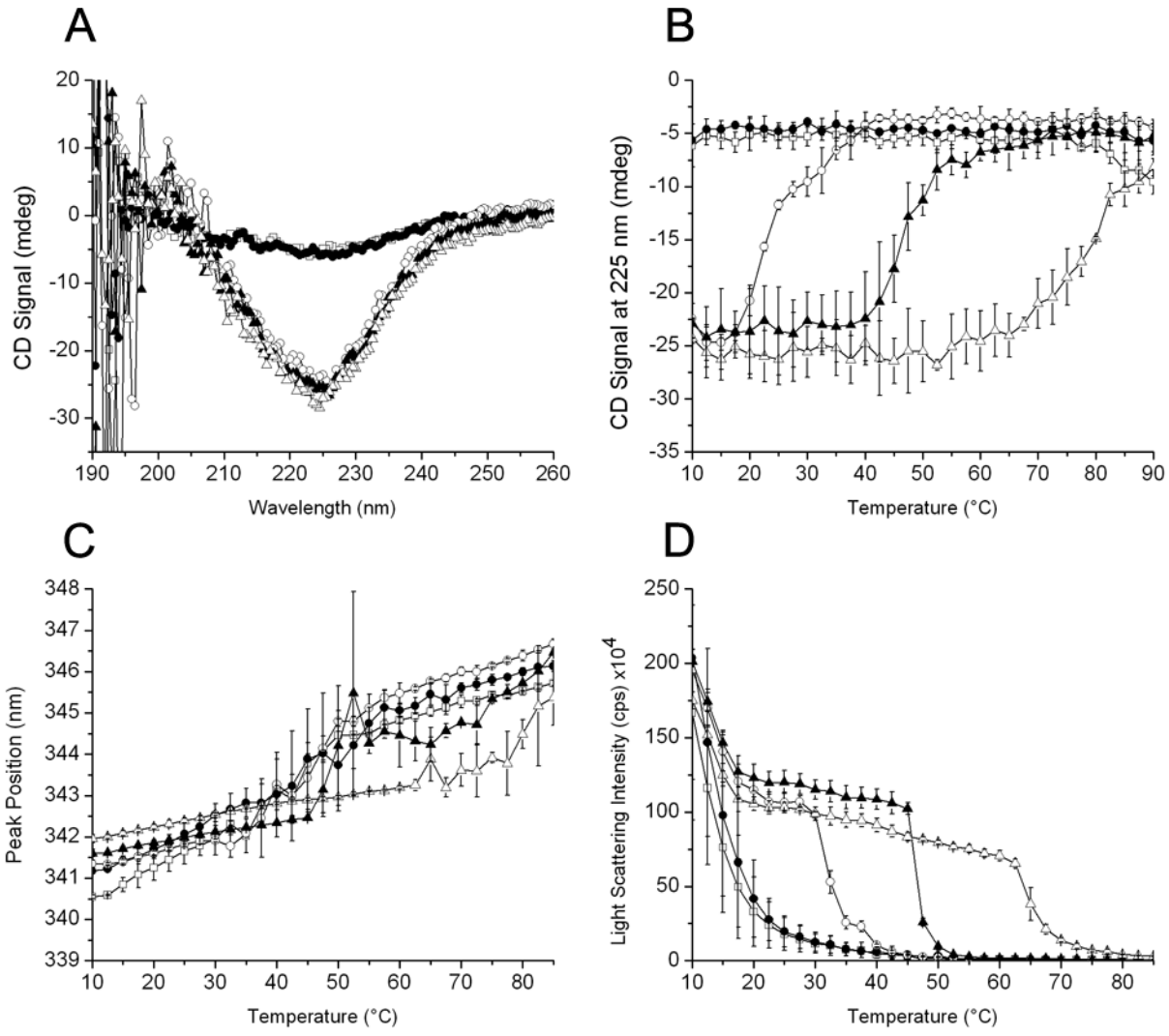

Figure 5.21: Biophysical characterization of IpaB-BLPs with the presence of LDAO. Far-UV Circular Dichroism (CD) spectra of IpaB-BLPs, recorded at different pH conditions (A). Far-UV CD molar ellipticity at 225 nm monitored as a function of temperature from 10 to 90 ˚C (B). Intrinsic Trp fluorescence peak position wavelength (C) and light scattering intensity monitored at 295 nm (D) as a function of temperature from 10 to 85 ˚C. Error bars represent standard deviation from three different experiments. Symbols: pH 4 (□), pH 5 (●), pH 6 (○), pH 7 (▲), pH 8 (Δ).

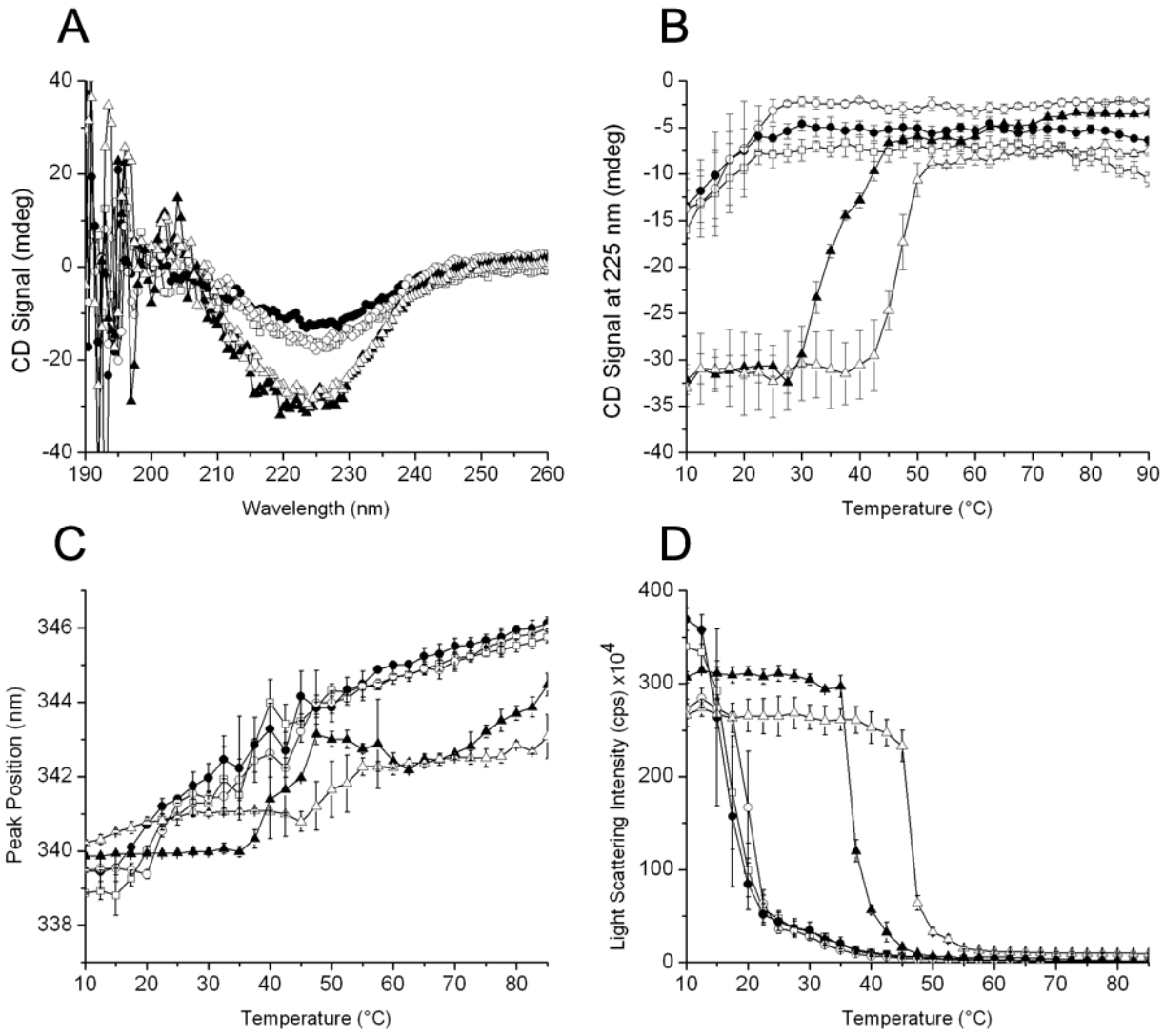

Figure 5 22: Biophysical characterization of SipB-BLPs with the presence of LDAO. Far-UV Circular Dichroism (CD) spectra of SipB-BLPs, recorded at different pH conditions (A). Far-UV CD molar ellipticity at 225 nm monitored as a function of temperature from 10 to 90 ˚C (B). Intrinsic Trp fluorescence peak position wavelength (C) and light scattering intensity monitored at 295 nm (D) as a function of temperature from 10 to 85 ˚C. Error bars represent standard deviation from three different experiments. Symbols: pH 4 (□), pH 5 (●), pH 6 (○), pH 7 (▲), pH 8 (Δ).

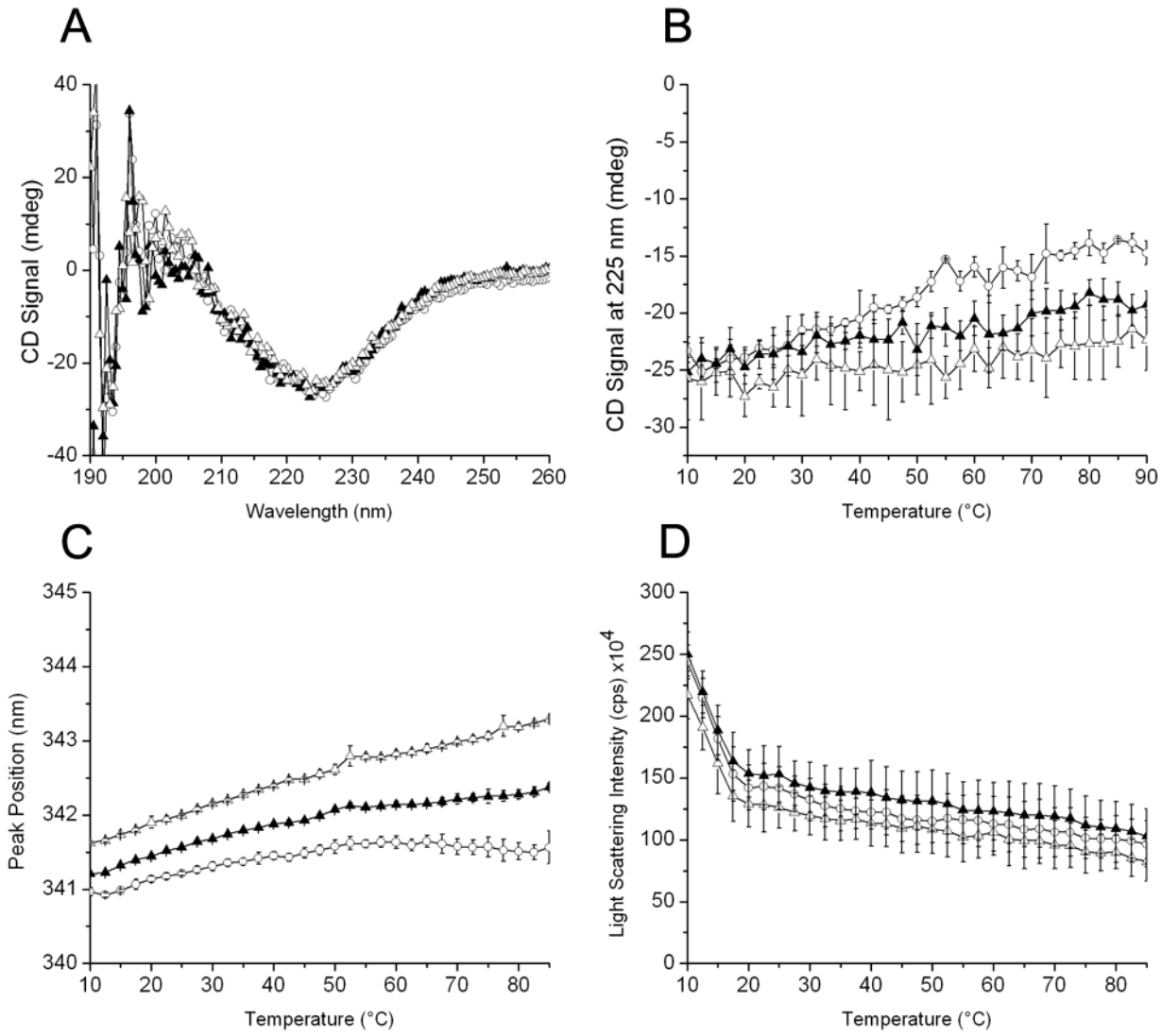

Figure 5.23: Biophysical characterization of YopB-BLPs with the presence of LDAO. Far-UV Circular Dichroism (CD) spectra of YopB-BLPs, recorded at different pH conditions (A). Far-UV CD molar ellipticity at 225 nm monitored as a function of temperature from 10 to 90 ˚C (B). Intrinsic Trp fluorescence peak position wavelength (C) and light scattering intensity monitored at 295 nm (D) as a function of temperature from 10 to 85 ˚C. Error bars represent standard deviation from three different experiments. Symbols: pH 6 (○), pH 7 (▲), pH 8 (Δ).

the melt process was done, however, the YopB-BLPs behaved very differently with the overall secondary structure retained throughout the process without significant changes (Fig. 5.23 B).

The tertiary structure was examined by fluorescence peak position changes as a function of temperature and pH (Fig. 5.21C, 5.22C and 5.23C). For IpaB-BLPs at pH 4 and 5, peak position went through a gradual red shift without sharp transition just like with the CD melt. Clear red shifts were seen at pH 6 to 8 at round same temperature as the transition in the CD signal. For SipB-BLPs, an increase of peak position at ~ 40 ˚C and ~45 ˚C were observed for pH 7 and 8 conditions, respectively. For both cases much less noise was seen at higher pH, suggesting they were more stable at the higher pH. Meanwhile, the tertiary structure of YopB-BLPs seemed to maintain itself rather well.

With regard to the aggregation state as monitored by static light scattering, the plot pattern was highly consistent with the CD melt. For IpaB-BLPs and SipB-BLPs, the rapid drop in signal was attributed to the protein rapidly aggregating and causing the BLPs to fall out of solution. Interestingly, a sharp drop of intensity was found for YopB-BLPs followed by a gradually decrease without complete aggregation observed as seen for the other two protein-BLP complexes. This might indicate a self-limited structural change happened at the beginning with the protein retained in this state as the temperature continues to increase. Overall, it is obvious that BLPs associated with translocator proteins prefer higher pH conditions.

The three-index EPDs for IpaB-BLP and SipB-BLP exhibited similar pattern with only two regions defined respectively (Fig. 5.24A and B). Region 1 at neutral pH and lower temperatures represents a more native-like state as indicated by the CD, FL peak and SLS panels on the right. As triggered by the settling of protein-BLPs system, sharp color transitions are observed as stress is applied. As before, the YopB-BLPs behave dramatically different relative to

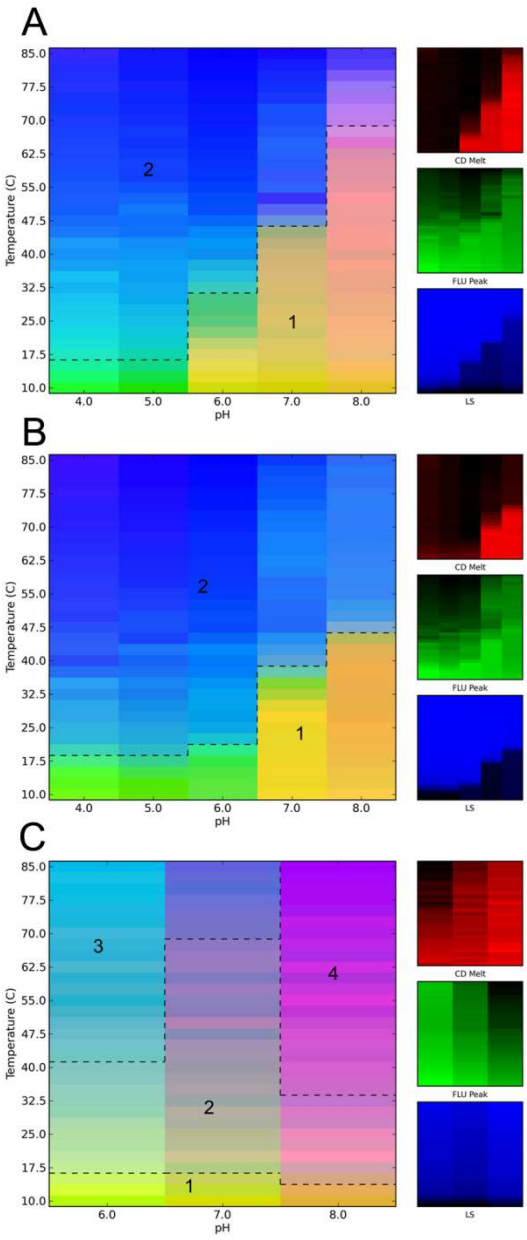

Figure 5.24: Three-index empirical phase diagrams (EPDs) with the presence of LDAO for IpaB-BLPs (A), SipB-BLPs (B) and YopB-BLPs (C), representing the conformational stability of the translocator proteins associated with BLPs as a function of pH and temperature. The red, green and blue panels at the right define individual component indices for secondary structure (CD), tertiary structure (fluorescence peak position) and aggregation behavior (SLS), respectively.

the other two. With an initial decrease in light scattering signal, the product quickly went into a sub-aggregation state. Meanwhile the color changes in secondary and tertiary panel came from the gradual yet obvious changes in the CD and peak position signals. The rather small region 1 thus represents the most stable state and regions 2, 3 and 4 represent various aspects of partial structural alterations that are from the combined effects of the different secondary and tertiary structure states seen under different stresses.

Discussion

The tip proteins and first translocator proteins from the type III secretion systems (T3SSs) of *S. flexneri*, *S.* typhimurium and *Y. enterocolitica* have been identified as potential protective antigens against infection caused by their corresponding bacterial pathogens. To enhance the immune response against these protein antigens, these proteins were genetically fused to a peptidoglycan anchor (PA) domain, which naturally binds to peptidoglycan, so they could be examined as part of a new vaccine delivery system. These PA fusion proteins were thus bound to Bacterium-like particles (BLPs) derived from *L. lactis*. The work presented here is a stability study to lay the foundation for future formulation studies which are required in order to avoid vaccine failure due to chemical modification, degradation and aggregation of the antigens. In this study, selected biophysical techniques were used to assess the structural stability of these proteins alone, their respective PA fusions, and the latter associated with BLPs under the pharmaceutically relevant stresses of temperature and pH. The acquired data set was then combined to generate a three index EPD, which is an improved diagram for visual interpretation of protein structural changes. EPDs are extremely useful in designing excipient screens for the final formulation of a stable vaccine.

The three T3SS tip proteins studied here have been previously shown to have a dumbbell-like structure with N-terminal and C-terminal domains supported by an anti-parallel coiled-coil [81,107,108], however, the shape and size of the two ends of the structure vary for each subfamily resulting in protein specific functions [109]. IpaD and SipD have over 25% sequence similarity and are composed of two independently folding domains with the N-terminal domain being thermal-liable, which might explain the similar pattern of their EPDs and the double thermal transitions observed at neutral pH [81,105]. Compared to IpaD and SipD, LcrV exhibits a distinct behavior under thermal and pH stress, which is not surprising because LcrV belong to a different subfamily of T3SS tip proteins. While IpaD and SipD stay unaffected by pH at lower temperatures, LcrV prefers neutral pH conditions with reduced structural integrity under acidic conditions. Nevertheless, all the three tip proteins maintain a native conformational state at neutral pH under low to moderate thermal stress.

The translocator proteins also play important roles in the virulence of these pathogens and they also appear to be potential vaccine candidates. IpaB, SipB and YopB all need to be co-expressed with their chaperones (IpgC, SicA and SycD, respectively), which are then removed with mild detergent which is needed to keep the translocator proteins soluble. The mild detergent LDAO was used here for the preparation of all three hydrophobic translocator proteins based on its success with IpaB [57]. Moreover, LDAO have been shown to prevent dramatic structural alterations and aggregation in our study of the DB Fusion and the SipDB fusion protein. As might thus be expected, IpaB and SipB were also found to retain many of their structural properties in response to thermal stress when LDAO was present. Data were not collected for IpaB and SipB at pH 3 because minor degradation was observed and this was also seen for PA-IpaB and PA-SipB. No aggregation activity was detected by light scattering during the melting process for these proteins. Unfortunately, LDAO didn’t counter the pH effect for YopB and significant conformational changes were seen for this protein, especially from pH 5 to 7.

For the tip proteins, the addition of the PA domain to the C-terminus had a significant negative impact on their resistance to thermal stress. The introduction of PA domain clearly changed the CD spectra for these proteins with a much stronger signal at 208 nm, thereby indicating the presence of more random coil as seen for the PA protein itself (Fig. 5.25A). Moreover, for secondary and tertiary structure, the signature double transition of IpaD and SipD was absent after fusing with PA, which is most likely attributed by the PA domain (Fig. 5.25B and C). Interestingly, the spectroscopic characteristics of LcrV-PA are less dominated by the PA domain, however, it is still different from the pattern of LcrV by itself. First, insoluble aggregates were formed during dialysis of LcrV-PA to pH 3 and 4. Moreover, LcrV-PA at pH 6, 7 and 8 was more sensitive to thermal stress than LcrV alone.

For translocator proteins, the addition of PA domain to the C-terminus led to degradation and significant instability, probably because effects on the protein's folding processes. Thus, the PA domain was genetically fused to the N-terminus of each protein and each fusion was successfully purified in the presence of LDAO. Unlike IpaB and SipB in LDAO, the PA domain is obviously affected by pH and thermal stress, especially at higher pH (Fig. 5.26). Therefore, PA-IpaB and PA-SipB exhibited very different characteristics than did IpaB and SipB alone. The structural integrity was more impacted at higher pH. The most obvious difference is that aggregation is observed at higher pH values for PA-IpaB and PA-SipB while no aggregation occurs for IpaB and SipB alone. It's not surprising to see these changes considering the PA portion is contributing to the conformational alterations, however, PA-YopB seemed to be much more intensely affected with insoluble aggregates appearing at low temperatures at pH 3 to 5 and it being highly sensitive to thermal stress at pH 6 to 8.

Due to protein degradation only five pH conditions were examined for IpaD-BLPs, SipD-BLPs, IpaB-BLPs and SipB-BLPs. Even fewer pH conditions were examined for LcrV-BLPs and YopB-BLPs due to aggregation. Although the majority of the spectroscopic signal is contributed

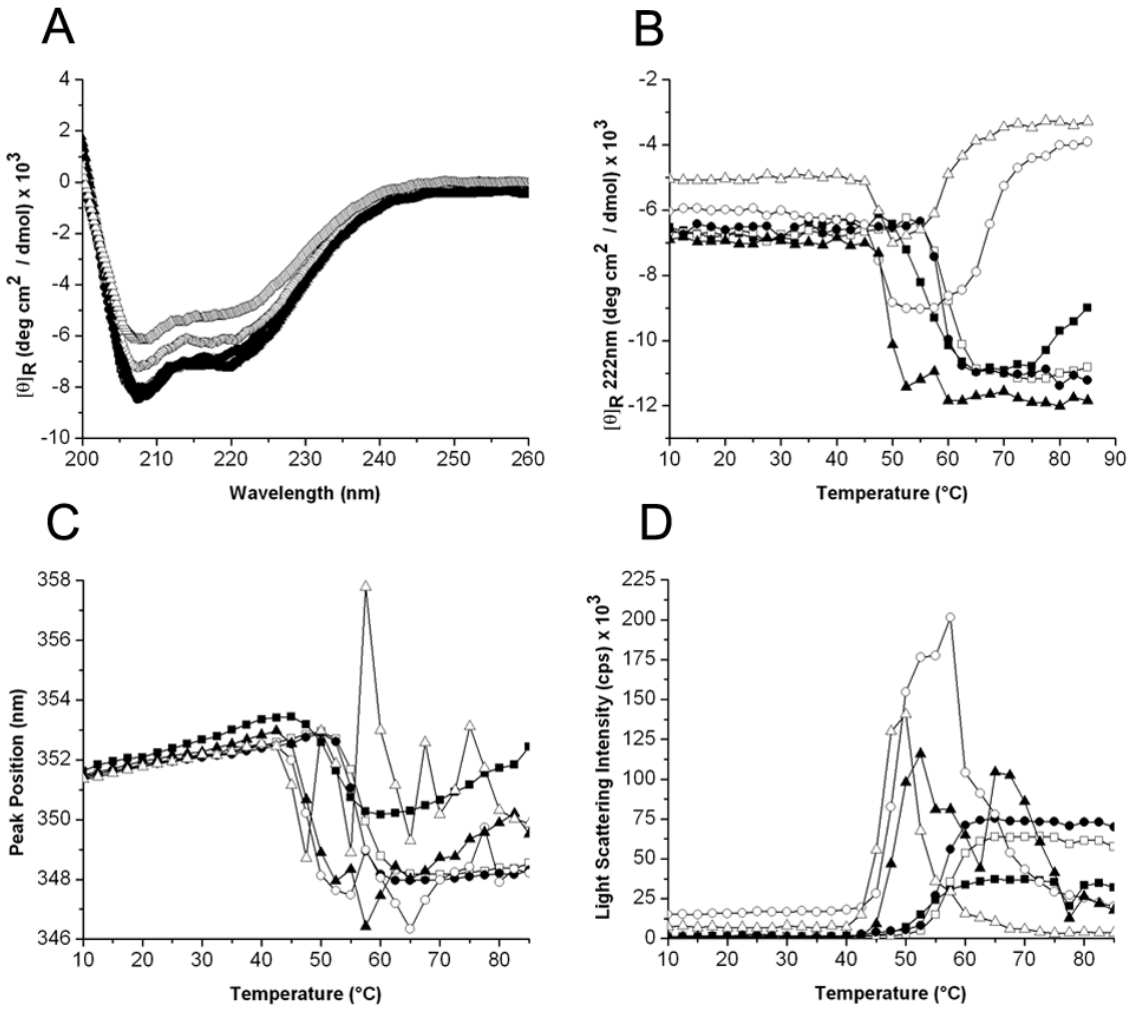

Figure 5.25: Biophysical characterization data for PA domain. Far-UV Circular Dichroism (CD) spectra of PA, recorded at different pH conditions (A). Far-UV CD molar ellipticity at 222 nm monitored as a function of temperature from 10 to 90 ˚C (B). Intrinsic Trp fluorescence peak position wavelength (C) and light scattering intensity monitored at 295 nm (D) as a function of temperature from 10 to 85 ˚C. Error bars represent standard deviation from three different experiments. Symbols: pH 3 (■), pH 4 (□), pH 5 (●), pH 6 (○), pH 7 (▲),pH 8 (Δ).

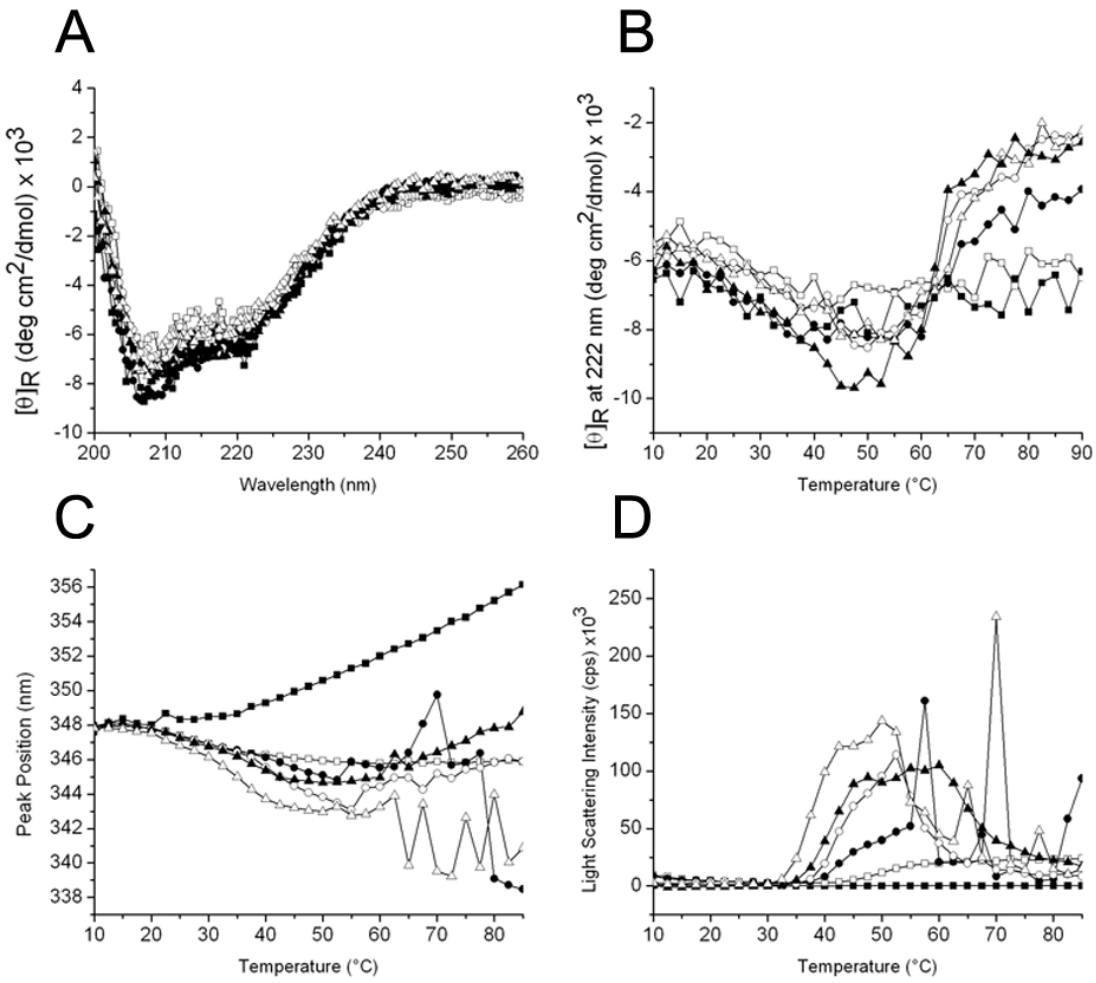

Figure 5.26: Biophysical characterization data for PA domain with the presence of LDAO. Far-UV Circular Dichroism (CD) spectra of PA, recorded at different pH conditions (A). Far-UV CD molar ellipticity at 222 nm monitored as a function of temperature from 10 to 90 ˚C (B). Intrinsic Trp fluorescence peak position wavelength (C) and light scattering intensity monitored at 295 nm (D) as a function of temperature from 10 to 85 ˚C. Error bars represent standard deviation from three different experiments. Symbols: pH 3 (■), pH 4 (□), pH 5 (●), pH 6 (○), pH 7 (▲),pH 8 (Δ).

by the BLPs, the structural changes of the associated proteins certainly influence the behavior of the BLPs and give rise to specific signal patterns. It's important to notice that the BLPs give a very strong initial light scattering signal because of their size, however, when the associated protein aggregates, the signal rapidly decreases due to the settling of the BLPs out of solution. For the tip protein-BLPs, despite the difference pattern exhibited by EPDs, pH 7 and 8 conditions are most favorable in general. This also applies to the translocator-BLPs although they are less stable than their respective tip protein-BLPs except for YopB-BLPs which are very stable in spite of the relative instability of PA-YopB. It seems like the binding activity alters the structure somehow and decreases the impact of the PA domain on the overall fusion protein structure.

In this study, a large amount of biophysical data was collected. In this situation, the EPD technique shows its advantage in that it's easier to interpret and more convenient to compare different proteins' behavior in solution, as well as different forms of the same protein (for example, with or without a PA domain fusion). The three-index EPDs revealed a tremendous amount of structural information for these T3SS proteins before and after binding to BLPs, and in response to pH and thermal stress. Most significantly, this study investigated the protein-specific stability conferred by the binding to BLPs and the ability to differentiate the different samples despite the fact that the BLP moiety is the major species in solution and the protein moiety is a more subtle, yet defining contributor to the observe spectroscopic observations. The generated EPDs will now be used to provide direction for designing excipient screens and in determining suitable conditions for vaccine storage. Excipients will need to be identified to expand the thermal and acidic boundaries of the EPDs for these proteins.

CHAPTER VI

CONCLUSIONS

The purpose of this work has been to characterize the conformational stability of a series of type three secretion system (T3SS) proteins that are candidates for creating protein-based subunit vaccines against *Shigella*, *Salmonella* and *Yersinia* infections using a novel biophysical analysis tool called the three-index Empirical Phase Diagram (EPD). The information obtained will now be used for pre-formulation studies and the creation of a final vaccine product.

Infectious diarrhea is an important public health problem and a major cause of morbidity all over the world, especially in developing countries. Infants and young children under 5 years old are the most vulnerable to enteric infections [110]. Limited improvements in sanitation and medical conditions have contributed to a reduction in mortality rate, however, the disability-adjusted life years lost caused by these diseases cannot be made up. Furthermore, even though the morbidity caused by infectious diarrhea is much lower in developed countries, the cost of hospitalizations and absences from work/school are still considerably high. *Shigella, Salmonella* and *Yersinia enterocolitica* are three highly virulent water and food borne pathogens that cause a high incidence of infectious diarrhea. Thus, the development of vaccines against these pathogens is urgently needed. Vaccination is one of the most important public health tools for the prevention of infectious diseases, however, formulation of safe and effective vaccines can be challenging

– especially since all of the easily developed vaccines are already on the market. A lot of effort has been made on the development of live, attenuated vaccines, but while these vaccines show promise, they fail to convey broad protection against closely related bacterial pathogens. In this study, we focused on the pre-formulation of subunit vaccines based on T3SS proteins.

The T3SS is a common virulence factor shared by many Gram-negative bacterial pathogens. Within a given species the T3SS components are highly conserved and have the potential to convey serotype-independent protection if developed into an efficacious vaccine. With the discovery of *Shigella* T3SS protein IpaD and IpaB as protective antigens, we developed two strategies for vaccine development based on T3SS proteins. The first is a fusion protein strategy based on the observation that the combination of IpaD and IpaB give better immunogenicity/protection than the individual proteins. (Data not published) We thus decided to make a fusion composed of both proteins, which simplifies the production and lowers the cost. During the generation of this vaccine candidate, we discovered that a mild detergent called LDAO can convey elasticity and resiliency properties to the hydrophobic proteins being examined here. Furthermore, LDAO is considered safe for use in humans and is less expensive that OPOE and cost is an important consideration when creating a vaccine for use in the developing world.

Following our initial success with the DB Fusion, we used the same strategy to construct a SipDB fusion for *Salmonella*. An alternative vaccine strategy that we tested is to bind multiple T3SS antigens onto Bacterium-Like Particles derived from *L. lactis.* This strategy is being used to target newborns because *L. lactis* is one of the probiotics which have been shown to be safe for children and even newborns [94]. T3SS tip proteins and translocator proteins from *Shigella, Salmonella* and *Yersinia* were fused with a protein anchor (PA) domain and attached to the surface of BLPs. The immunogenicity of these vaccine candidates is currently under investigation

at the Center for Vaccine Development (CVD) at the University of Maryland, School of Medicine.

Based on the two strategies mentioned above, we've successfully constructed a series of vaccine candidates. For the protein based vaccines, stability is an important issue in formulation, storage and shipping. The chemical and structural integrity of the proteins is easy to be compromised by environmental stress like pH and temperature, which can jeopardize the efficacy of the vaccine. Thus, an approach to characterize the stability of protein products efficiently is born at the right moment called three-index empirical phase diagram (EPD) which is a colored representation of protein structural integrity and conformational stability in response to various of environmental stress. To generate an EPD, multiple biophysical techniques measuring the protein secondary, tertiary and quaternary structural changes under environmental perturbations need to be applied. Meaningful colors are assigned to represent the protein structural changes, which makes the three-index EPD a friendly and efficient visualization technique for understanding of the proteins' properties under a variety of pharmaceutically relevant stresses. In chapter II, the use of the biophysical techniques and EPD clearly showed the different impact of detergent OPOE and LDAO had on DB fusion proteins, and helped us to define a better detergent for formulation. Furthermore, we extended the use of these techniques and generate EPDs for protein antigens associated with bacterium-like particles in chapter IV. Although the biophysical techniques used for monitoring structural changes of proteins might not be perfect suitable for antigen-BLPs considering the dominant signal come from BLPs, the alteration can still be monitored. Significant information has been obtained from the EPDs and will be of great value for further development like excipient screening.

To summarize this dissertation, I focused on the biophysical characterization of T3SS protein-based subunit vaccine candidates against *Shigella, Salmonella* and *Yersinia*. The large data set obtained for each protein or protein derivative was then summarized using an improved

data visualization technique, the three-index EPD, which allows for easy interpretation of the overall structural changes that occur in a protein as a function of pH and thermal stress. Based on the information acquired, we learned a great deal about the conformational changes that occur in these recombinant proteins in response to environmental stresses and discovered the importance of using the proper detergent in the pre-formulation of these subunit vaccines. Further studies that include excipient screening can now be guided with the information generated here.

REFERENCES

[1] K. Shiga, Sekiri byogen kenkyu hokoku dai-ichi (first report on etiologic research on dysentery), Saikingaku Zasshi 25 (1897) 790.

[2] T.L. Hale, Genetic basis of virulence in Shigella species, Microbiological reviews 55 (1991) 206-224.

[3] K. Kotloff, J. Winickoff, B. Ivanoff, J.D. Clemens, D. Swerdlow, P. Sansonetti, G. Adak, M. Levine, Global burden of Shigella infections: implications for vaccine development and implementation of control strategies, Bulletin of the World Health Organization 77 (1999) 651-666.

[4] G.N. Schroeder, H. Hilbi, Molecular pathogenesis of Shigella spp.: controlling host cell signaling, invasion, and death by type III secretion, Clinical microbiology reviews 21 (2008) 134-156.

[5] WHO, Initiative for vaccine research: diarrheal diseases (up-dated February 2009), WHO, Geneva, Switzerland. www.who.int/vaccine_research/diseases?diarrhoeal/en/index6.html. (2009).

[6] J. Gorden, P. Small, Acid resistance in enteric bacteria, Infection and immunity 61 (1993) 364-367.

[7] G.H. Gudmundsson, P. Bergman, J. Andersson, R. Raqib, B. Agerberth, Battle and balance at mucosal surfaces–The story of< i> Shigella</i> and antimicrobial peptides, Biochemical and biophysical research communications 396 (2010) 116-119.

[8] D. Islam, L. Bandholtz, J. Nilsson, H. Wigzell, B. Christensson, B. Agerberth, G.H. Gudmundsson, Downregulation of bactericidal peptides in enteric infections: a novel immune escape mechanism with bacterial DNA as a potential regulator, Nature medicine 7 (2001) 180-185.

[9] A.L. Man, M.E. Prieto-Garcia, C. Nicoletti, Improving M cell mediated transport across mucosal barriers: do certain bacteria hold the keys?, Immunology 113 (2004) 15-22.

[10] J.S. Wassef, D.F. Keren, J.L. Mailloux, Role of M cells in initial antigen uptake and in ulcer formation in the rabbit intestinal loop model of shigellosis, Infection and immunity 57 (1989) 858-863.

[11] A. Zychlinsky, B. Kenny, R. Ménard, M.C. Prévost, I.B. Holland, P.J. Sansonetti, IpaB mediates macrophage apoptosis induced by Shigella flexneri, Molecular microbiology 11 (1994) 619-627.

[12] A. Zychlinsky, M.C. Prevost, P.J. Sansonetti, Shigella flexneri induces apoptosis in infected macrophages, Nature 358 (1992) 167-169.

[13] K. Le-Barillec, J.G. Magalhaes, E. Corcuff, A. Thuizat, P.J. Sansonetti, A. Phalipon, J.P. Di Santo, Roles for T and NK cells in the innate immune response to Shigella flexneri, The Journal of Immunology 175 (2005) 1735-1740.

[14] P.J. Sansonetti, A. Phalipon, J. Arondel, K. Thirumalai, S. Banerjee, S. Akira, K. Takeda, A. Zychlinsky, Caspase-1 Activation of IL-1β and IL-18 Are Essential for< i> Shigella flexneri</i>–Induced Inflammation, Immunity 12 (2000) 581-590.
[15] P. Clerc, P.J. Sansonetti, Entry of Shigella flexneri into HeLa cells: evidence for directed phagocytosis involving actin polymerization and myosin accumulation, Infection and immunity 55 (1987) 2681-2688.
[16] P.J. Sansonetti, A. Ryter, P. Clerc, A. Maurelli, J. Mounier, Multiplication of Shigella flexneri within HeLa cells: lysis of the phagocytic vacuole and plasmid-mediated contact hemolysis, Infection and immunity 51 (1986) 461-469.
[17] T. Kubori, Y. Matsushima, D. Nakamura, J. Uralil, M. Lara-Tejero, A. Sukhan, J.E. Galán, S.-I. Aizawa, Supramolecular structure of the Salmonella typhimurium type III protein secretion system, Science 280 (1998) 602-605.
[18] A. Blocker, N. Jouihri, E. Larquet, P. Gounon, F. Ebel, C. Parsot, P. Sansonetti, A. Allaoui, Structure and composition of the Shigella flexneri 'needle complex', a part of its type III secreton, Molecular microbiology 39 (2001) 652-663.
[19] S. Chatterjee, S. Chaudhury, A.C. McShan, K. Kaur, R.N. De Guzman, Structure and biophysics of type III secretion in bacteria, Biochemistry 52 (2013) 2508-2517.
[20] J.E. Deane, P. Roversi, F.S. Cordes, S. Johnson, R. Kenjale, S. Daniell, F. Booy, W.D. Picking, W.L. Picking, A.J. Blocker, Molecular model of a type III secretion system needle: Implications for host-cell sensing, Proceedings of the National Academy of Sciences 103 (2006) 12529-12533.
[21] E.M. Barry, M.F. Pasetti, M.B. Sztein, A. Fasano, K.L. Kotloff, M.M. Levine, Progress and pitfalls in Shigella vaccine research, Nature Reviews Gastroenterology and Hepatology 10 (2013) 245-255.
[22] A.I. Camacho, J.M. Irache, C. Gamazo, Recent progress towards development of a Shigella vaccine, (2013).
[23] J.H.*e.a.* Passwell, Safety and immunogenicity of *Shigella sonnei*-CRM9 and *Shigella flexneri* type 2a-rEPAsucc conjugate vaccines in one-to for-year-old children, *Pediatr. Infect. Dis. J.* 22 (2003) 701-706
[24] D. Cohen, S. Ashkenazi, M. Green, Y. Lerman, R. Slepon, G. Robin, N. Orr, D.N. Taylor, J.C. Sadoff, C. Chu, Safety and immunogenicity of investigational Shigella conjugate vaccines in Israeli volunteers, Infection and immunity 64 (1996) 4074-4077.
[25] J.H. Passwell, S. Ashkenzi, Y. Banet-Levi, R. Ramon-Saraf, N. Farzam, L. Lerner-Geva, H. Even-Nir, B. Yerushalmi, C. Chu, J. Shiloach, Age-related efficacy of< i> Shigella</i> O-specific polysaccharide conjugates in 1–4-year-old Israeli children, Vaccine 28 (2010) 2231-2235.
[26] K.L. Kotloff, M.F. Pasetti, E.M. Barry, J.P. Nataro, S.S. Wasserman, M.B. Sztein, W.D. Picking, M.M. Levine, Deletion in the Shigella enterotoxin genes further attenuates Shigella flexneri 2a bearing guanine auxotrophy in a phase 1 trial of CVD 1204 and CVD 1208, Journal of Infectious Diseases 190 (2004) 1745-1754.
[27] K.M. Rahman, S.E. Arifeen, K. Zaman, M. Rahman, R. Raqib, M. Yunus, N. Begum, M.S. Islam, B.M. Sohel, M. Rahman, Safety, dose, immunogenicity, and transmissibility of an oral live attenuated< i> Shigella flexneri</i> 2a vaccine candidate (SC602) among healthy adults and school children in Matlab, Bangladesh, Vaccine 29 (2011) 1347-1354.
[28] G. Adamus, M. Mulczyk, D. Witkowska, E. Romanowska, Protection against keratoconjunctivitis shigellosa induced by immunization with outer membrane proteins of Shigella spp, Infection and immunity 30 (1980) 321-324.

[29] D. Pore, N. Mahata, A. Pal, M.K. Chakrabarti, Outer membrane protein A (OmpA) of Shigella flexneri 2a, induces protective immune response in a mouse model, PloS one 6 (2011) e22663.
[30] F.B. Scorza, A.M. Colucci, L. Maggiore, S. Sanzone, O. Rossi, I. Ferlenghi, I. Pesce, M. Caboni, N. Norais, V. Di Cioccio, High yield production process for Shigella outer membrane particles, PloS one 7 (2012) e35616.
[31] A. Maurelli, B. Baudry, H. d'Hauteville, T. Hale, P. Sansonetti, Cloning of plasmid DNA sequences involved in invasion of HeLa cells by Shigella flexneri, Infection and immunity 49 (1985) 164-171.
[32] J.M. Buysse, C.K. Stover, E.V. Oaks, M. Venkatesan, D.J. Kopecko, Molecular cloning of invasion plasmid antigen (ipa) genes from Shigella flexneri: analysis of ipa gene products and genetic mapping, Journal of bacteriology 169 (1987) 2561-2569.
[33] M. Espina, A.J. Olive, R. Kenjale, D.S. Moore, S.F. Ausar, R.W. Kaminski, E.V. Oaks, C.R. Middaugh, W.D. Picking, W.L. Picking, IpaD localizes to the tip of the type III secretion system needle of Shigella flexneri, Infection and immunity 74 (2006) 4391-4400.
[34] A.J. Olive, R. Kenjale, M. Espina, D.S. Moore, W.L. Picking, W.D. Picking, Bile salts stimulate recruitment of IpaB to the Shigella flexneri surface, where it colocalizes with IpaD at the tip of the type III secretion needle, Infection and immunity 75 (2007) 2626-2629.
[35] M.S. Riddle, R.W. Kaminski, C. Williams, C. Porter, S. Baqar, A. Kordis, T. Gilliland, J. Lapa, M. Coughlin, C. Soltis, Safety and immunogenicity of an intranasal< i> Shigella flexneri</i> 2a Invaplex 50 vaccine, Vaccine 29 (2011) 7009-7019.
[36] D. Tribble, R. Kaminski, J. Cantrell, M. Nelson, C. Porter, S. Baqar, C. Williams, R. Arora, J. Saunders, M. Ananthakrishnan, Safety and immunogenicity of a< i> Shigella flexneri</i> 2a Invaplex 50 intranasal vaccine in adult volunteers, Vaccine 28 (2010) 6076-6085.
[37] F.J. Martinez-Becerra, J.M. Kissmann, J. Diaz-McNair, S.P. Choudhari, A.M. Quick, G. Mellado-Sanchez, J.D. Clements, M.F. Pasetti, W.L. Picking, Broadly protective Shigella vaccine based on type III secretion apparatus proteins, Infection and immunity 80 (2012) 1222-1231.
[38] N.R. Maddux, S.B. Joshi, D.B. Volkin, J.P. Ralston, C.R. Middaugh, Multidimensional methods for the formulation of biopharmaceuticals and vaccines, Journal of pharmaceutical sciences 100 (2011) 4171-4197.
[39] B.S. Chang, S. Hershenson, Practical approaches to protein formulation development, Rational Design of Stable Protein Formulations, Springer, 2002, pp. 1-25.
[40] D.T. Brandau, L.S. Jones, C.M. Wiethoff, J. Rexroad, C.R. Middaugh, Thermal stability of vaccines, Journal of pharmaceutical sciences 92 (2003) 218-231.
[41] S.Y. Venyaminov, J.T. Yang, Determination of protein secondary structure, Circular dichroism and the conformational analysis of biomolecules, Springer, 1996, pp. 69-107.
[42] C.S. Braun, L.A. Kueltzo, C.R. Middaugh, Ultraviolet absorption and circular dichroism spectroscopy of nonviral gene delivery complexes, Nonviral Vectors for Gene Therapy, Springer, 2001, pp. 253-284.
[43] W. Jiskoot, Visser, A. J. W. G., Herron, J. N., and Sutter, M., Fluorescence spectroscopy, in Methods for Structural Analysis of Protein Pharmaceuticals, American Association of Pharmaceutical Scientists (AAPS) pp. 27-82 (2005).
[44] M. Cardamone, N. Puri, Spectrofluorimetric assessment of the surface hydrophobicity of proteins, Biochem. J 282 (1992) 589-593.
[45] L.A. Kueltzo, B. Ersoy, J.P. Ralston, C.R. Middaugh, Derivative absorbance spectroscopy and protein phase diagrams as tools for comprehensive protein characterization: A bGCSF case study, Journal of pharmaceutical sciences 92 (2003) 1805-1820.

[46] S.B. Joshi, A. Bhambhani, Y. Zeng, C.R. Middaugh, An Empirical Phase Diagram–High-Throughput Screening Approach to the Characterization and Formulation of Biopharmaceuticals, Formulation and Process Development Strategies for Manufacturing Biopharmaceuticals (2010) 173-205.
[47] J.H. Kim, V. Iyer, S.B. Joshi, D.B. Volkin, C.R. Middaugh, Improved data visualization techniques for analyzing macromolecule structural changes, Protein Science 21 (2012) 1540-1553.
[48] F.J. Martinez-Becerra, X. Chen, N.E. Dickenson, S.P. Choudhari, K. Harrison, J.D. Clements, W.D. Picking, L.L. Van De Verg, R.I. Walker, W.L. Picking, Characterization of a Novel Fusion Protein from IpaB and IpaD of Shigella spp. and Its Potential as a Pan-Shigella Vaccine, Infection and immunity 81 (2013) 4470-4477.
[49] N. SK., Shigellosis, J. Microbiol 43:133-143 (2005).
[50] F.J. Martinez-Becerra, M. Scobey, K. Harrison, S.P. Choudhari, A.M. Quick, S.B. Joshi, C.R. Middaugh, W.L. Picking, Parenteral immunization with IpaB/IpaD protects mice against lethal pulmonary infection by< i> Shigella</i>, Vaccine 31 (2013) 2667-2672.
[51] P. Cossart, P.J. Sansonetti, Bacterial invasion: the paradigms of enteroinvasive pathogens, Science 304 (2004) 242-248.
[52] J.E. Galán, H. Wolf-Watz, Protein delivery into eukaryotic cells by type III secretion machines, Nature 444 (2006) 567-573.
[53] N.E. Dickenson, L. Zhang, C.R. Epler, P.R. Adam, W.L. Picking, W.D. Picking, Conformational changes in IpaD from Shigella flexneri upon binding bile salts provide insight into the second step of type III secretion, Biochemistry 50 (2010) 172-180.
[54] A. Blocker, P. Gounon, E. Larquet, K. Niebuhr, V. Cabiaux, C. Parsot, P. Sansonetti, The tripartite type III secreton of Shigella flexneri inserts IpaB and IpaC into host membranes, The Journal of cell biology 147 (1999) 683-693.
[55] S.E. Birket, A.T. Harrington, M. Espina, N.D. Smith, C.M. Terry, N. Darboe, A.P. Markham, C.R. Middaugh, W.L. Picking, W.D. Picking, Preparation and characterization of translocator/chaperone complexes and their component proteins from Shigella flexneri, Biochemistry 46 (2007) 8128-8137.
[56] C.S. Dickenson NE, Adam PR, Kramer RM, Joshi SB, Middaugh CR, Picking WL, Picking WD, Oligomeric states of the Shigella translocator protein IpaB provide structural insights into formation of the type III secretion translocon., Protein Science 22:614-627 (2013).
[57] N.E. Dickenson, S.P. Choudhari, P.R. Adam, R.M. Kramer, S.B. Joshi, C.R. Middaugh, W.L. Picking, W.D. Picking, Oligomeric states of the Shigella translocator protein IpaB provide structural insights into formation of the type III secretion translocon, Protein Science 22 (2013) 614-627.
[58] A.P. Markham, B.S. Barrett, R. Esfandiary, W.L. Picking, W.D. Picking, S.B. Joshi, C.R. Middaugh, Formulation and immunogenicity of a potential multivalent type III secretion system-based protein vaccine, Journal of pharmaceutical sciences 99 (2010) 4497-4509.
[59] J. Miller, E.D. Williamson, J.H. Lakey, M.J. Pearce, S.M. Jones, R.W. Titball, Macromolecular organisation of recombinant Yersinia pestis F1 antigen and the effect of structure on immunogenicity, FEMS Immunology & Medical Microbiology 21 (1998) 213-221.
[60] S. Hermeling, L. Aranha, J.M.A. Damen, M. Slijper, H. Schellekens, D.J. Crommelin, W. Jiskoot, Structural characterization and immunogenicity in wild-type and immune tolerant mice of degraded recombinant human interferon alpha2b, Pharmaceutical research 22 (2005) 1997-2006.

[61] A.S. Rosenberg, Effects of protein aggregates: an immunologic perspective, The AAPS journal 8 (2006) E501-E507.
[62] J.F. Carpenter, T.W. Randolph, W. Jiskoot, D.J. Crommelin, C.R. Middaugh, G. Winter, Y.X. Fan, S. Kirshner, D. Verthelyi, S. Kozlowski, Overlooking subvisible particles in therapeutic protein products: gaps that may compromise product quality, Journal of pharmaceutical sciences 98 (2009) 1201-1205.
[63] B. Coburn, G.A. Grassl, B.B. Finlay, Salmonella, the host and disease: a brief review, Immunol Cell Biol 85 (2007) 112-118.
[64] Salmonella, Available from: http://www.cdc.gov/salmonella/index.html (May 2012).
[65] M.M. Levine, Typhoid Fever Vaccines, Vaccines p. 1057-1093 (2004).
[66] J. Holmgren, A.-M. Svennerholm, Vaccines against mucosal infections, Current opinion in immunology 24 (2012) 343-353.
[67] S. Ohtake, R. Martin, A. Saxena, B. Pham, G. Chiueh, M. Osorio, D. Kopecko, D. Xu, D. Lechuga-Ballesteros, V. Truong-Le, Room temperature stabilization of oral, live attenuated< i> Salmonella enterica</i> serovar Typhi-vectored vaccines, Vaccine 29 (2011) 2761-2771.
[68] M.M. Arshad, M.J. Wilkins, F.P. Downes, M.H. Rahbar, R.J. Erskine, M.L. Boulton, M. Younus, A.M. Saeed, Epidemiologic attributes of invasive non-typhoidal Salmonella infections in Michigan, 1995–2001, International Journal of Infectious Diseases 12 (2008) 176-182.
[69] M.M. Levine, Typhoid vaccines ready for implementation, New England Journal of Medicine 361 (2009) 403-405.
[70] M.M. Levine, C. Ferreccio, P. Abrego, O.S. Martin, E. Ortiz, S. Cryz, Duration of efficacy of Ty21a, attenuated< i> Salmonella typhi</i> live oral vaccine, Vaccine 17 (1999) S22-S27.
[71] R. Figueira, K.G. Watson, D.W. Holden, S. Helaine, Identification of Salmonella pathogenicity island-2 type III secretion system effectors involved in intramacrophage replication of S. enterica serovar Typhimurium: implications for rational vaccine design, MBio 4 (2013) e00065-00013.
[72] A.J. Bäumler, R.M. Tsolis, P.J. Valentine, T.A. Ficht, F. Heffron, Synergistic effect of mutations in invA and lpfC on the ability of Salmonella typhimurium to cause murine typhoid, Infection and immunity 65 (1997) 2254-2259.
[73] K.L. Penheiter, N. Mathur, D. Giles, T. Fahlen, B.D. Jones, Non-invasive Salmonella typhimurium mutants are avirulent because of an inability to enter and destroy M cells of ileal Peyer's patches, Molecular microbiology 24 (1997) 697-709.
[74] B.D. Jones, N. Ghori, S. Falkow, Salmonella typhimurium initiates murine infection by penetrating and destroying the specialized epithelial M cells of the Peyer's patches, The Journal of experimental medicine 180 (1994) 15-23.
[75] J.E. Galán, Salmonella interactions with host cells: type III secretion at work, Annual review of cell and developmental biology 17 (2001) 53-86.
[76] A.W. Van der Velden, S.W. Lindgren, M.J. Worley, F. Heffron, Salmonella Pathogenicity Island 1-Independent Induction of Apoptosis in Infected Macrophages bySalmonella enterica Serotype Typhimurium, Infection and immunity 68 (2000) 5702-5709.
[77] M. Hensel, J.E. Shea, C. Gleeson, M.D. Jones, E. Dalton, D.W. Holden, Simultaneous identification of bacterial virulence genes by negative selection, Science 269 (1995) 400-403.
[78] S.A. Khan, R. Stratford, T. Wu, N. Mckelvie, T. Bellaby, Z. Hindle, K.A. Sinha, S. Eltze, P. Mastroeni, D. Pickard, < i> Salmonella typhi</i> and< i> S. typhimurium</i> derivatives

harbouring deletions in aromatic biosynthesis and< i> Salmonella</i> Pathogenicity Island-2 (SPI-2) genes as vaccines and vectors, Vaccine 21 (2003) 538-548.
[79] S.P. Salcedo, M. Noursadeghi, J. Cohen, D.W. Holden, Intracellular replication of Salmonella typhimurium strains in specific subsets of splenic macrophages in vivo, Cellular microbiology 3 (2001) 587-597.
[80] D. Chakravortty, M. Rohde, L. Jäger, J. Deiwick, M. Hensel, Formation of a novel surface structure encoded by Salmonella Pathogenicity Island 2, The EMBO journal 24 (2005) 2043-2052.
[81] Z.D. Chatterjee S, Nordhues BA, Battaile KP, Lovell S, De Guzman RN., The crystal structures of the Salmonella type III secretion system tip protein SipD in complex with deoxycholate and chenodeoxycholate., Protein Sci 20:75-86 (2011).
[82] M.L. Barta, N.E. Dickenson, M. Patil, A. Keightley, G.J. Wyckoff, W.D. Picking, W.L. Picking, B.V. Geisbrecht, The structures of coiled-coil domains from type III secretion system translocators reveal homology to pore-forming toxins, Journal of molecular biology 417 (2012) 395-405.
[83] M.L. Bennish, B.J. Wojtyniak, Mortality due to shigellosis: community and hospital data, Review of infectious diseases 13 (1991) S245-251.
[84] E.J. Gangarosa, D.R. Perera, L.J. Mata, C. Mendizábal-Morris, G. Guzmán, L.B. Reller, Epidemic Shiga bacillus dysentery in Central America. II. Epidemiologic studies in 1969, Journal of Infectious Diseases 122 (1970) 181-190.
[85] S.M. Ray, S.D. Ahuja, P.A. Blake, M.M. Farley, M. Samuel, T. Fiorentino, E. Swanson, M. Cassidy, J.C. Lay, T. Van Gilder, Population-based surveillance for Yersinia enterocolitica infections in FoodNet sites, 1996–1999: higher risk of disease in infants and minority populations, Clinical infectious diseases 38 (2004) S181-S189.
[86] T.L. Cover, R.C. Aber, Yersinia enterocolitica, New England Journal of Medicine 321 (1989).
[87] B. Metchock, D. Lonsway, G. Carter, L. Lee, J. McGowan, Yersinia enterocolitica: a frequent seasonal stool isolate from children at an urban hospital in the southeast United States, Journal of clinical microbiology 29 (1991) 2868-2869.
[88] C. Hanski, U. Kutschka, H. Schmoranzer, M. Naumann, A. Stallmach, H. Hahn, H. Menge, E. Riecken, Immunohistochemical and electron microscopic study of interaction of Yersinia enterocolitica serotype O8 with intestinal mucosa during experimental enteritis, Infection and immunity 57 (1989) 673-678.
[89] C. Mueller, P. Broz, G. Cornelis, The type III secretion system tip complex and translocon, Molecular microbiology 68 (2008) 1085-1095.
[90] G.I. Viboud, J.B. Bliska, Yersinia outer proteins: role in modulation of host cell signaling responses and pathogenesis, Annu. Rev. Microbiol. 59 (2005) 69-89.
[91] S.A. Audouy, M.L. Van Roosmalen, J. Neef, R. Kanninga, E. Post, M. Van Deemter, H. Metselaar, S. Van Selm, G.T. Robillard, K.J. Leenhouts, < i> Lactococcus lactis</i> GEM particles displaying pneumococcal antigens induce local and systemic immune responses following intranasal immunization, Vaccine 24 (2006) 5434-5441.
[92] K. Leenhouts, Mimopath™-Based Vaccine Delivery, Novel Immune Potentiators and Delivery Technologies for Next Generation Vaccines, Springer, 2013, pp. 245-265.
[93] A. Mattia, R. Merker, Regulation of probiotic substances as ingredients in foods: premarket approval or “generally recognized as safe” notification, Clinical infectious diseases 46 (2008) S115-S118.
[94] M. Mshvildadze, J. Neu, V. Mai, Intestinal microbiota development in the premature neonate: establishment of a lasting commensal relationship?, Nutrition reviews 66 (2008) 658-663.

[95] K. Ramirez, Y. Ditamo, L. Rodriguez, W.L. Picking, M.L. van Roosmalen, K. Leenhouts, M.F. Pasetti, Neonatal mucosal immunization with a non-living, non-genetically modified Lactococcus lactis vaccine carrier induces systemic and local Th1-type immunity and protects against lethal bacterial infection, Mucosal immunology 3 (2010) 159-171.
[96] C. Keijzer, T. Meijerhof, P. Voorn, A. de Haan, B. Haijema, K. Leenhouts, M. van Roosmalen, W. van Eden, F. Broere, Inactivated influenza vaccine adjuvanted with bacterium-like particles induce systemic and mucosal influenza A virus specific t-cell and b-cell responses after nasal administration in a tlR2 dependent fashion, Nanoparticles for Nasal Delivery of Vaccines (2013).
[97] T. Bosma, R. Kanninga, J. Neef, S.A. Audouy, M.L. van Roosmalen, A. Steen, G. Buist, J. Kok, O.P. Kuipers, G. Robillard, Novel surface display system for proteins on non-genetically modified gram-positive bacteria, Applied and environmental microbiology 72 (2006) 880-889.
[98] S.A. Audouy, S. van Selm, M.L. van Roosmalen, E. Post, R. Kanninga, J. Neef, S. Estevão, E.E. Nieuwenhuis, P.V. Adrian, K. Leenhouts, Development of lactococcal GEM-based pneumococcal vaccines, Vaccine 25 (2007) 2497-2506.
[99] K. Nganou-Makamdop, M.L. van Roosmalen, S. Audouy, G.-J. van Gemert, K. Leenhouts, C.C. Hermsen, R.W. Sauerwein, Bacterium-like particles as multi-epitope delivery platform for Plasmodium berghei circumsporozoite protein induce complete protection against malaria in mice, Malar J 11 (2012) 50.
[100] A. Rigter, I. Widjaja, H. Versantvoort, F.E. Coenjaerts, M. Van Roosmalen, K. Leenhouts, P.J. Rottier, B.J. Haijema, C.A. de Haan, A protective and safe intranasal RSV vaccine based on a recombinant prefusion-like form of the F protein bound to bacterium-like particles, PloS one 8 (2013) e71072.
[101] C. Epler, N. Dickenson, E. Bullitt, W. Picking, Ultrastructural Analysis of IpaD at the Tip of the Nascent MxiH Type III Secretion Apparatus of Shigella flexneri, Microscopy and Microanalysis 19 (2013) 122-123.
[102] M. Lara-Tejero, J.E. Galán, Salmonella enterica serovar typhimurium pathogenicity island 1-encoded type III secretion system translocases mediate intimate attachment to nonphagocytic cells, Infection and immunity 77 (2009) 2635-2642.
[103] C.A. Mueller, P. Broz, S.A. Müller, P. Ringler, F. Erne-Brand, I. Sorg, M. Kuhn, A. Engel, G.R. Cornelis, The V-antigen of Yersinia forms a distinct structure at the tip of injectisome needles, Science 310 (2005) 674-676.
[104] A.P. Markham, S.E. Birket, W.D. Picking, W.L. Picking, C.R. Middaugh, pH sensitivity of type III secretion system tip proteins, Proteins: Structure, Function, and Bioinformatics 71 (2008) 1830-1842.
[105] M. Espina, S.F. Ausar, C.R. Middaugh, M.A. Baxter, W.D. Picking, W.L. Picking, Conformational stability and differential structural analysis of LcrV, PcrV, BipD, and SipD from type III secretion systems, Protein Science 16 (2007) 704-714.
[106] Y. Zeng, H. Fan, G. Chiueh, B. Pham, R. Martin, D. Lechuga-Ballesteros, V.L. Truong, S.B. Joshi, C.R. Middaugh, Towards development of stable formulations of a live attenuated bacterial vaccine, Human vaccines 5 (2009) 322-331.
[107] M. Espina, S.F. Ausar, C.R. Middaugh, W.D. Picking, W.L. Picking, Spectroscopic and calorimetric analyses of invasion plasmid antigen D (IpaD) from Shigella flexneri reveal the presence of two structural domains, Biochemistry 45 (2006) 9219-9227.
[108] U. Derewenda, A. Mateja, Y. Devedjiev, K.M. Routzahn, A.G. Evdokimov, Z.S. Derewenda, D.S. Waugh, The Structure of< i> Yersinia pestis</i> V-Antigen, an Essential Virulence Factor and Mediator of Immunity against Plague, Structure 12 (2004) 301-306.

[109] S. Johnson, P. Roversi, M. Espina, A. Olive, J.E. Deane, S. Birket, T. Field, W.D. Picking, A.J. Blocker, E.E. Galyov, Self-chaperoning of the type III secretion system needle tip proteins IpaD and BipD, Journal of Biological Chemistry 282 (2007) 4035-4044.
[110] M. Kosek, C. Bern, R.L. Guerrant, The global burden of diarrhoeal disease, as estimated from studies published between 1992 and 2000, Bulletin of the World Health Organization 81 (2003) 197-204.

APPENDICES

Appendix A: Recipes

Agarose gel for DNA electrophoresis

25 ml 1X TAE

15 µl 6 mM Ethidium bromide

0.3 g agarose (electrophoresis grade)

1X TAE (running buffer for agarose gel electrophoresis)

4.84g Tris

1.142ml Glacial acetic acid

2ml 0.5 M EDTA

Q.S. to 1 L

12% SDS-PAGE Separating Gel (Sufficient for two gels)

3.00 ml diH20

2.50 ml 1.5 M Tris-HCl, pH 8.8

100 µl 10% (w/v) SDS

4.00 ml 29:1% (w/v) acrylamide:bisacrylamide

0.15 ml 10% (w/v) ammonium persulfate (APS)

10 µl N,N,N′,N′-Tetramethylethylenediamine (TEMED)

5% SDS-PAGE Stacking Gel (Sufficient for two gels)

2.85 ml diH2O

1.25 ml 0.5 M Tris-HCl, pH 6.8

50.0 µl 10% (w/v) SDS

1.00 ml 29:1% (w/v) acrylamide:bisacrylamide

0.2ml 10% (w/v) APS

15µl TEMED

Maleimide-Labeling buffer:

50 mM 4-(2-Hydroxyethyl)piperazine-1-ethanesulfonic acid (HEPES)

150 mM NaCl

5 mM Tris(2-carboxyethyl)phosphine hydrochloride (TCEP)

pH: 7.0

SDS-PAGE destain

5% (v/v) methanol

7.5% (v/v) glacial acetic acid

SDS-PAGE running buffer

2.42g Tris

14.41g glycine

1.0g SDS

Q.S. to 1 L

SDS-PAGE stain

0.1% (w/v) Coomassie Brilliant Blue R-250

5% (v/v) methanol

7.5% (v/v) glacial acetic acid

IMAC Binding Buffer

20 mM Tris-HCl

500 mM NaCl

5mM imidazole

pH: 7.9

IMAC Charge Buffer

50 mM $NiSO_4$

IMAC Elution Buffer

20 mM Tris-HCl
500 mM NaCl
400 mM imidazole
pH: 7.9

IMAC Strip Buffer
20 mM Tris-HCl
500 mM NaCl
100 mM EDTA
pH: 7.9

IMAC Wash Buffer
20 mM Tris-HCl
500 mM NaCl
60 mM imidazole
pH: 7.9

Hydrophobic Interaction Chromatography (HIC) Buffer A
20 mM NaPO4
1M ammonium sulfate
pH: 7.0

HIC Buffer B
20 mM NaPO4
pH: 7.0

Q Column Start Buffer.
10 mM Tris-HCl
10 mM NaCl
pH: 7.5

Q Column Elution Buffer.
10 mM Tris-HCl
1.0 M NaCl

pH: 7.5

Phosphate-Buffered Saline (PBS)

130 mM NaCl

10 mM Na2HPO4

1.5 mM K2HPO4

3 mM KCl

Citrate Phosphate buffer recipe (2L, 20mM)

Solution 1

0.4 M sodium phosphate dibasic

Sodium phosphate dibasic anhydrous	56.78
Distilled water	1000 ml

Solution 2

0.4M Citric acid

Citric acid anhydrous	76.85
Distilled water	1000 ml

Desired pH	Vol Sol'n 1 (ml)	Vol Sol'n 2 (ml)	NaCl (g) (I = 150mM)	Vol Water (ml)
3	40	60	15.81	1900
4	60	40	14.82	1900
5	70	30	14.00	1900
6	80	20	13.33	1900
7	90	10	12.22	1900
8	97	3	10.88	1900

Appendix B: Bacterial Growth Media

LB Agar

37.0 g LB agar (ready-made mix)

Q.S. to 1 L

Luria-Bertani (LB) Broth

25.0 g LB broth (ready-made mix)

Q.S. to 1 L

Terrific broth (TB):

To prepare 1L of TB, combine 900 ml of tryptone-yeast (Component A) with 100 ml of TB salts (Component B). Components A and B must be prepared and sterilized separately. If combined prior to autoclave sterilization, the salts will precipitate.

Component A (tryptone-yeast):

12 g Tryptone

24 g Yeast extract

4 ml Glycerol

900 ml nanopure H2O

Component B (TB Salts):

Combine the following in ~600 ml of nanopure H2O:

125.41 g K2HPO4

23.12 g KH2PO4

Q.S. to 1 L

Auto-induction media 1L

5 g yeast extract

10 g tryptone

930 mL H_2O

Autoclave

1 mL of 1M $MgSO_4$, 50 mL of 20X NPS solution, 20 mL of 50X 5052 solutions were added in 1 L of the media before incubated with pre-culture.

20X NPS

66 g $(NH_4)_2SO_4$

136 g KH_2PO_4

142 g Na_2HPO_4

900 mL H_2O

Autoclave

50X 5052

100 g α-lactose

25 g glucose

250 g glycerol

900 mL H_2O
Autoclave

Dissolving lactose can be accelerated by warming up in microwave.

Appendix C: Abbreviations

AI: auto-induction

Amp: ampicillin

AUC: analytical ultracentrifugation

BLPs: bacterium-like particles

BSA: bovine serum albumin

CD: circular dichroism

DB: fusion protein IpaD-IpaB

DTT: dithiothreitol

EPD: empirical phase diagram

IL: interleukin

Ipa: invasion plasmid antigen

IPTG: isopropyl thio-β-D-glactoside

kDa: kiloDaltons

LB: Luria-Bertani broth

LDAO: N,N-Dimethyl-n-dodecylamine N-oxide

LPS: lipopolysaccharide

M: molar

Min: minute

MW: molecular weight

Mxi: membrane expression of invasion plasmid antigens

OD: optical density

OPOE: n-Octyl-oligo-oxyethylene

PA: protein anchoring domain

PBS: phosphate-buffered saline

PCR: polymerase chain reaction

PMN: polymorphonuclear leukocytes

SDS-PAGE: sodium dodecyl sulfate-polyacrylamide gel electrophoresis

SipDB: fusion protein SipD-SipB

SLS: static light scattering

spp: species

T3SA: type III secretion apparatus

T3SS: type III secretion system

TB: terrific broth

Tris: tris-hydroxymethyl aminomethane

UV: ultroviolet

VITA

Xiaotong Chen

Candidate for the Degree of

Doctor of Philosophy

Thesis: AN EMPIRICAL PHASE DIAGRAM APPROACH TOWARD BIOPHYSICAL CHARACTERIZATION OF VACCINE CANDIDATES AGAINST SHIGELLA, SALMONELLA AND YERSINIA

Major Field: Microbiology and Molecular Genetics

Biographical:

Education:

Completed the requirements for the Doctor of Philosophy in Microbiology and Molecular Genetics at Oklahoma State University, Stillwater, Oklahoma in July, 2014.

Completed the requirements for the Bachelor of Biotechnology at Shandong University Jinan, China in 2010.

Experience and Selected Awards:

Two accepted peer-reviewed manuscripts (Second-author)
One submitted manuscript (First-author)
One manuscript in preparation (First-author)
Two awards for excellence in presentation
Four presentations at national professional meetings
Nine presentations at regional/local professional meetings

Professional Memberships:

American Society for Microbiology
American Society for Microbiology Missouri Valley Branch